

Comparative Evaluation of Acoustic and Electric Signals of Partial Discharges

Von der Fakultät für Elektrotechnik und Informatik
der Gottfried Wilhelm-Leibniz-Universität Hannover
zur Erlangung des akademischen Grades
Doktor-Ingenieur (Dr.-Ing.)
genehmigte Dissertation

von Herrn
M. Sc. Seyed Amir Mahmood Najafi
geboren am 20.09.1984
in Teheran/Iran

2023

1. Referent: Prof. Dr.-Ing. Ernst Gockenbach

2. Referent: Prof. Dr.-Ing. Michael Hartje / Hochschule Bremen

Vorsitz: Prof. Dr.-Ing. Peter Werle

Tag der Promotion: 24.04.2023

Acknowledgement

I would like to thank my parents and my wife for their support and love during my PhD journey. I would like to express my deep gratitude to Professor Ernst Gockenbach and Professor Hosein Borsi for their patient guidance, enthusiastic encouragement, and useful critiques of this research work since the beginning of the project. Also, I would like to offer my special thanks to Professor Peter Werle for his advice during the project since 2015. I am particularly grateful for the assistance given by MSc. Mohammad Taghi Imani and other colleagues during my investigations. The assistance provided by our workshop staff (Karl-Heinz Maske, Claus-Dieter Hasselberg and Erich Semke) was greatly appreciated.

I would like to thank Senvion GmbH and Siemens-Energy AG for their support during writing period.

Abstract

Failures of power electric components such as transformers and outages can lead to a huge economical loss in the electric power grid. One of the main parts of a power electric components is the insulation system, namely, insulation oil, impregnated pressboard and paper. Several methods exist for diagnostics of these insulation materials. Partial discharge (PD) measurement known as one of the main non-destructive monitoring systems of the insulation materials. However, it has been mainly done off-line in maintenance periods, and the existing on-line methods generally provide less information due to environment electric noises. In contrast to electric PD measurement system, the acoustic emission (AE) measurement system is well known for its immunity against environment electrical noises.

In this thesis comparative evaluation of acoustic and electric signals of PD events generated in oil impregnated pressboard and papers is investigated. The thesis is focused on the characteristic of PD activity and the consequence of that on the electric and AE signal. PD classification is defined by using the relation between acoustic and electric signals of PD events. Although the sensitivity of the AE sensors has been improved over the years, but the detection of the acoustic signals from PD activity in power equipment mainly transformers remain the main challenge of acoustic measurement. Lack of information regarding evaluation of electric PD signals and AE signals beside the mechanical attenuation are two main disadvantages of AE measurement method. Due to mechanical and electrical mechanism of waves generated during PD activities, the mechanical and electrical behaviour of the waves is discussed in more detail to have better understanding about the electric and acoustic signals. PD sources were generated at different electrode configurations such as needle-plane and electrode ball arrangement within a sample in the tank to investigate different types of PD. Electric characteristics of PD and different PD measuring technics such as electric, UHF and acoustic beside the mechanical behaviour of the acoustic waves are also discussed.

The corona in oil results regarding the relation between AE and electric PD signals shows the correlated behaviour between AE and PD apparent charge magnitude. However, in surface discharges these behaviours are uncorrelated. In this regards the surface discharge is studied in more detail, leading to the first results of PD with very low acoustic (no acoustic) activity. Regarding these results two different categories in term of AE signals of PDs are defined, silent PD and non-silent PD. Silent PDs are those PD activities without or with very low acoustic signal and non-silent PDs are with acoustic signal.

The existence of the silent PD is validated via oscilloscope and digital signal processing (DSP) devices. Also, with different innovative methods and arrangements such as needle plane and ball electrodes with and without oil gap, the probable reasons of creation this phenomenon (silent PD) is investigated.

It is found that the carbonization patterns start with non-silent PD and remain the same during silent PD activities even with very high electric apparent charges. It means the development in carbonization traces produce electric and AE signals and in contrast no changes in carbonization traces produce only electric signals with no AE signal. These results verify the advantages of using acoustic technics and electric measurement in terms of PD classification and localization.

Keywords: Partial Discharge, Silent Partial Discharge, non-Silent Partial Discharge, Acoustic, PD, AE, Acoustic Emission

Abstrakt

Ausfälle von Komponenten in elektrischen Energiesystemen wie Transformatoren können zu einem enormen wirtschaftlichen Verlust im Energiesystem führen. Einer der Hauptbestandteile der Komponenten in elektrischen Energiesystemen ist das Isoliersystem, nämlich Öl, imprägniert Pressboard und Papier. Es gibt mehrere Methoden zur Diagnose dieser Isoliermaterialien. Die Messung der Teilentladung (TE) ist als eines der wichtigsten zerstörungsfreien Überwachungssysteme für Isoliermaterialien bekannt. Jedoch wird dies in Wartungsperioden hauptsächlich offline durchgeführt, und die existierenden Online-Verfahren liefern im Allgemeinen weniger Informationen aufgrund von elektromagnetischen Störungen. Im Gegensatz zum elektrischen TE-Messsystem ist das Schallemissionsmesssystem für seine Immunität gegen elektrische Umgebungsgeräusche bekannt.

In dieser Arbeit wird die vergleichende Auswertung von akustischen und elektrischen Signalen von TE-Ereignissen untersucht, die in ölprägnierten Pressboard und Papieren erzeugt werden. Sie konzentriert sich auf die Charakteristik der TE-Aktivität und deren Einfluss auf akustische Signale. Die TE-Klassifizierung wird definiert, indem die Beziehung zwischen akustischen und elektrischen Signalen von TE-Ereignissen verwendet wird. Obwohl die Empfindlichkeit der akustischen Sensoren im Laufe der Jahre verbessert wurde, bleibt die Erkennung der akustischen Signale von TE-Aktivität das Hauptproblem bei Komponenten in elektrischen Energiesystemen, hauptsächlich Transformatoren. Fehlende Informationen zur Auswertung von elektrischen TE-Signalen und akustischen Signalen sind neben der mechanischen Dämpfung zwei Hauptnachteile der akustischen Messung.

Wegen der mechanischen und elektrischen Mechanismen von Wellen, die während der TE-Aktivitäten erzeugt werden, wird deren Verhalten ausführlicher diskutiert, um ein besseres Verständnis über die elektrischen und akustischen Signale zu erhalten. An verschiedenen Elektrodenkonfigurationen innerhalb einer Probe im Öltank werden TE-Quellen an verschiedenen Elektrodenkonfigurationen wie Spitze-Platte und Elektrodenkugelanordnung innerhalb einer Probe im Tank erzeugt, um verschiedene Arten von TE zu untersuchen. Neben dem mechanischen Verhalten der akustischen Wellen werden auch elektrische Eigenschaften von TE und verschiedene TE-Messtechniken wie elektrisch, UHF und akustisch behandelt.

Die Ergebnisse bezüglich des Verhältnisses zwischen AE- und elektrischen TE-Signalen für Korona im Öl zeigen das korrelierte Verhalten zwischen AE- und TE-Signalen. Bei Oberflächenentladungen sind diese Verhaltensweisen jedoch unkorreliert. Die Oberflächenentladung wird genauer untersucht, was zu den ersten Ergebnissen von TE mit sehr geringer akustischer (keine akustischen Signale) Aktivität führt. In Bezug auf diese Ergebnisse werden zwei verschiedene Kategorien in Bezug auf elektrische und AE-Signale von TE definiert, stille TE und nicht-stille TE. Stille TE sind elektrische TE-Signale ohne oder mit sehr geringer akustischer Aktivität, und nicht-stille TE sind elektrische TE-Signale mit akustischer Aktivität.

Die Existenz der stillen PD wird über Oszilloskope und digitale Signalverarbeitungsgeräte (DSP) validiert. Auch mit verschiedenen innovativen Methoden und Anordnungen wie Nadel und Kugelelektroden mit und ohne Ölspalt werden die wahrscheinlichen Entstehungsursachen dieses Phänomens (Silent TE) untersucht.

Es wurde festgestellt, dass die Karbonisierungsmuster mit nicht-stiller TE beginnen und während stiller TE-Aktivitäten selbst bei sehr hohen scheinbaren elektrischen Ladungen unverändert bleiben. Dies bedeutet, dass bei der Entwicklung der Karbonisierungsspuren elektrische und AE-Signale erzeugt werden und im Gegensatz dazu ohne Änderungen der Karbonisierungsspuren nur elektrische Signale (ohne AE-Signale) erzeugt werden. Diese Differenzierung ist nur möglich bei gleichzeitigem Einsatz der akustischen Technik und elektrischen Messung im Hinblick auf die TE-Klassifizierung und Lokalisierung.

Schlagwörter: Teilentladung, TE

Table of Contents

Abbreviations and symbols	1
Introduction and Motivation	3
1 Fundamental Study	8
1.1 Partial discharge (PD).....	9
1.1.1 Internal partial discharge.....	13
1.1.2 Surface discharge.....	14
1.1.3 Corona	15
1.1.4 Dielectric barrier discharge.....	15
1.1.5 Space charge	15
1.2 PD measurement and detection.....	15
1.2.1 Electric PD Measurement.....	16
1.2.2 UHF.....	16
1.2.3 Acoustic measurement.....	17
1.2.4 DGA	17
1.3 Localization via different methods	18
1.3.1 PD pattern	19
1.3.2 Acoustic method with an electric PD trigger.....	20
1.3.3 All-acoustic method.....	21
1.4 Acoustic emission (AE)	22
1.4.1 Acoustic Impedance.....	22
1.4.2 Reflected and Transmitted waves	23
1.4.3 Longitudinal and Transverse waves	24
1.4.4 Attenuation	26
1.4.5 Blast wave	27
1.4.6 Velocity of acoustic waves	29
2 Measurement Setup	30
2.1 Photography	30
2.2 Sample preparation	31
2.3 PD acoustic measuring system.....	35
2.3.1 Oscilloscope decoupling method.....	37
2.3.2 DSP Measuring device.....	37
2.4 Electric PD measuring system	39
2.4.1 Measuring via coupling capacitor	39
2.4.2 UHF measurement.....	41
2.5 Setup for corona in oil.....	41
2.6 Setup for surface discharge	42
2.7 Setup for acoustic and electric PD	43
3 Basic Examinations	45
3.1 Corona in oil	45
3.1 AE measurement.....	45
3.1.1 The effect of overlapping on accuracy.....	45
3.1.2 The effect of wavelength on accuracy	47
3.1.3 Results	49
3.1.4 Discussion	50
3.2 Surface discharge.....	51
3.2.1 Results	51
3.2.2 Discussion	53
3.3 Effect of carbonized patterns on AE signals	55

3.3.1	Voltage courses	55
3.3.2	Carbonized patterns.....	56
3.3.3	Acoustic emission signals	58
3.4	Summary.....	60
4	Silent and Non-silent Partial Discharges	61
4.1	Acoustic destructive effect	66
4.1.1	Example 1: Delay between two PD activities	67
4.1.2	Example 2: Distance between AE sensor and PD source	69
4.2	Material Attenuation.....	71
4.3	Electric and UHF characteristic.....	78
4.4	The effect of pressboard material on creation of silent PD.....	87
4.4.1	Effect of different voltage courses on AE signals	89
4.4.2	Effect of water content on creation of AE signals	93
4.4.3	Gas Generation	95
4.5	Degradation of Silent and non-Silent PD	98
4.5.1	Scenario 1	100
4.5.2	Scenario 2	102
4.5.3	Scenario 3	104
4.5.4	Scenario 4	106
4.5.5	Energy of silent PD	107
4.6	Summery.....	107
	Conclusion	109
	References	111

Abbreviations and symbols

AC	Alternating current
AE	Acoustic emission
CD	Coupling device
CT	Current transformer
CC	Connecting cable
DBD	Dielectric barrier discharge
DC	Direct current
DSP	Digital signal processing
DGA	Dissolved gas analysis
EA	AE number to PD number ratio
EM	Electromagnetic
EMI	Electromagnetic interferences
FEM	Finite element method
HDT	Hit definition time
HLT	Hit lockout time
HV	High voltage
MI	Measuring instrument
PD	Partial discharge
PDT	Peak definition time
PDIV	Partial discharge inception voltage
PRPD	Phase resolved partial discharge
PSA	Pulse sequential analysis
UHF	Ultra high frequency
s	Second
A	Displacement amplitude / dimension area
C_a	Capacitor or capacitance of entire dielectric
C_b	Capacitor or capacitance of bordering of cavity
C_c	Capacitor or capacitance of cavity
C_k	Coupling capacitor
C_t	Total capacitor of the test sample
D	Dielectric flux density
D	Distance from the partial discharge source to sensor
E	Electric field
I	Electric current
I_r	Energy intensity of reflected acoustic signal

I_i	Energy intensity of incident acoustic signal
J	Current density vector
P	Dielectric polarisation / acoustic pressure wave
Q	Charge
R_c	Resistor for simulating the time delay of discharge in cavity
X	Susceptibility
Z	Electric / acoustic impedance
Z_0	Acoustic characteristic impedance
t	Time
T	Time period
V	Applied voltage
V_a	Voltage of the sample with cavity
V_c	Voltage of cavity
λ	Wavelength or free path length
k	Wave number
v	Acoustic velocity
h	Volumetric modulus of elasticity / Plank constant
y_m	Maximum displacement amplitude
z	Specific acoustic impedance
σ	Electric conductivity
σ_0	Electric dc conductivity
ω	Angular frequency
u	Particle velocity
p	Acoustic pressure
$p_{r,max}$	Peak reflected pressure
f	Electric frequency
q_c	Charge of the cavity
q_{ap}	Apparent charge
q_m	Measured charge
X	Linear susceptibility
t_d	Negative phase duration
ρ	Medium density
ϵ_0	Permittivity of free space
ϵ_r	Relative permittivity of dielectric

Introduction and Motivation

The insulation system of high voltage equipment, especially power transformers, is subjected to combined electric, mechanic, thermal and environmental stresses during operation which may alter the dielectric properties [1]-[5]. The condition of the electrical insulation system of high voltage equipment will strongly influence the economic and technical lifetime as well as the reliability of the supply of the generated or distributed electric power [6]-[8].

Recent studies show the failure rate of 1 % per year during the period of 1996 to 2010 by considering the total production of 167,459 transformer per year above 69 kV [8]. However, the failure rate of the medium voltage transformers below 69 kV seems to be higher based on a study showing the mean life of the power transformers in 2007 the Australian distribution utility publication [10]. The variable output due to variable parameters of the renewal distributed energy identified as one of the main stresses on medium voltage transformers [11]-[15].

Since the electric stress imposed on insulating materials of the transformers has been increased significantly over the past few years due to optimizing the size of transformers specially in renewable energy segments and less material cost, there is a greater need for monitoring the actual state of insulation ageing or deterioration. Various diagnostic methods are applied for investigating the conditions of the insulating materials[16]-[20]. Partial discharges (PD) are known as one of the early sources of insulation failures and main source of ageing in high voltage apparatus also PD measurements and analyses have been widely used as a non-destructive diagnostic tool to monitor and to examine the long term degradation of power transformers [21]-[23]. The very fast signals released from a PD activity could be measured electrically, or via ultra-high frequency UHF, or acoustic or even light emission sensors [24]-[33]. Also, PD has some chemical effects especially inside the oil which could be detected via gas detectors, which is known as Dissolved Gas Analysing or DGA [34]-[35].

Localization of PDs could improve the reliability of power systems and reduce the maintenance cost intensely. UHF and acoustic emission (AE) PD localization became more favourable due its immunity against electromagnetic (EM) interferences. These methods are mainly based on time difference information. UHF signals are in the range of some GHz compared to the AE signals in the range of some kHz. It means a higher sampling rate system is required for UHF method compare to the AE method; however some other localization methods based on a received signal strength indicator could be a solution for this problem [36], but limitation related to the placing of the UHF sensors inside the power transformers makes this method not as practical as acoustic method, since the AE sensors could be mounted outside the transformers [37]. In addition to the localization, over the years an immense effort has been put into the development of methods to investigate the degradation phenomena in HV components [38].

In a case study at Leibniz University of Hannover, it has been tried to localize the PDs inside a 2.5 MVA oil insulated transformer via acoustic method. Electrical measurements showed the existence of the partial discharge in this transformer. The electric pattern of the discharges showed that the discharges are either surface or internal discharges but not corona in oil. Furthermore, electric three phase localization proved the existence of the PD in one of the coils, but the exact location of the PD was not clear. After searching for acoustic signals over the whole body of the transformer via acoustic sensors, the only AE measurable location could be detected. Fig. 0.1

shows the placing of the AE sensors mounted between the air convection cooled heat exchangers via special AE sensor casing to reach to the transformer tank.



Fig. 0.1: Part of a transformer with special casing of the AE sensors to install in large dimension of cooling system

Fig. 0.2 shows the schematic top view of mounted AE sensors on the transformer tank. More information regarding localization calculation can be found in Chapter 1.

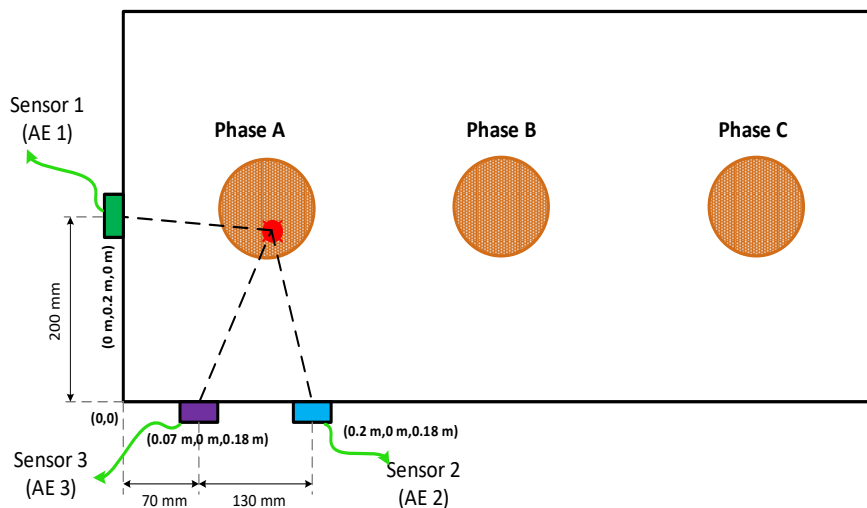


Fig. 0.2: Schematic view of mounted sensors on the transformer tank from top

The localization of PD has been done by using the electric trigger as reference point. Fig. 0.3 shows the time delay between electric trigger and the acoustic signals captured by different AE sensors. The time delay between electric trigger and first AE signal above the AE threshold could be used to calculate the distances between the AE sensors and PD source.

By considering the time delay between electric and acoustic signals and 1400 m/s speed of the AE velocity in oil and 700 μ s, 800 μ s and 1300 μ s delay time (Fig. 0.3)

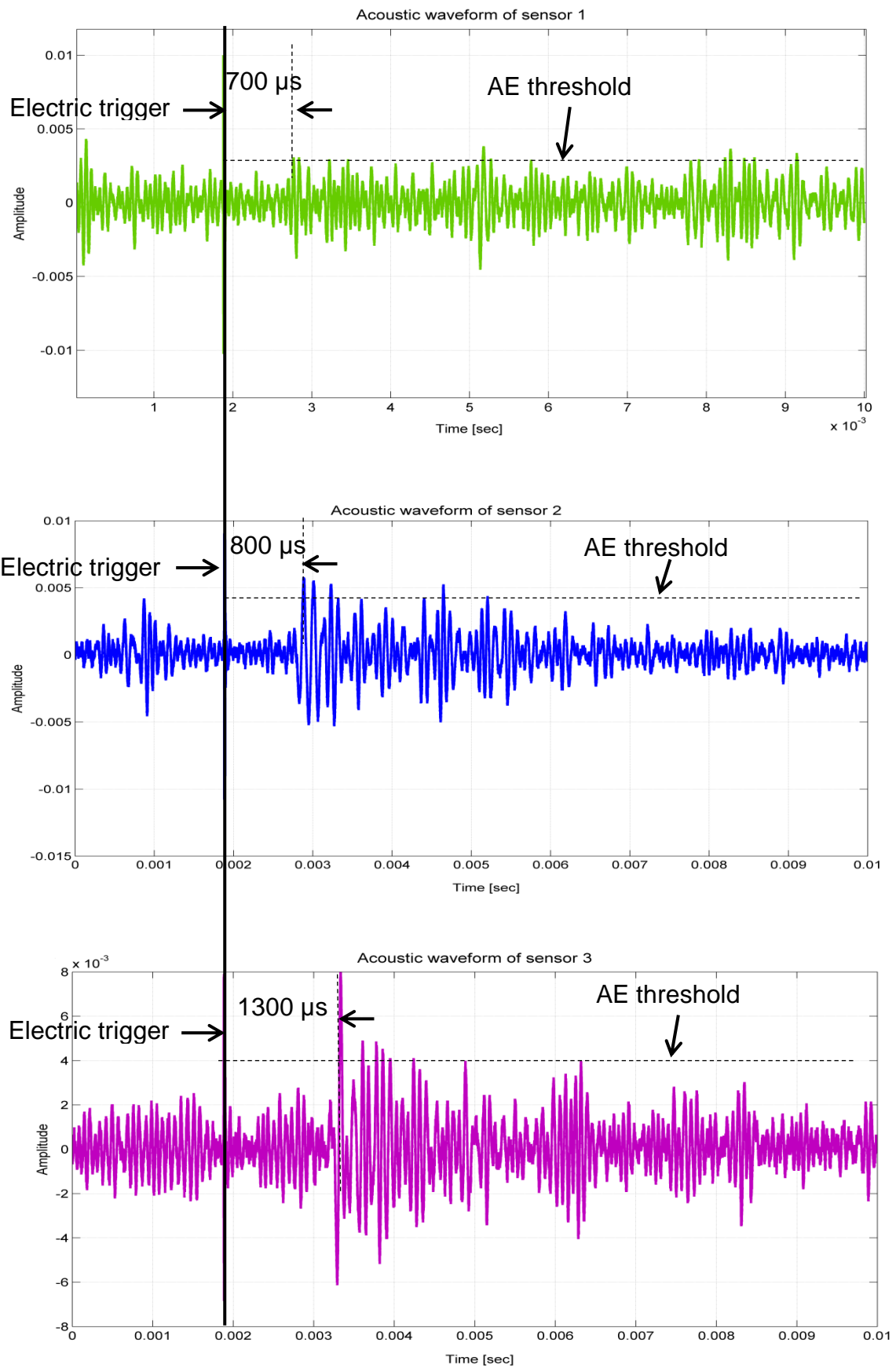


Fig. 0.3: Time delay between electric and AE signals captured by different AE sensors

the following equations could be arrived (for more information please refer to chapter 1.3.3):

$$(x)^2 + (y - 0.2)^2 + (z)^2 = (1400 \cdot 700 \cdot 10^{-6})^2 \quad (1)$$

$$(x - 0.07)^2 + (y)^2 + (z - 0.18)^2 = (1400 \cdot 800 \cdot 10^{-6})^2 \quad (2)$$

$$(x - 0.2)^2 + (y)^2 + (z - 0.18)^2 = (1400 \cdot 1300 \cdot 10^{-6})^2 \quad (3)$$

The coordinates calculated by these equations would be $x = 87$ mm, $y = 86$ mm, $z = 101$ mm. However, the exact location of the PD could be difficult because of some errors regarding the speed variation of AE waves propagation in oil at different temperatures and acoustic reflections. To find out the accuracy of localization, the electric and acoustic signals have been compared together. Large number of electric PDs could be detected by AE sensors at the mentioned place during the measuring time, since not all acoustic signals generated by PDs could be detected at this location. This unmeasurable AE signals could be because of high attenuation of AE signals or other electric PD sources outside the localization area. Also, the amplitude of the acoustic signals varies at the same amount (around 2 nC) of electric discharges during the measurement. This magnitude variation showed an uncorrelated behaviour between electric and acoustic signals of PD. This uncorrelated behaviour of AE and PD signals has been observed also by other investigations as well. Fig. 0.4 shows acoustic activities during surface discharges [60].

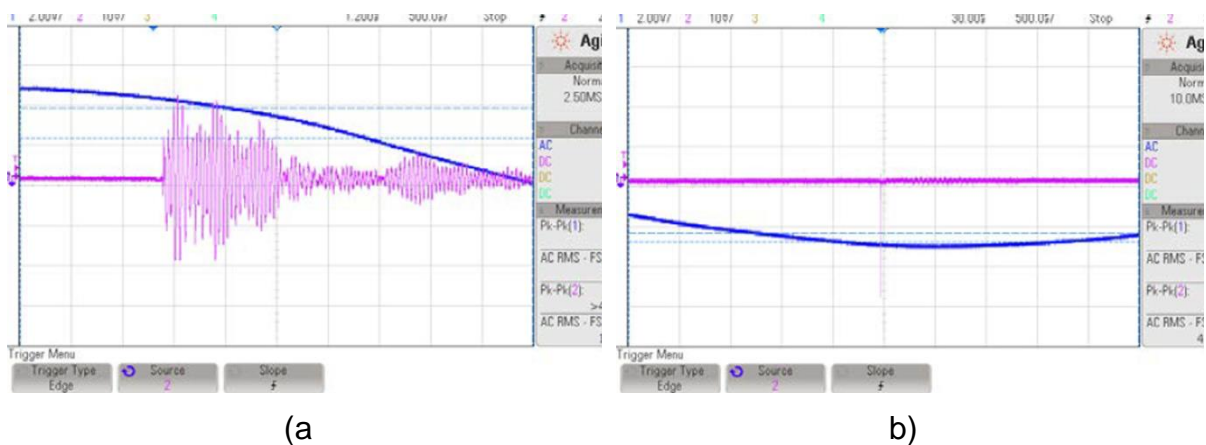


Fig. 0.4: AC input voltage in yellow colour and AE signal in green colour captured during surface discharge [60]

- a) AE signal visible
- b) AE signal is not visible

Fig. 0.5 shows the schematic view of the sensor locations and also the possible location of the PD source (red ball).

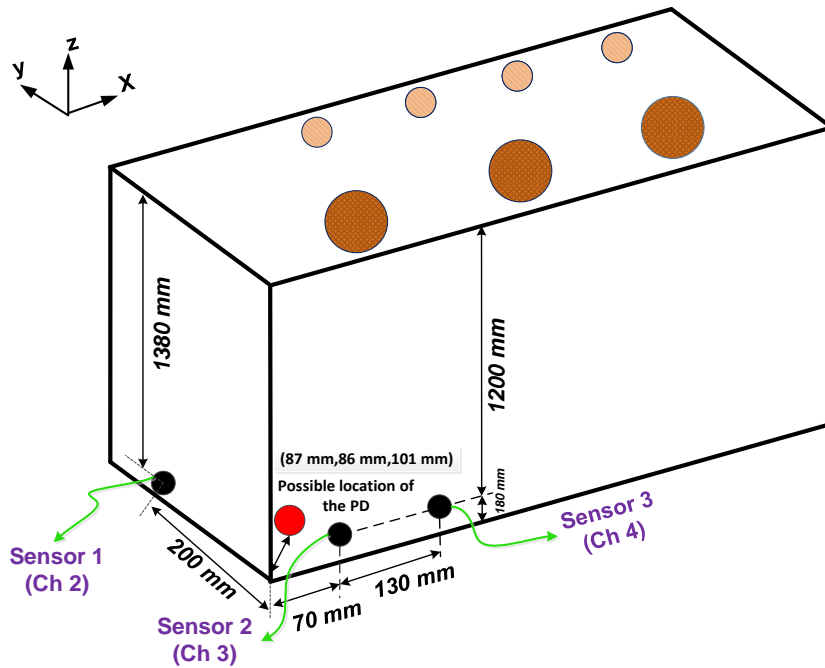


Fig. 0.5: Schematic view of the AE sensors and possible location of PD

In recent years many studies have been done on localization of PDs inside transformers via UHF method [39] and acoustic method [40]. However there are not much studies in correlation between electric PD and AE signals. Lack of these information impose some uncertainties in localization of PD via acoustic methods.

The aim of this work is to experimentally investigate the comparative evaluation of acoustic and electric signals of PD in more detail. The main objectives are:

1. Studying the correlated and uncorrelated behaviour of the AE and electric PD signals
2. Classification of PD in terms of AE behaviour
3. Investigating the effect of different PD types in terms of AE signals at different levels of deterioration of insulation materials
4. Validation of the results by using different measuring devices

1 Fundamental Study

Transformers are one of the main electrical components in power distributions. Transformer replacement could cost even more than transformers due to the delay of replacement and preparation cost especially in offshore wind turbines. By increasing the demand of offshore wind platforms, the reliability of even smaller distribution transformers becomes more important than before. By considering the lifetime expectation of wind turbine more than 20 years [88], the lifetime of the power transformers is expected to be more than 25 years and more by considering 5 years margin. It makes the transformer one the complex structure in terms of fault analyses. Fig. 1.1 shows the classification of fault in power transformers [89].

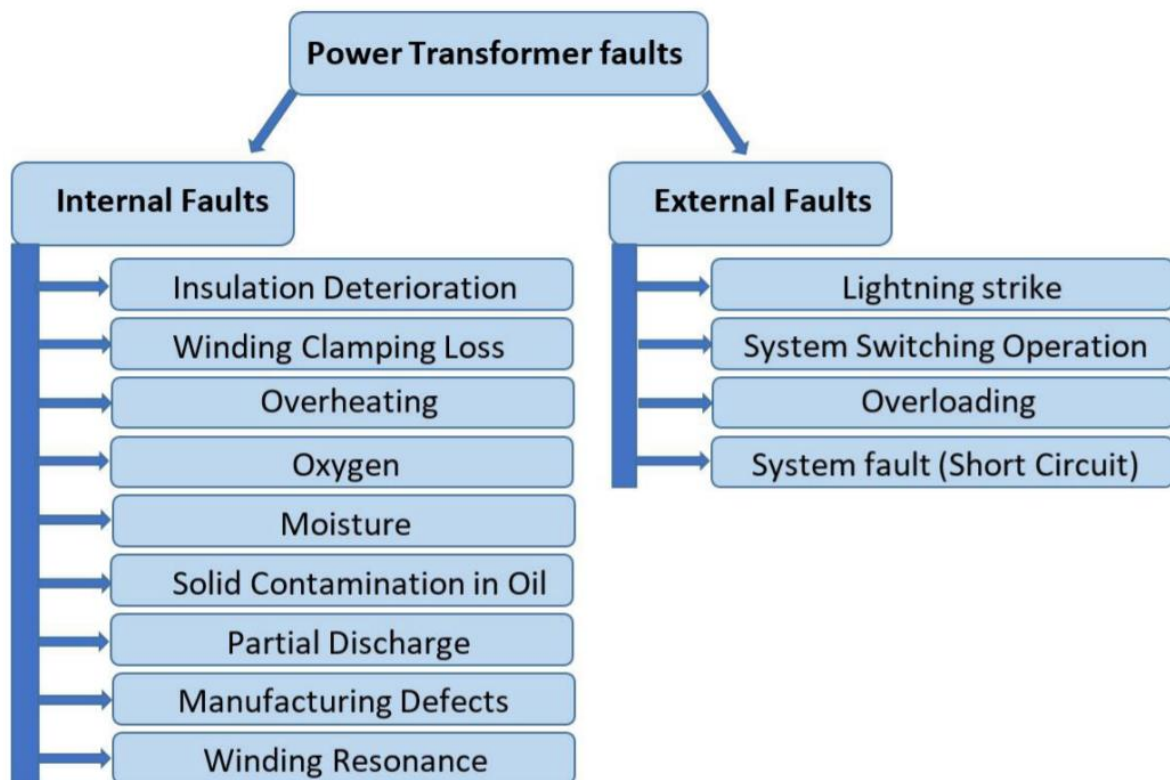


Fig. 1.1: Classification of faults in power transformers [89]

Statistics show that 70 % - 80 % of transformer faults are internal faults [90]. Internal faults happen at different location which include the high voltage windings [91], insulation fluid (oil), tank [92], core [93], terminals [94] and cooling systems [95]. External faults occur due to different reasons including the external short-circuit of power system, over-flux and overload. Fig. 1.2 shows failure statistic of transformers at substations > 100 kV.

The factory acceptance tests could check all parameters of transformer and detect any deviations in design or production of the transformers. These tests are categorized in three major categories i. e. type test, routine tests and special tests. Partial discharge (PD) measurement considered as one of the main non-destructive test technics. Non-destructive tests are occurring when transformers are exposed to lower field stresses compared to destructive tests (like impulse test), thereby avoiding any destructive or non-linear effects. Power transformer condition monitoring after production could be essential to increase the reliability of a transformer. Among different condition

monitoring tests, PD monitoring again can effectively diagnose the transformer's condition with the possibility of advancement in the future [97].

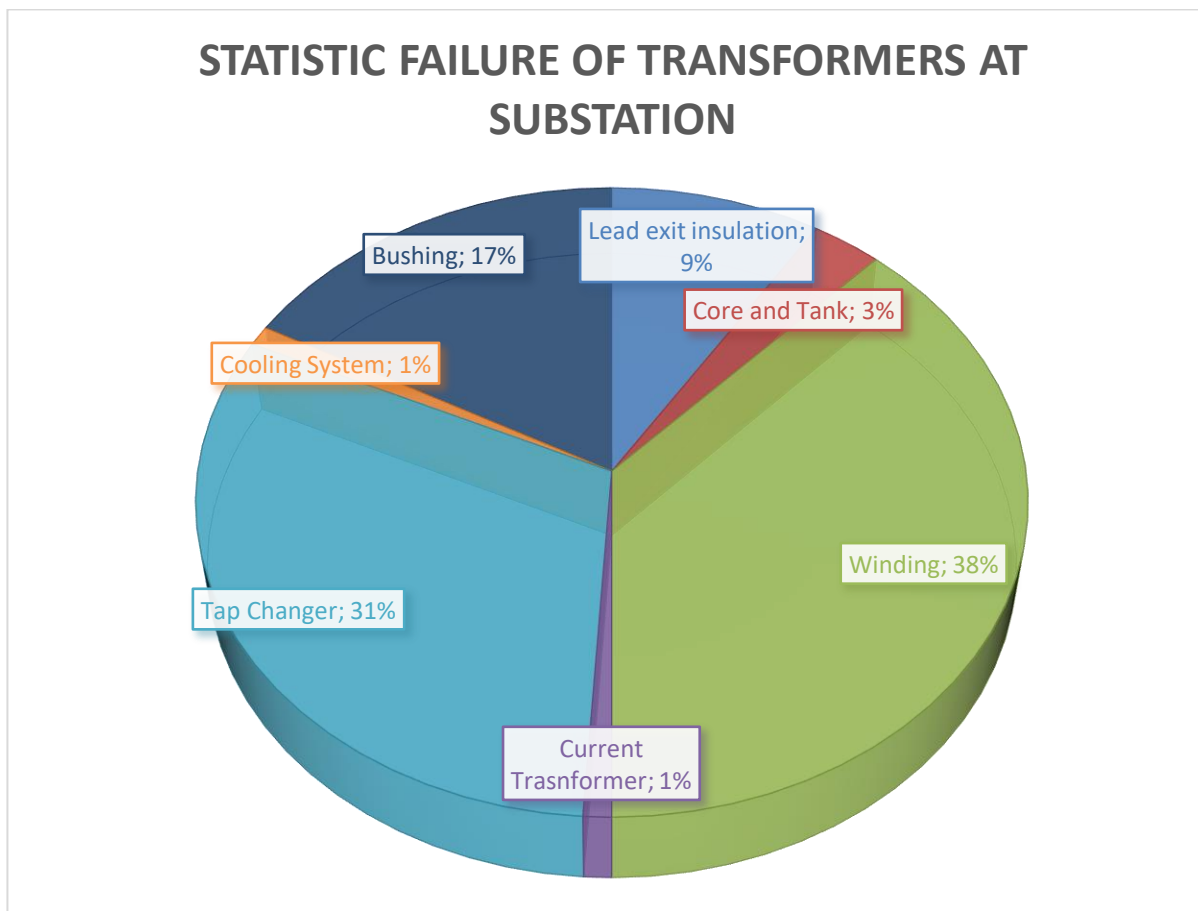


Fig. 1.2: Failure statistic of transformers at substation > 100 kV [96]

1.1 Partial discharge (PD)

When dielectric materials are exposed to an electric field, the atoms or molecules of the dielectric arrange themselves in the electric field. This displacement is known as dielectric polarization P . Generally, gases are not considered as material, because of the large distance between atoms or molecules per unit volume. Under the influence of electric field E , the dipoles will only partly be oriented. In general dielectric polarization depends slightly on strength of the electric field, so that in a normal electric field a linear dependency of P with E can still be assumed. Dipolar polarization is a quite fast effect and can follow AC frequencies up to MHz or GHz. Interfacial polarization is effective in insulating materials composed from different dielectric materials such as oil-impregnated paper. The mismatch of the products of permittivity and conductivity for the different dielectrics forces moveable charges to become attached on interfaces. Normally this phenomenon is very slow and follows the power frequency. During all these processes, the electric field is not strong enough to force the charges to move fast inside material and create electric discharges and causes deterioration in materials [98].

Any material, which is isotropic and homogenous in microscopic or even at macroscopic level, the following relation exists between polarization P and electric field E :

$$P = P_0 + \epsilon_0 X E + \epsilon_0 X^{(2)} E^2 + \dots \quad (4)$$

Where $\epsilon_0 = 8.85 \cdot 10^{-12} \text{ Fm}^{-1}$ is the permittivity of vacuum and the first X is the linear susceptibility of the matter. While the nonlinear susceptibilities ($X^{(n)}$) can be generalized to anisotropic materials in which the susceptibility is not uniform in every direction. The linear susceptibility is a dimensionless number and with a value of zero for vacuum. In vacuum insulation material dielectric flux density " D " is proportional to the applied electric field E as follow:

$$D = \epsilon_0 E \quad (5)$$

E and D are dependent on the applied voltage. If the voltage is time-dependent, both D and E are of identical time dependency with no time delay between their magnitudes. If the vacuum is replaced by a dielectric material, the displacement increases by macroscopic polarization P as below:

$$D(t) = \epsilon_0 E(t) + P(t) \quad (6)$$

The time dependency of P , however, will not be the same as that of E , as the different polarization processes will have different delays with respect to the appearance of E caused by the time-dependent behaviour of the susceptibility. The time dependency of P can be divided in two different categories. First part is electronic and ionic polarization of vacuum, which could be considered as the prompt response. Second part is the rest polarization, which is slower compared to the first part and could be evaluated separately. More information regarding polarization behaviour could be found in [98].

Polarization $P(t)$ produce a main part of displacement current inside the materials. Regarding to the Maxwell equation, an electric field $E(t)$ applied to a dielectric material generates a current density as follow:

$$j(t) = \sigma_0 E(t) + \frac{dD(t)}{dt} \quad (7)$$

where σ_0 is the DC conductivity of the material and $j(t)$ is the current flow inside the insulation materials [36]. This shows the current flow inside the insulation materials depending on applied voltage, which is responsible for the electric field.

In case the local electric field in a small region of the insulating material gets higher than the electric strength of the dielectric material in this region, a local breakdown as known as PD occurs.

This partial breakdown generates a small avalanche of charge carriers that may or may not lead to a local degradation of the material. It is still the aim of many investigations to relate partial discharge to the lifetime of specified materials. Such a quantitatively defined relationship is, however, difficult to ensure. Independent to the actual situation, degradation or not, the partial discharge modifies the local field distribution, this could lead to tiny voltage drop depending on impedance and capacitance of the voltage source. PD occurs normally due to high electric stress related to design or manufacturing problem or aging of the high voltage insulation systems. Depending on the discharge event, it could cause a deterioration of the material by the energy impact of high energy electrons or accelerated ions, causing chemical transformations of many types like carbonization.

Generally, such discharges appear as pulses of duration of much less than 1 μs . More continuous (without pulses) forms may, however, occur, as for example the so-called pulse-less discharges in gaseous dielectrics. The detection and measurement of partial discharges is based on the exchange of energy taking place during the discharge. These exchanges are manifested as: electric pulse currents, dielectric losses, electromagnetic radiation (light), sound (noise), increased gas pressure, and chemical reactions [98]. Electrical PD measurement technique was already applied over the past decades, but it is still a topic of research and increasing application. Since PD cannot be measured directly, its energy by-products such as electric transients, chemical changes, electromagnetic emissions, vibration, sound, light, and heat can be measured. Regarding to the high frequency of the PD event compared to the input AC voltage, different electrical methods could be used to decouple and detect this phenomenon. PD measuring could be done by using coupling capacitor, through high frequency current transformer and Rogowski coils or UHF and very high frequency (VHF) antenna. Acoustical detection methods utilizing ultrasonic transducers can successfully be used to detect and localize the discharges. Other measuring methods such as dissolve gas analysis (DGA), ultraviolet light measurement, power factor tip-up measurement also could be used [8], [42], [123].

Fig. 1.3 shows simple a-b-c model of a cavity inside the insulation material (C_c) with an equivalent circuit. This cavity could be related to a manufacturing failure due to not complete impregnation process. This cavity could become the origin of PD.

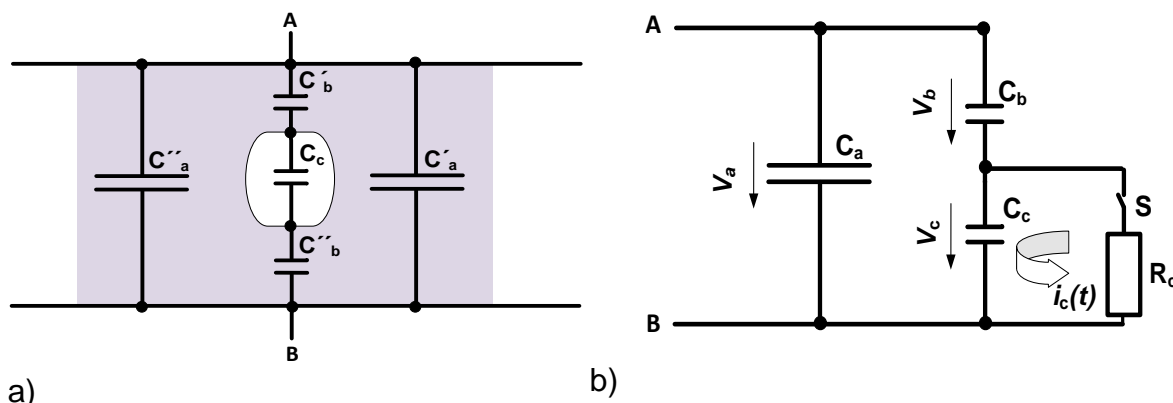


Fig. 1.3: PD schematic view

- a) Model of a cavity inside the insulation material
- b) PD equivalent circuit

By considering the a-b-c model the C_b and C_c could be calculated by following relation. Where C_c represents the capacitance of the cavity, C_b and C_a are the capacitance of

the rest of the dielectric material. Capacitance size of the cavity (C_c) depends on the size of the cavity. Smaller cavity size in thickness compared to the C_b , could lead to a larger C_c compared to the C_b , despite the lower relative permittivity of C_c .

$$C_a = C'_a + C''_a ; C_b = \frac{C'_b C''_b}{C'_b + C''_b} \quad (8)$$

$$C_a \gg C_c \gg C_b \text{ or } C_a \gg C_b \gg C_c \quad (9)$$

Fig. 1.3b shows a schematic view of PD activity. Switch S is controlled by the voltage V_c across the void capacitance C_c , and S is closed only for a short time, during which the flow of a current $i_c(t)$ takes place. The resistor R_c simulates the delay time of the discharge development.

By considering the ΔV_c as the voltage change after discharge and $\Delta q_c = C_c \Delta V_c$, the voltage across the cavity can be calculated by calculating the voltage division:

$$\Delta V_a = \frac{C_b}{C_a + C_b} \Delta V_c \quad (10)$$

This voltage drop calculation contains no information about the charge Δq_c . On the other hand, the voltage drop ΔV_a is directly proportional to $C_c \Delta V_c$, which causes the value to be related to the cavity geometry. ΔV_a is a quantity which could be measured. It has a very small magnitude; however, ΔV_c has higher magnitude (around kV) [98]. Due to these facts, the detection of ΔV_a is very challenging and therefore the detection circuits are based upon another quantity. C_t is the total capacity of the test sample which consists of C_a , C_b and C_c . C_k is coupling capacitor which should be placed near to the test sample C_t . It should be of low inductance design and should exhibit a sufficiently low level of partial discharges at the specified test voltage. During the short circuit inside the cavity C_c , coupling capacitor C_k acts as a stable voltage source. Fig. 1.4 shows the circuit during short circuit of C_t . Where, impedance "Z" is the total impedance of the connection between the source and test sample. It releases a charging current (PD current pulse) between C_k and C_t and tries to cancel the voltage drop ΔV_a across C_t . If $C_k \gg C_t$ then the charge transfer could completely compensate the ΔV_a during the discharge and the charge could be calculated as follow:

$$C_t = C_b + C_a , \quad q_{ap} = \int i(t) \approx \Delta V_a (C_a + C_b) = \Delta V_a C_t \quad (11)$$

where q_{ap} is the apparent charge. With equation (10) this charge becomes

$$q_{ap} = C_b \Delta V_c \quad (12)$$

this charge is so called "apparent charge", which is the most fundamental quantity of all PD measurements. It calls apparent charge because this charge is not equal to the

exact amount of charge locally discharged during the discharge activity in the capacitance of C_c of the cavity.

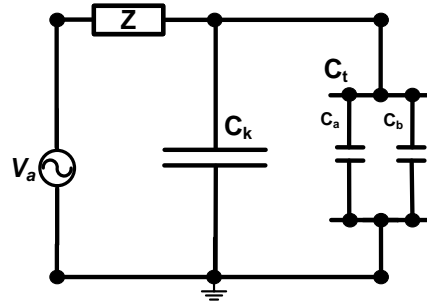


Fig. 1.4: PD measurement system after PD event

Finding a correlation between q_{ap} value and PD is more realistic than ΔV_a and PD because it would be less related to the capacitance C_a of the test object. Capacitance C_t of the test object could be as large as coupling capacitor C_k . Following equation shows the relation between measured quantity q_m over apparent charge q_{ap} , when C_k is not large enough.

$$\frac{q_m}{q_{ap}} = \frac{C_k}{C_k + C_t} \quad (13)$$

To reduce the difference between q_m and q_{ap} , the coupling capacitance (C_k) should be larger than testing object capacitance (C_t). However, the value of coupling capacitor is limited to price, weight, dimension, and imaginary power capability of the main input source power.

The calibration of a partial discharge measuring system is carried out to determine its scale factor at different test object capacitance (C_t). This operation is performed by injecting a calibrated known electric charge to the system (near to test object) and indicating the value of apparent charge by the measuring device (please refer to chapter 2.4.1 for more information). The test object may consist of solid, liquid or gaseous insulation materials, or any combination of these [98].

1.1.1 Internal partial discharge

PD inside the insulating liquids and solid dielectrics due to imperfection are classified as internal discharges (Fig. 1.5a). Normally self-sustaining electron avalanches are only created in gaseous inclusions. Thus, discharges in solid insulations may be ignited in gas-filled cavities, such as voids and cracks and even in defects of the molecular structure. In liquid insulation partial discharges may appear in gas-bubbles due to lower permittivity and lower breakdown voltage in gases. In fact, creation of insulation materials free from any kind of defects would be almost impossible. Due to this fact an acceptance value as a limit for PD apparent charge based on experiences has been dedicated in standards [98], [100].

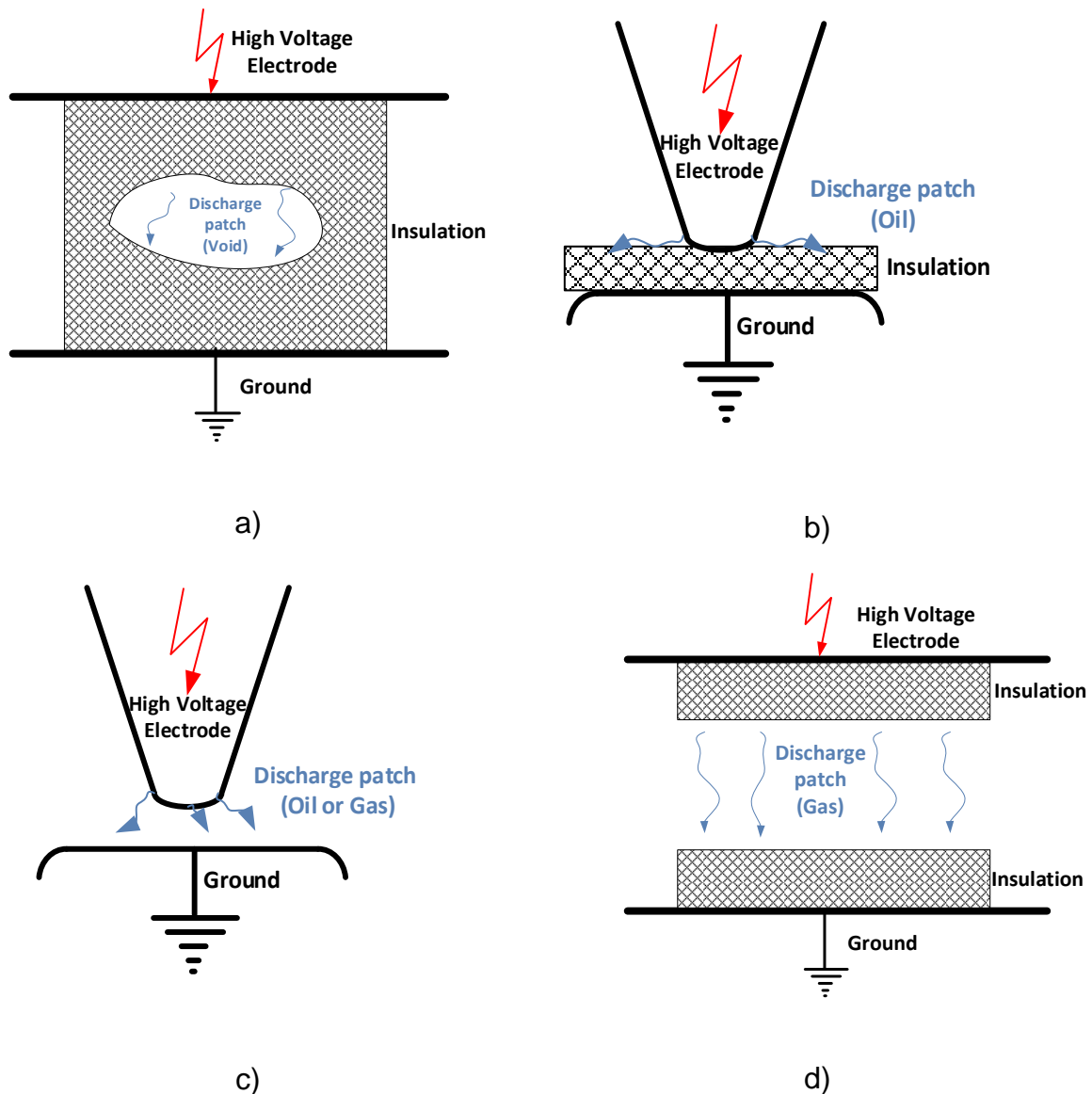


Fig. 1.5: Schematic view of the different discharges

- a) Internal PD
- b) Surface discharge
- c) Corona
- d) Dielectric barrier discharge (DBD)

1.1.2 Surface discharge

The inhomogeneity of material and strong non-uniform electric field at the interface can lead to surface discharge. In fact the weakest point in high voltage systems is generally associated with interactions involving boundaries and electric fields between two different dielectric materials (Fig. 1.5b) with different relative permittivity [104]. This phenomenon is known also as electric double layer, first proposed by Helmholtz [105].

Thermal and electronic action of surface discharges over solid insulation could result in mechanical and chemical damage of the material. Surface damage is known as tracking, whereas damage through the bulk of the (solid) material is termed treeing, which in both cases, results in a permanent conductive path that reduces the effective withstand voltage of the material [106].

1.1.3 Corona

Corona discharges occurring in gaseous dielectrics in the presence of inhomogeneous fields (Fig. 1.5c). Due to the self-replacement of the air, the corona discharges in air normally would have no effect on lifetime of the insulation materials [98]. Due to the self-replacement of the liquid insulation materials (like insulation oil), the discharges occurring in gas dissolve of oil in presence of inhomogeneous fields are also called as corona (corona in oil) [99].

1.1.4 Dielectric barrier discharge

Dielectric barrier discharges (DBD) are generated by the presence of one or more insulating layers in the current path between metal electrodes in addition to the discharge gap. Due to locally micro charge build up on the electrodes, the field at the location of a micro discharge would be reduced within a few ns after breakdown. In this way micro partial discharges are produced along the dielectric layers in discharge gap. Discharge gap should consist of one or different type of gases. Rising the external voltage causes additional micro discharges at new positions. DBDs have duration of 1-10 ns, total charges from some pC up to several nC and electron energy of 1 - 10 eV [101].

DBDs have been used in several variety of applications like coherent infrared radiation in CO₂ lasers, incoherent ultraviolet exciter lamps, surface treatment and in plasma display panels. Fig. 1.5d shows one of the most popular geometrical configurations of DBD. In 1857 Werner von Siemens came up with an idea of a special discharge that could be used to produce ozone from air or oxygen. Siemens refers to his product as “electrolysis of the gas phase”. Later, they named this discharge as “silent discharge” because of very low sound creation (almost no sound) of these discharges. Silent discharges also known as DBDs which could be operated at about atmospheric pressure [113].

1.1.5 Space charge

The charges could be trapped inside the insulation materials and create an additional electric field, known as space charge. Space charge accumulation affect the dielectric properties and breakdown strength of the material. The formation of space charge can distort the electric field distribution along insulation thickness. Such localised electric stress enhancement can lead to the premature failure of the insulation at stresses well below the anticipated or designed values in the extreme situation. Simulation results showed a highest risk of partial discharge inception when heterocharges are accumulated inside dielectrics [107]-[94].

1.2 PD measurement and detection

Apparent charge, partial discharge inception voltage as well as number and distribution of PD pulses are most important quantities. Identification with certain PD patterns in time and frequency domains as well as localization of PD are most important aspects by implementing AC input voltage. PD measuring technics can be divided in two main categories namely conventional charge-based measurement (conventional method) and signal-based measurement (unconventional methods).

1.2.1 Electric PD Measurement

Electric PD measurement also known as charge-based PD detection method is standardized method based on international standard IEC 60270 [102]. Fig. 1.6 shows a conventional PD measurement system with coupling device CD in series with the coupling capacitor. Where U_{\sim} is high-voltage supply, Z_{mi} represents input impedance of measuring system, CC is connecting cable, C_a is test object, C_k is coupling capacitor, CD is coupling device, MI is measuring instrument and Z is filter. The PD current generated in C_a would be compensated by C_k and measured via MI. Since the C_a depending on the testing component, the whole system should be calibrated by a PD calibrator before measurement. However, this method has the advantage of universal calibration possibility independent to the position of the PD and test object, but the independency to the location of PD makes this method impossible for localization PD.

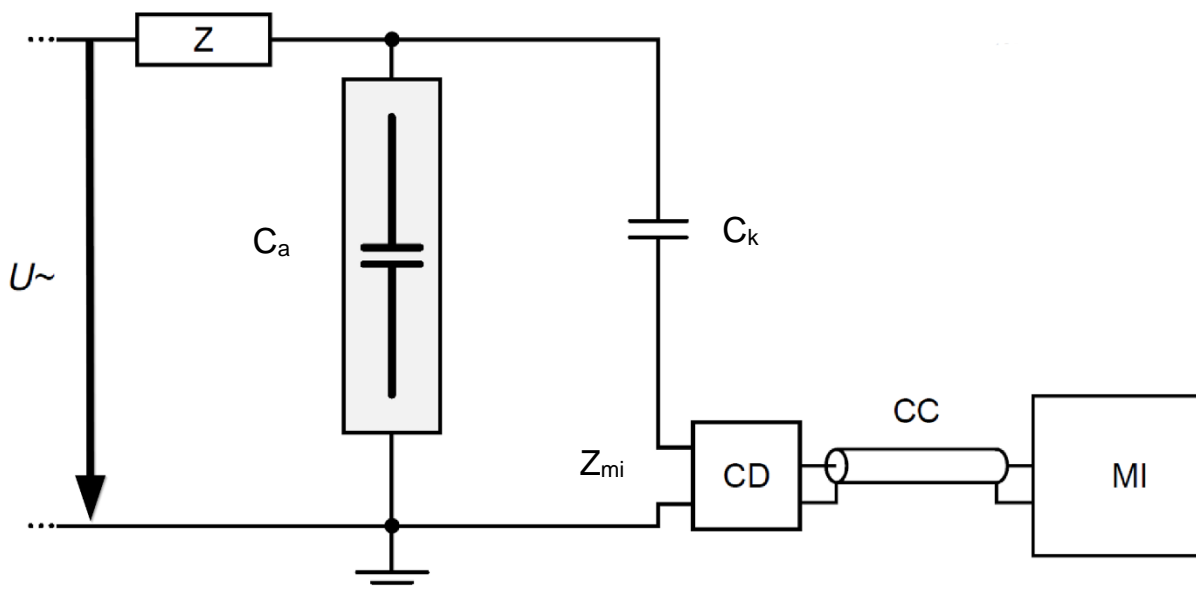


Fig. 1.6: Conventional PD measurement system with coupling device CD in series with the coupling capacitor [102]

The coupling device (CD) could be also installed in series with test object (C_a) and coupling capacitor (C_k) in parallel to the whole system. However, this configuration has two drawbacks, first the coupling device and measuring instrument could be damaged in case of major failure of the test object and second the test object grounding should be disconnected so that the coupling device can be installed in series to the test object.

1.2.2 UHF

UHF method (unconventional PD detection) is based on the measurement of electromagnetic radiated waves by PD [108].

The UHF method needs an antenna inside the tank of the transformer to detect the signals. The electromagnetic signals of PD radiate in the space of the transformer. The UHF sensors inside the transformer tank could be considered as shielded against external electromagnetic interferences, since the grounded transformer tank acts as Faraday cage. However low-noise UHF measurement have been established for online and onsite measurements, but localization of PD by using UHF method is difficult due to very high speed of electromagnetic wave propagations [109].

1.2.3 Acoustic measurement

In addition to the chemical and electromagnetic effects of the PD phenomenon, PDs can also generate acoustic signals, which are known as acoustic emission (AE) signals. In the subsequent chapters, the comparative evaluation of acoustic and electric signals of PDs would provide a more detailed explanation of the relationship between AE signals and electric PD signals.

1.2.4 DGA

Dissolved gas analysis (DGA) is known as one of the most practical condition monitoring tools for detecting damages inside the power transformers. In this method different gases (mainly H_2 , CH_4 , C_2H_6 , C_2H_4 , and C_2H_2) inside the transformer oil would be investigated. Several ways have been developed to increase the possibility of fault detection regarding to the concentrations and rates of these gases. Duval investigations showed that some of the failures with the same results (like T3 and T2) could be named as less dangerous or very dangerous depending on the failure location [41]. It emphasizes the importance of the fault localization inside the power transformers not only for the maintenance cost reduction, but also for better estimation of the insulation degradation. Fig. 1.7 shows the Duval triangle method to detect PD inside the power transformer by using DGA method [103]. The level of PD could be not detected by this method.

IEEE Std C57.104-2019
IEEE Guide for the Interpretation of Gases Generated in Mineral Oil-Immersed Transformers

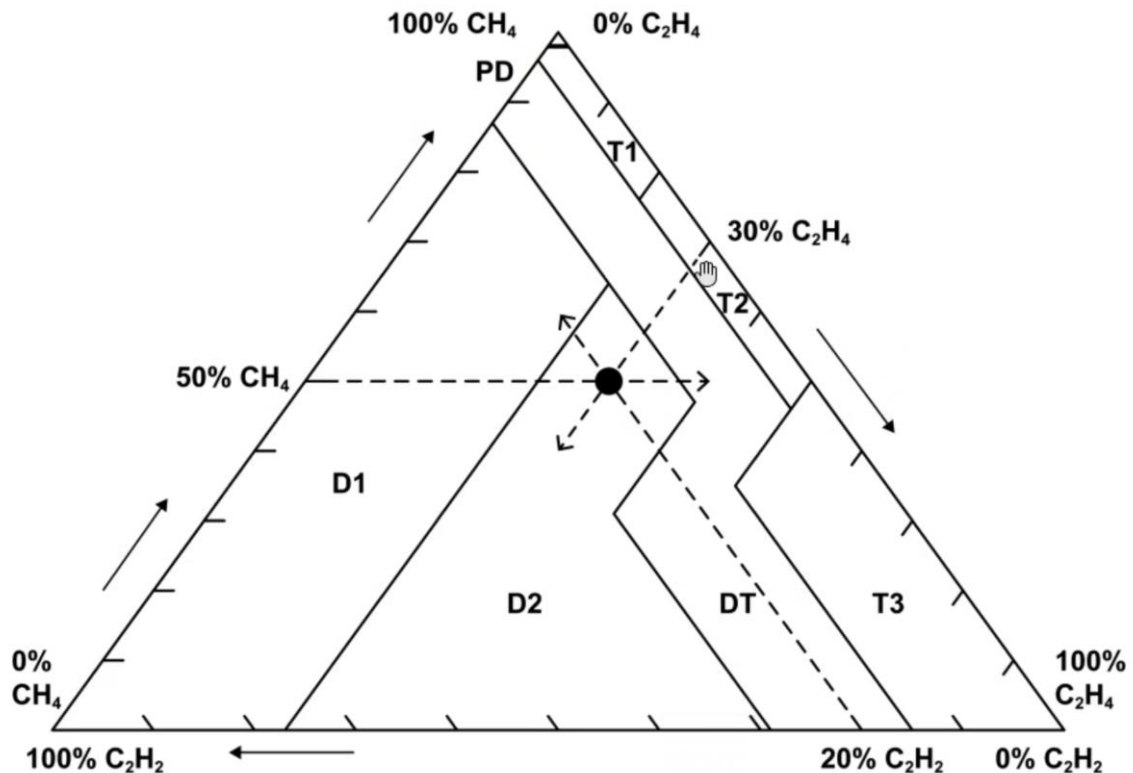


Fig. 1.7: Example of Duval Triangle method [103]

1.3 Localization via different methods

Electrical measuring method could be used also to localize the PD inside at power transformer. Phase resolved partial discharge (PRPD) pattern has been used for several years to locate the source of PD inside the power transformers. In this method the PD could be localized by using three phase measurements [126]. It is well-known that different types of PD sources can generate different discharge patterns. The discharge pattern is represented by a set of features, which can be extracted from PD measurement data. Two sets of features are commonly adopted in PD source classification. They are the phase resolved discharge pulse magnitude and repetition rate distribution, and the time resolved discharge pulse shape and magnitude. However, the localization based on this method is limited to differentiate between the PD inside the transformers and outside the transformers [129]. Beside all these advantages unfortunately still this method has some drawbacks and limitation in terms of online monitoring regarding its sensitivity to disturbances [130]. Another electrical method based on traveling wave theory could be used to localize the PD inside the power transformer based on transient behaviour of the coil [131]. This method needs very high frequency and precise PD measurement as well as electric transfer function of power transformer with high accuracy.

UHF and acoustic methods are known as the best localization unconventional PD measurement methods. In addition to that, they have following advantages: first immunity against external disturbing signals, second the sensors are electrically not connected to the testing object, third the localization of PD based on the arrival time

difference of the signals would be possible [130]. However, the UHF method is not sensitive to noise inside a transformer oil tank because of faraday shield. In UHF method, the UHF antenna normally should go through holes into the transformer tank. This makes the installation not as easy as AE sensors, which could be mounted outside the tanks. Also, very high speed of UHF signals (near speed of light) needs more precise measurement devices compared to AE measuring devices.

Small explosion of PD could produce AE waves around the PD source. Detecting PD by AE signals is known also as unconventional method. Depending on the location of source the AE waves would propagate along the oil tank. The immunity to the electromagnetic interferences (EMI) makes this method one of the most practical PD detection methods in terms of noise cancellation. The investigation on correlation between AE and PD signals are mostly limited to some practical investigation and the exact correlation between AE and electric PD is still not known [42]. Due to this fact this method is not used as a judgment for level of insulation deterioration in HV components. Digital signal processing (DSP) devices are normally used to capture the AE signals over a long period of time to increase the precision of localization by using this method. There are several methods of locating the discharge source using time delays between AE sensors. Reflections, refractions and attenuations have a very important role in precision of the localization [44], [45]. The all-acoustic method and acoustic method with an electric trigger method are two common localizing methods which could be used to localize the PD inside transformers. Each of them has their own advantages and disadvantages.

1.3.1 PD pattern

There are two techniques of measuring and analysing PD activities which are widely used; they are pulse sequential analysis (PSA) techniques and PRPD pattern. The PSA is based on the evaluation of data sets in which the individual sequence or partial discharge events are registered [46].

The PRPD technique makes use of the phase and charge magnitude of PD occurrences. The x-axis (phase axis) consists of one complete cycle of the applied voltage while the PD charge magnitude axis (y-axis) consists of the range of magnitude detected. PD data within certain number of the applied voltage cycle is plotted on the x-axis of one voltage cycle. Therefore, a PRPD pattern shows PD occurrences at a specific phase of the applied voltage with certain charge magnitude within certain number of the applied voltage cycles [47].

However, the PSA has the advantages of evaluating the time dependent phenomenon like memory effect and space charge [48], but the more advanced PRPD measuring devices nowadays could be able to stream the data in time domain. This ability could be used to evaluate the PRPD patterns at different time intervals.

Fig. 1.8 shows some samples of PRPD patterns of void and corona discharge with their arrangements. When the applied voltage is higher, the numbers of PDs per cycle, total charge per cycle and the maximum magnitude of corona discharges are higher. This can be seen in the publication that by a higher number of PDs in each applied voltage cycle at higher applied voltage [47].

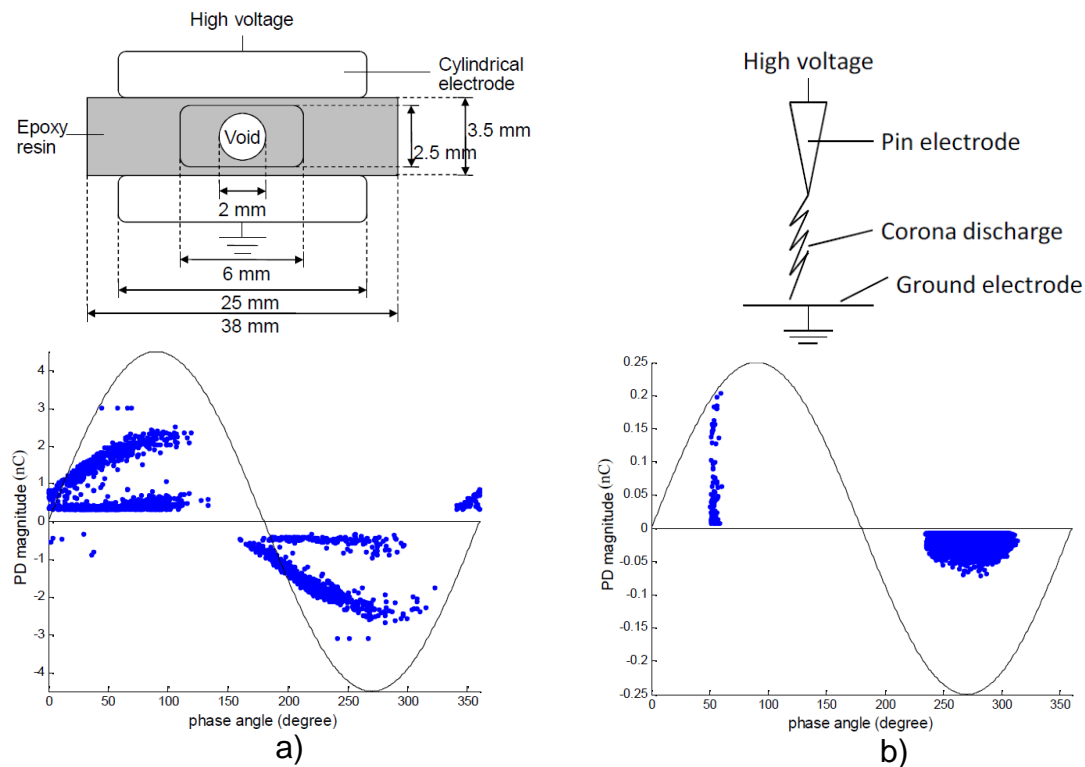


Fig. 1.8 Arrangement (top) and PRPD (bottom) of [47]

- a) void discharge
- b) corona discharge

1.3.2 Acoustic method with an electric PD trigger

Because of very fast velocity of the PD electromagnetic waves compared to the acoustical waves, an electric signal would be used as a trigger point at this method. Electric triggers could be also captured by coupling capacitors or using very high frequency or ultra-high frequency (UHF) antenna. Using electric trigger via coupling capacitor could determine the existence of the PD activity almost independent to the location of source. UHF sensors are normally inserted into the tank through the tank oil valve. This could also reduce the outside electromagnetic interferences by using transformer tank as a faraday cage.

In contrast to all acoustic method, at localization with electric trigger method, the tank dimensions for localization could be eliminated (because of very high velocity of electric trigger). The appropriate nonlinear observation equations are in the simplest case characterized by sphere functions which intersect at the PD origin. Mathematically this corresponds to an absolute time measurement, illustrated in Fig. 1.9. The approximation of a vanishing propagation delay of the electromagnetic PD signal (nanosecond range) is valid because the acoustic signals show typical delay times in the range of microsecond up to millisecond range.

The correlation between electric and acoustic signals could help us to increase the accuracy of the localization by corresponding the exact electric signal to its acoustic signal. Wrong interpretation of electric and acoustic signals would decrease the accuracy of the localization.

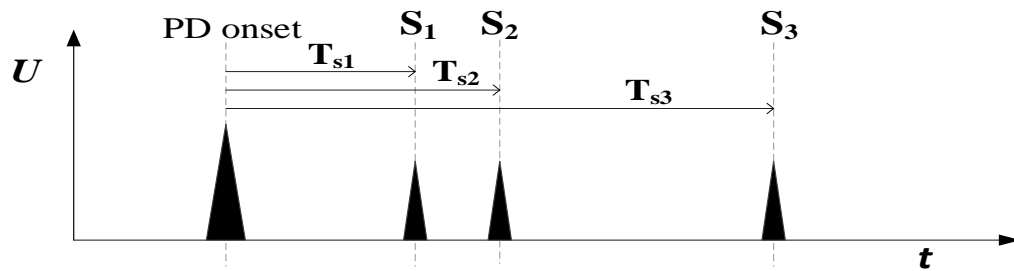


Fig. 1.9: Schematic visualization of acoustic arrival times in reference to the known PD onset (electric/electromagnetic PD signal) [42]

1.3.3 All-acoustic method

This method consists of several AE sensors, which could be mounted outside on the tank wall of a transformer. The location of the PD would be determined by AE sensors. All acoustic measurement (without any electric input) is one of the most isolated measuring methods in terms of electromagnetic interferences, but it increases the probability of not detecting AE signals because of not enough sensitivity of AE sensors or large distances between PD source and AE sensors [42].

In all acoustic method the localization would only be based on the acoustic wave signals with the same speed.

$$D_1 = v \cdot t_0 \quad (14)$$

$$D_2 = v \cdot (t_0 + \Delta t_1) \quad (15)$$

$$D_3 = v \cdot (t_0 + \Delta t_2) \quad (16)$$

$$D_4 = v \cdot (t_0 + \Delta t_3) \quad (17)$$

Fig. 1.10 shows a schematic view of the investigated oil tank. For localization at this method, the tank dimensions should be known. Let's assume the velocity of the acoustic signal is v , then the distance D_1 , D_2 , D_3 and D_4 from the AE sensors S_1 , S_2 , S_3 and S_4 in Fig. 1.10 can be calculated as following equations:

In Fig. 1.10 the distances between sensors and PD source (D_1 , D_2 , D_3 and D_4) could be calculated by $D_i = \sqrt{(x - x_{si})^2 + (y - y_{si})^2 + (z - z_{si})^2}$ where i is the index of the sensors and Δt is the time difference between acoustic waves and electric signal trigger. For all acoustic method there would be at least 4 sensors needed to localize the PD in three dimensions since the t_0 is not known.

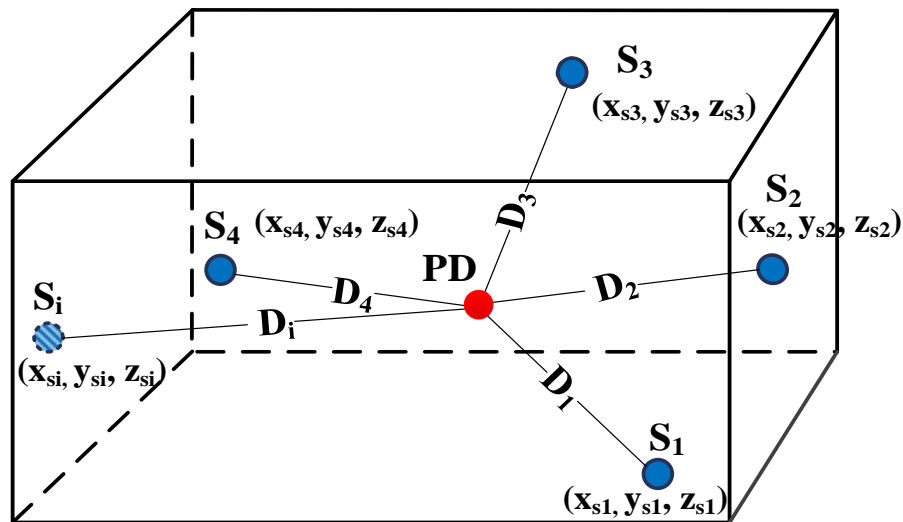


Fig. 1.10: Principle of localization of PD by acoustic method [42]

1.4 Acoustic emission (AE)

A sound wave is a mechanical vibration of molecules of a substance or substances (for example oil or air) transmitted in space. These substances are known also as transmission medium. As a result of any displacement from original position of equilibrium, there would be a pressure drop at the following point, when the main substance (surrounded around the “body”) compressed during the motion, which result in excessive pressure pushing the surrounding substance (it could be the same or not the same as main substance). The pressure differences after transition produce oscillation. The frequency of the oscillation depending on the substance properties. The chain after initial disturbance transmits in space from one point to another. The “body”, which produce this distortion is called source of sound. Due to this oscillation, this phenomenon has been compared with spring-mass oscillations (known as Hooke's law) in different contributions [49], [51].

1.4.1 Acoustic Impedance

Sound travels through materials under the influence of sound pressure. The specific acoustic impedance is a ratio of acoustic pressure to specific flow, which is the same as flow per unit area (velocity). Acoustic impedance is the ratio of acoustic pressure to flow. By considering the particle displacement y as a function of position x and time t :

$$y = y_m \sin(kx - \omega t) \quad (18)$$

Where y_m is the maximum displacement amplitude, k is the wave number ($k = 2\pi/\lambda$), λ is wavelength and ω is the angular frequency ($\omega = 2\pi f$) [49]. The particle velocity u is given by:

$$u = \frac{\partial y}{\partial t} = -y_m \omega \cos(kx - \omega t) \quad (19)$$

The acoustic pressure increase of p could be calculated as follow:

$$p = -h \frac{\partial y}{\partial x} = -hy_m k \cos(kx - \omega t) \quad (20)$$

where h is the volumetric modulus of elasticity. Acoustic impedance is the ratio of acoustic pressure to particle velocity (p/u). So that we have the following equation:

$$z = \frac{-hy_m k \cos(kx - \omega t)}{-y_m \omega \cos(kx - \omega t)} = hk/\omega \quad (21)$$

where z is the specific acoustic impedance. In the absence of reflection, the characteristic impedance Z_0 is as follow:

$$Z_0 = \frac{z}{A} \quad (22)$$

where A is one dimensional wave passing area. The acoustic impedance at a particular frequency indicates how much sound pressure is generated by a given acoustic flow at that frequency [49].

1.4.2 Reflected and Transmitted waves

Reflection occurs when acoustic waves propagate through media of different densities or elasticity. The energy and pressure of the transmitted wave will be reduced.

The pressure of sound at the boundary of two materials with Z_1 and Z_2 acoustic impedances would be calculated as below [50]:

$$R_p = \frac{p_r}{p_i} = \frac{Z_2 - Z_1}{Z_2 + Z_1}, T_p = \frac{p_t}{p_i} = \frac{2Z_2}{Z_2 + Z_1} \quad (23)$$

Where p_r , p_i and p_t represents respectively the reflection, incident, and transmitted pressure. Also, R_p and T_p are the reflection pressure coefficient and transmitted pressure coefficient. The transmission intensity co-efficient is determined by the difference in acoustic impedance for the two media. This is given by:

$$\alpha_{\text{Transmission}} = \frac{I_r}{I_i} = \frac{4Z_1 Z_2}{(Z_1 + Z_2)^2} \quad (24)$$

Here, I_r is energy intensity of reflected signal, I_i is energy intensity of incident signal, Z_1 and Z_2 are acoustic impedance of medium 1 and medium 2 respectively. For a given pressure wave, the transmission coefficient between oil and steel is 0.11, and the transmission co-efficient between air and steel is 0.0016. The acoustic waves would be reduced by transmission from oil to steel about 89%. The medium in tank is important for the signal amplitude outside the tank and better acoustic signal to noise ratio. Beside the effect of different characteristic impedances on reflection of the acoustic waves, the angle of hitting could also affect the reflections. Equation below shows the effect of hit angle to characterise acoustic impedance.

$$Z_i = \frac{\rho_i v_i}{\cos \theta_i} \quad (25)$$

Where i is the medium index and θ is the angle of wave at hitting position (Fig. 1.11) [58]. Fig. 1.11 shows the transmission and reflection at two different angles [59].

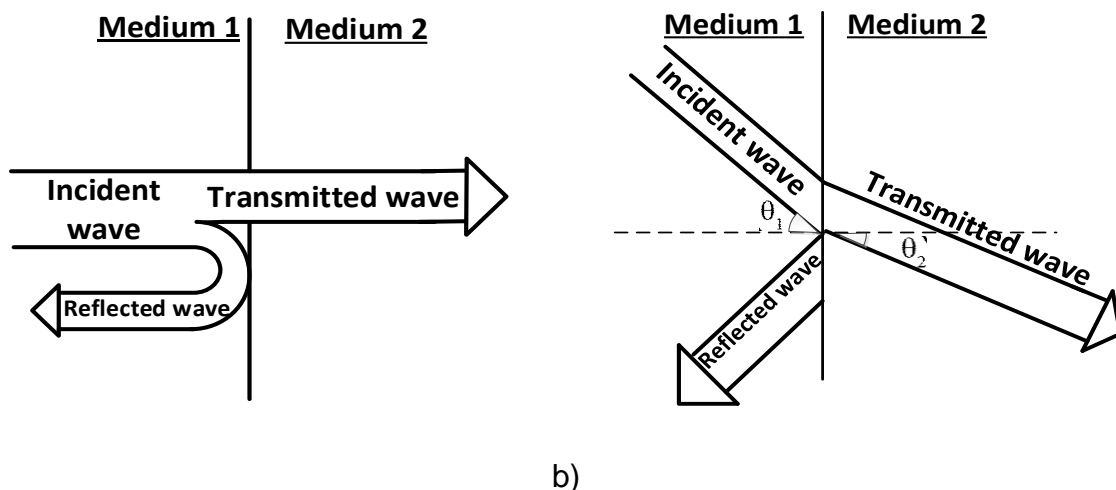


Fig. 1.11: Transmission and reflection of a wave that is incident to two different mediums with different acoustic impedance at different angles [59]

- a) Low reflection
- b) High reflection

Acoustic waves bend around corners and obstacles. This occurs as a result of wave diffraction. The bending of the acoustic waves because of diffraction becomes less obvious as the wavelength of the wave decreases relative to the dimensions of the obstacle. Diffraction is called scattering when many obstacles are present.

1.4.3 Longitudinal and Transverse waves

Longitudinal waves consist of periodic compressions and rarefactions (dark and light grey colours in Fig. 1.12). Longitudinal waves produce forces in direction of propagation. In this regard, they are known also as pressure waves. Longitudinal or pressure waves occur in both liquid and solid materials. A shock wave in the oil impinging at normal incidence on the tank will generate other motion in the tank wall that is perpendicular to the propagation direction. These kinds of waves are known as transverse or shear waves. A shear wave requires an acoustically solid material for

effective propagation and therefore does not exist in the oil; it exists only in solid materials like steel. Fig. 1.12 shows both longitudinal and transverse waves [42].

In Fig. 1.12 also the influence of the angle of hit on propagation of waves could be seen. By changing the angle from perpendicular direction (90°) to lower angles the waves propagation changes from longitudinal to transvers waves inside the tank wall. This procedure continues until critical angle. Above the critical angle, all the sound waves would be only reflected.

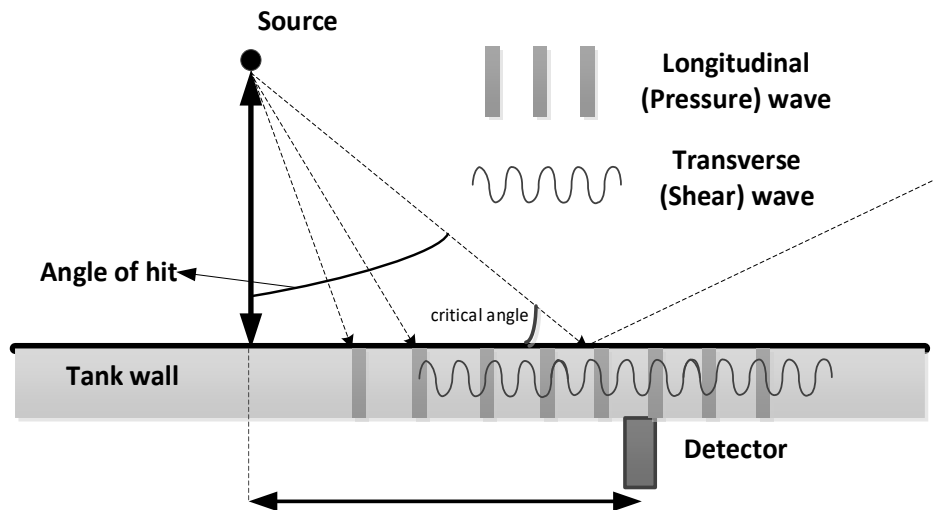
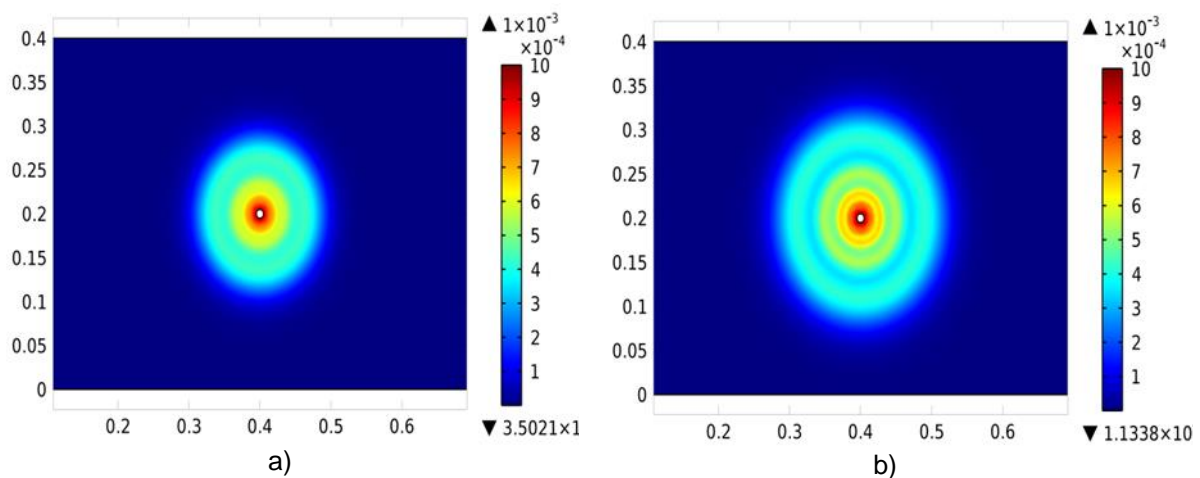


Fig. 1.12: Illustration of the longitudinal and transversal waves in the enclosure [42]

Fig. 1.13 shows a Finite Element Method (FEM) calculation of acoustic wave propagation inside a tank at different stages. It shows the longitudinal sound wave propagation at $t = 70 \mu\text{s}$ until $t = 270 \mu\text{s}$. Fig. 1.11 also shows the effect of reflection on wave propagation.



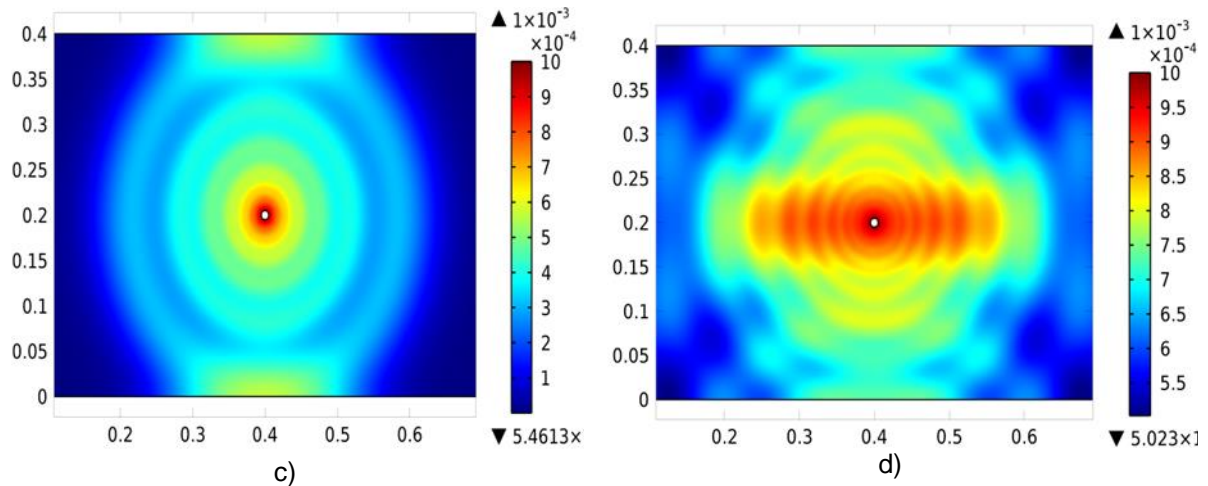


Fig. 1.13: Acoustic wave propagation in an oil tank

- a) $t = 70 \mu\text{s}$
- b) $t = 96 \mu\text{s}$
- c) $t = 130 \mu\text{s}$
- d) $t = 270 \mu\text{s}$

1.4.4 Attenuation

Dissipative or frictional forces arise whenever a real body is set to oscillation. Sound waves are also not an exception [49]. Table tennis is also popular with its nickname ping pong. This nickname most probably derived from the sound of the ball bouncing off the drum or table. But why the same ball could produce two different sounds? To answer this question, some basics about the propagation of the sound waves are illustrated.

The effect of attenuation plays an important role in many applications such as ultrasound second harmonic imaging or high-intensity focused ultrasound beam for therapeutic surgeries [54].

$$P(x + \Delta x) = P(x)e^{-\alpha(\omega)\Delta x} \quad (26)$$

$$\alpha(\omega) = \alpha_0 \omega^y, y \in [0,2] \quad (27)$$

Where P is the amplitude of an acoustic pressure and ω represents the angular frequency; Δx is distance; specific coefficients α_0 and y could be calculated by fitting the measured data.

The equations (25) and (26) show how the attenuation increases with increasing frequency.

The “l” letter sound consists of more high frequencies contents compared to the “O” letter. It could be concluded that the “Ping” word represents the sound hearing from bouncing balls near to the person and “Pong” represents the sounds of the bouncing balls from longer distances. This shows the effect of acoustic wave frequency on attenuation, which plays important role in choosing propel AE sensor.

1.4.5 Blast wave

PD activity is a short release of energy in a very short time and tiny space. Because of that, the PD could be known as a small explosion. The gas and/or oil around the PD source expands rapidly and displaces the surrounding air and/or oil, which causes a pressure disturbance to propagate away from the centre of the PD source. After realizing the energy, the pressure decays until ambient pressure is reached, this duration is known as the positive phase duration. The positive phase could be described as follow by Friedlander equation [52].

$$p_r(t) = p_{r,\max} \left(1 - \frac{t}{t_d}\right) e^{-bt/t_d}, \quad t \leq t_d \quad (28)$$

where $p_{r,\max}$ is the peak reflected pressure, t_d is the positive phase duration and b is the coefficient that describes the rate of decay of the pressure-time curve, known as the waveform or decay parameter.

After the positive phase comes a period of 'negative' pressure (below the normal pressure); a partial vacuum caused by over-expansion of the shocked air and/or oil. The negative phase could be then described as follow:

$$p_r(t) = -p_{r,\min} \left(\frac{6.75(t - t_d)}{\bar{t}_d}\right) \cdot \left(1 - \frac{(t - t_d)}{t_d}\right)^2, \quad (29)$$

$$t_d < t \leq t_d + \bar{t}_d$$

where $p_{r,\min}$ is the peak under pressure, \bar{t}_d is the negative phase duration. An idealized pressure-time profile for a reflected blast wave is shown in Fig. 1.14 where i_r and $i_{\bar{r}}$ are integral of the positive and negative phase pressure respectively [53].

In order to investigate the blast wave creation during a discharge activity, a needle (connected to the high voltage electrode) is placed with 30° angle to the surface of the pressboard. The pressboard is also placed vertically on the plane electrode. All the following arrangements are placed in a transparent oil-filled cylinder.

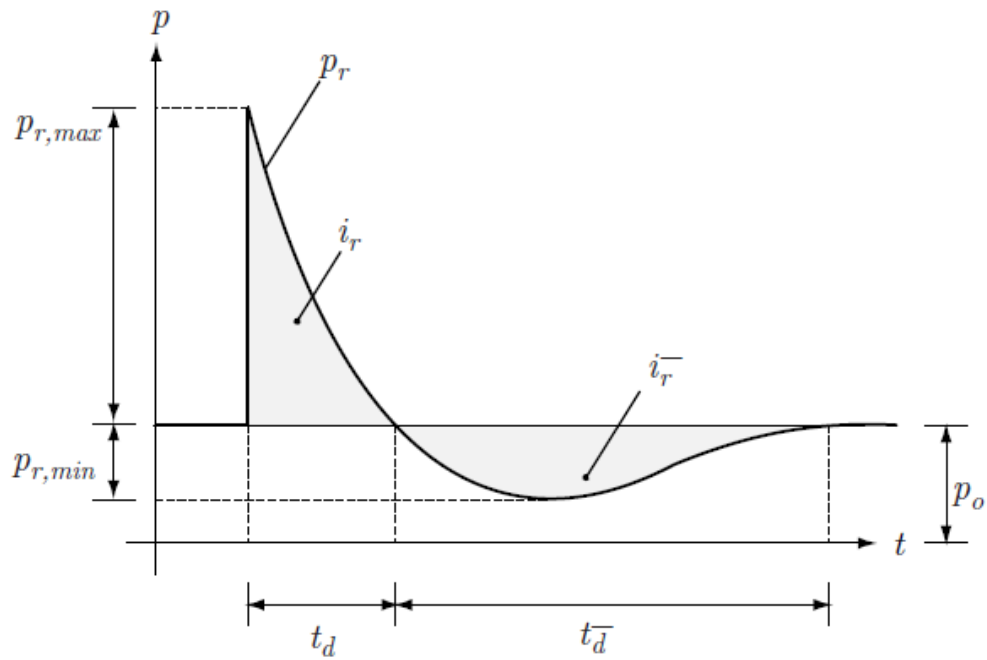


Fig. 1.14: Idealized pressure-time profile for a reflected blast wave [53]

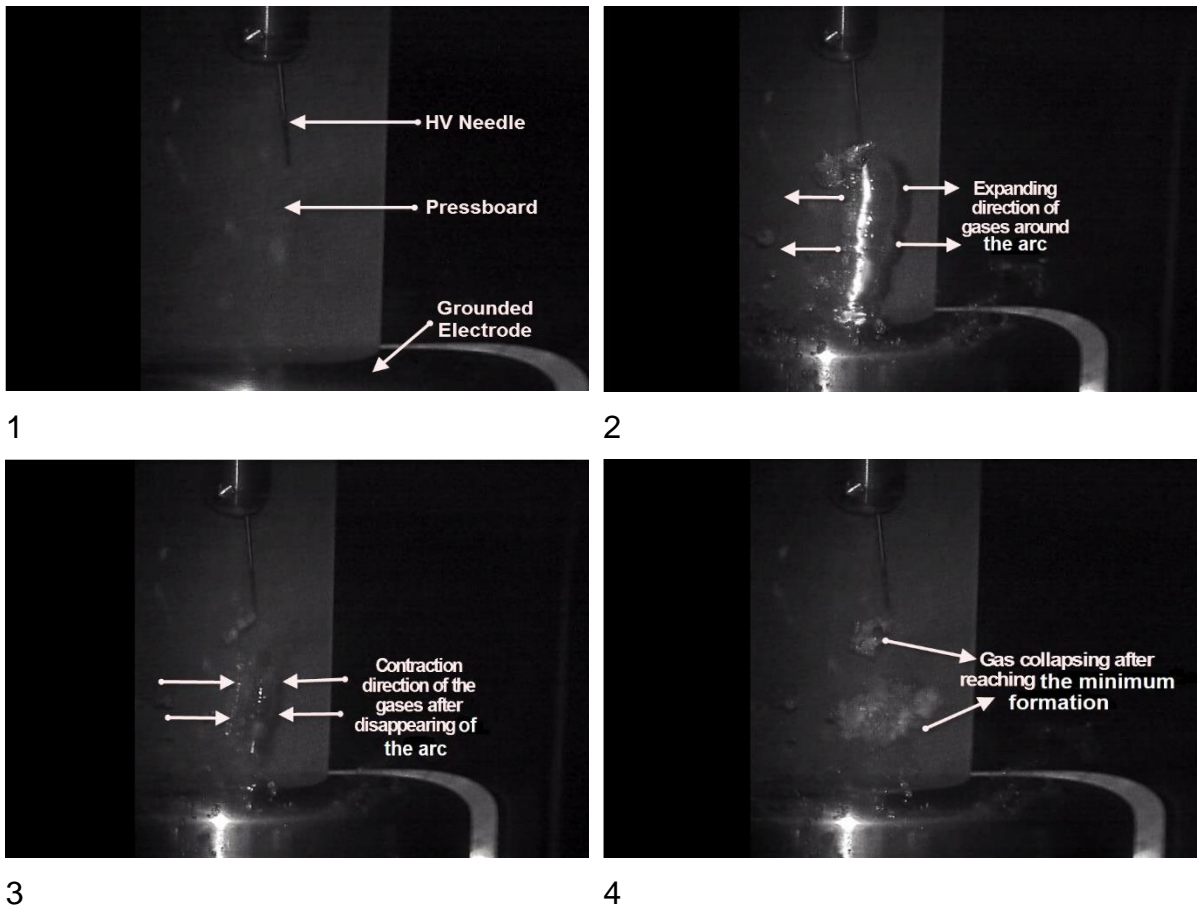


Fig. 1.15: The pictures from a high speed camera from the blast wave creation procedure during a discharge phenomenon

By using this arrangement, the possibility of surface discharges along the pressboard and the possibility of capturing a better image in terms of light reflection from the surface of the pressboard would be increased. Fig. 1.15 shows the procedure of the blast wave creation during a discharge activity captured by very high-speed camera. This fast expansion and contraction movement of oil/gas around the discharge area could generate an AE signal, which could be resonant depending on the characteristics of the surrounding medium (here oil) from the source to the sensor.

1.4.6 Velocity of acoustic waves

The speed of sound is faster in solid materials and slower in liquids and slower in gases. The speed of sound is even different for different types of solids, liquids, and gases. One of the reasons for this is that the elastic properties are different for different materials. Elastic properties relate to the tendency of a material to maintain its shape and not deform when a force is applied to it. A material such as steel will experience a smaller deformation than rubber when a force is applied to the material. Steel is a rigid material while rubber deforms easily and is a more flexible material.

By considering the Newton's second law at the boundary between two different mediums (with different acoustic impedances) following statement is calculated [49]:

$$v^2 = h/\rho \quad (30)$$

where ρ is the medium density, h is the volumetric modulus of elasticity and v shows the speed of sound. The velocity of a sound wave is affected by two properties of matter: the elastic properties and density. By considering the following relation between velocity and angular velocity:

$$\frac{\omega}{k} = \frac{\lambda}{T} = v \quad (31)$$

where k is the wave number ($k = 2\pi/\lambda$), ω is the angular frequency ($\omega = 2\pi f$), T is the time period, v the velocity and λ the wavelength. By replacing Eq. 29 and 30 in 31, the following statement is achieved:

$$z = \rho v \quad (32)$$

This shows the relation of acoustic impedance, sound velocity and medium density. Since the density as well as elasticity of oil varies at different temperatures, the velocity of sound also varies from 1000 m/s to 1600 m/s in transformer oil, whereby lower temperature shows higher sound velocity compared to higher temperature [59]. The sound speed variation has an influence on localization of the PD inside power transformers. In this regard, this correlation should be considered by using the acoustic measurement as an online measurement system during the operation of transformers at different oil temperatures [49].

2 Measurement Setup

2.1 Photography

VHX digital microscope has been used to capture and magnify 1000 times the samples of the PD carbonized patterns on the surface of insulating papers (Fig. 2.1).

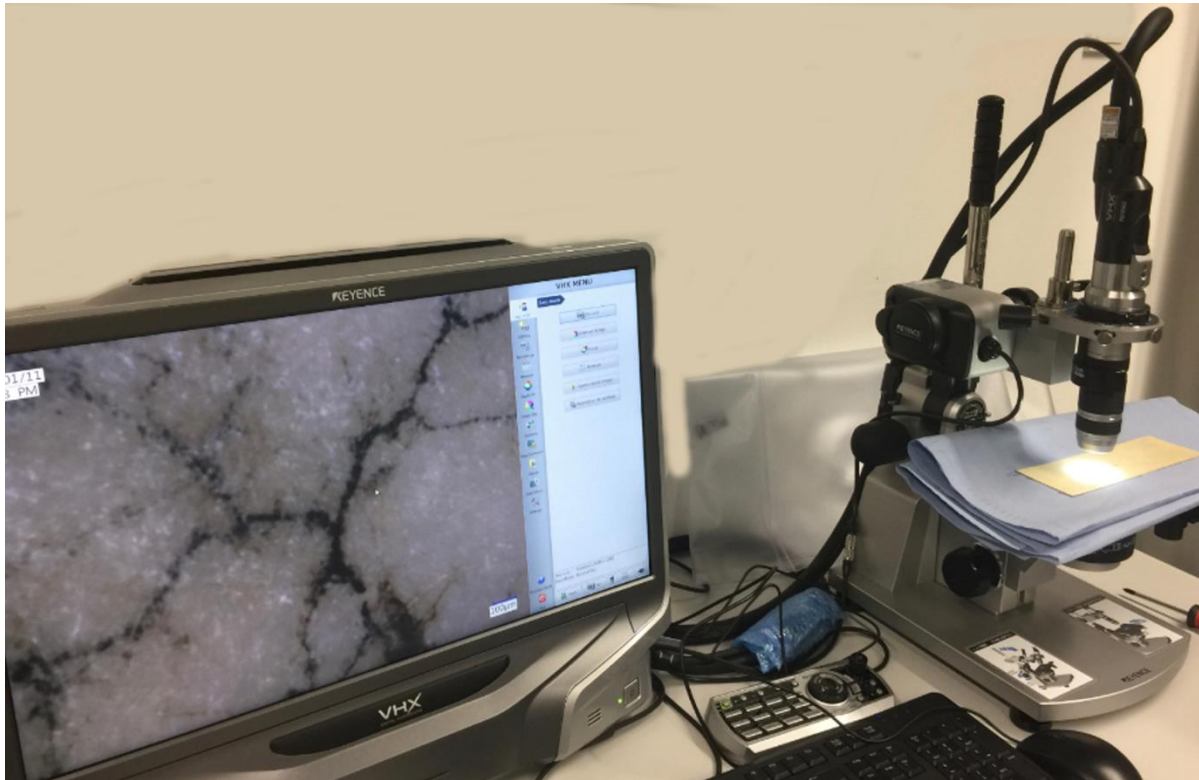


Fig. 2.1: VHX digital microscope

To investigate the samples visually during the test, a Nikon Camera with 300 mm objective was used (Fig. 2.2). To take picture of PD with low light emissions, 20 second shutter speed at ISO 1600 in a dark room was implemented. The dark room has been lightened for less than 20 ms to have a vision on objects/samples around the PD activity without PD light. This could help us to understand the carbonizations at different PD activity types in terms of acoustic and electric measurements.



Fig. 2.2: Camera for measuring the carbonization of pressboard during the test

2.2 Sample preparation

To measure if the water content inside transformer oil could have influence on creation of acoustic signals by PD activities, the water content of the oil is measured at different steps. The water content of the oil could decrease the insulation level of oil and also could even have some effects on creation of different kind of PDs [132], [133]. The amount of moisture in the oil and paper could have some impact on the measurement results. To reduce the moisture content below 7 ppm in oil the following procedure has been implemented. Fig. 2.3 shows the drying equipment.

First, high moisture oil is poured in the collection flask (1), the temperature of the heat exchanger (5) and two packed columns (8, 11) increased to 55°C by using a heating system (4). Via two vacuum pumps (7, 10), the air inside the two columns (8, 11) are removed and by means of an analogue pressure measurement device (6), vacuuming procedure is monitored. The pressure in the first column (8) reaches 0.4 mbar. In the second packed column (11) the pressure would decrease lower than 0.1 mbar.

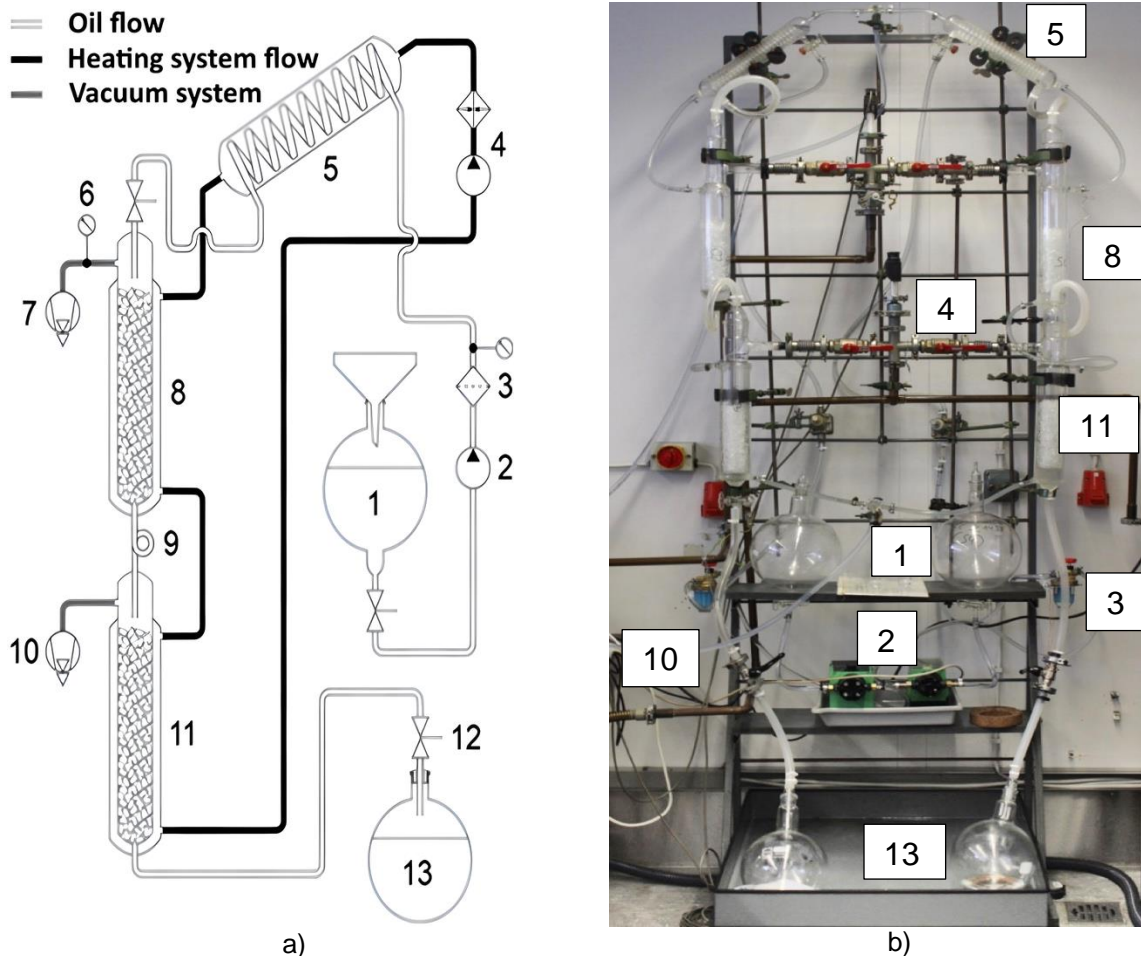
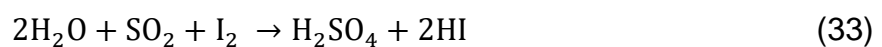


Fig. 2.3: Oil drying system
 a) Schematic view
 b) Real view

The siphon (9) maintains the differences of pressure between the two columns at a constant level. The pump (2) transports the fluid through the filter (3). For increasing the oil surface and accelerating the degassing and drying procedure, high temperature oil with lower viscosity flows around cylinders fillers inside columns. The primary degassing and drying procedure were done at the first column and then in the second column, lower pressure causes this process repeated extremely. Finally, dried oil with very low dissolved gases is collected in the glass flask (13) for further use.

Determination of absolute water content of the samples (oil and pressboard) is performed under ASTM D1533-00 by means of the 831 Karl Fischer coulometer made by Metrohm AG, which is shown in

Fig. 2.4. The idea behind this traditional method is based on reaction between sulphur dioxide (SO_2) and iodine (I_2) in the presence of water. In the coulometric titration method, when iodine (I_2) meets the water in the sample, water is titrated according to following reaction:



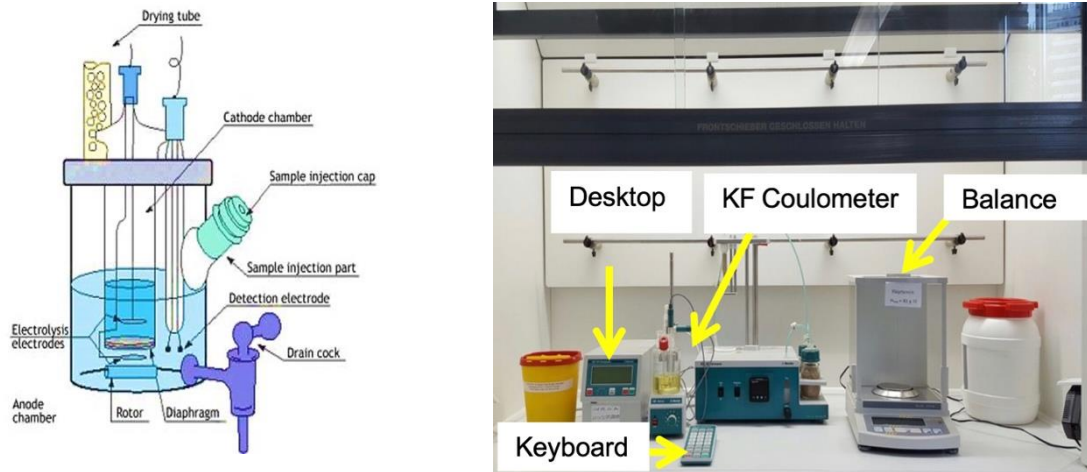


Fig. 2.4: KF coulometer used for water content measurement [134]

The detection limit of coulometric titration reaches down to some μg of water. Once all the water available has reacted, the reaction is complete. The amount of water in the sample is calculated by measuring the current needed for the electrochemical generation of iodine (I_2) from iodide ion (I^-) according to the following:



For paper/pressboard water content measurement, the samples were heated in heating device and the gas streamed with water vapour was led into the reaction vessel. To improve the accuracy and minimizing the external influences, four measurements were performed, and the mean value of these measurements assumed as the absolute water content. Water content value of the sample under consideration was between 2 ppm and 5 ppm as the acceptable error in this study.

Impregnation process is performed by a system which is shown in

Fig. 2.5. Samples are placed in a stainless-steel container at a temperature of $85\text{ }^\circ\text{C}$ and vacuum pressure of 0.5 mbar in a thermal vacuum chamber for 24 hours. Afterward, the oil content is added slowly to stainless-steel container through a pipe connected to oil vessel located at the top of the thermal-vacuum chamber.

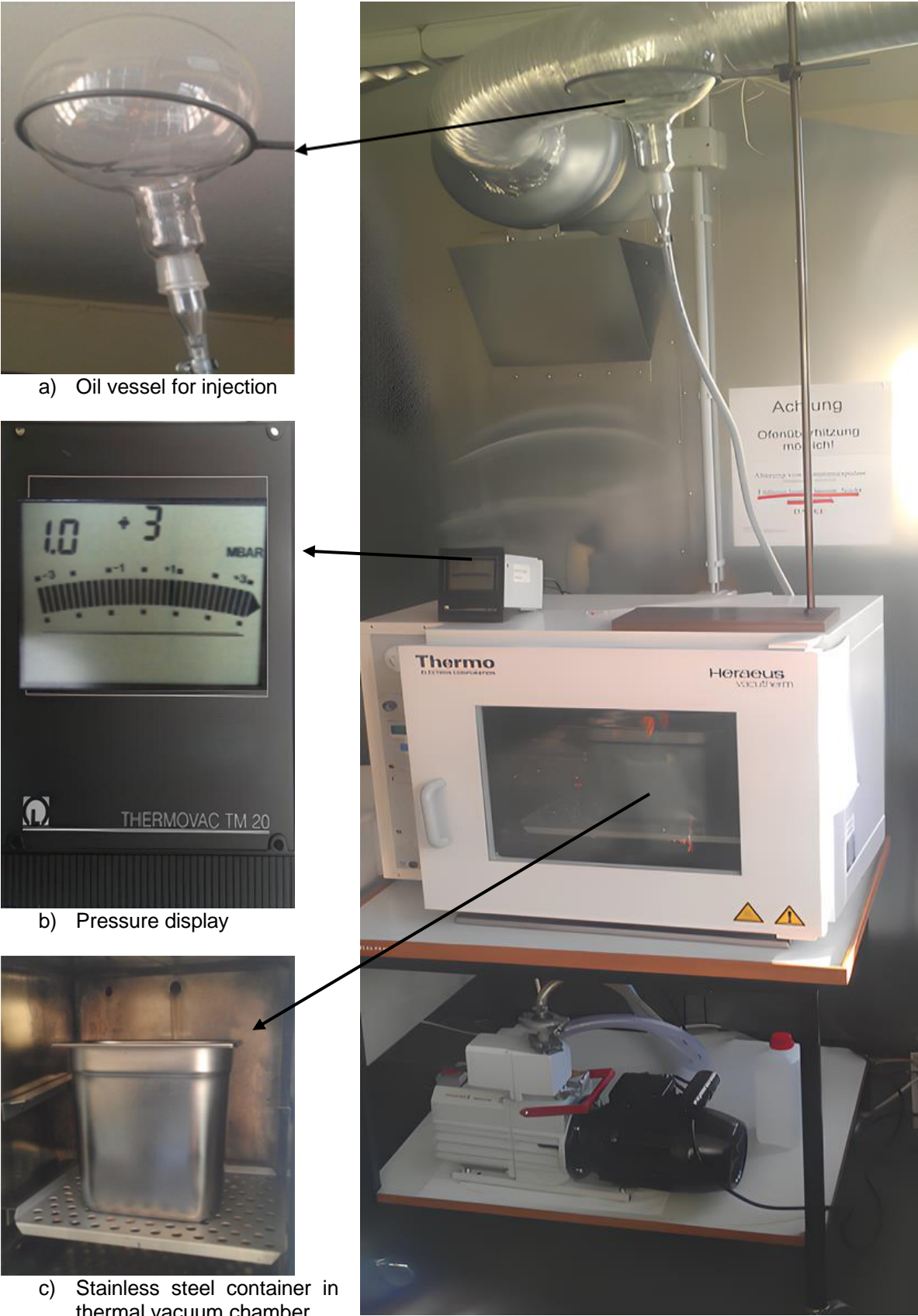


Fig. 2.5: Arrangement of oil-paper impregnation system a) oil vessel for injection, b) pressure display and c) stainless-steel container

After 24 hours of oil injection into the container, the heater is turned off to naturally cool down the samples for half a day until reach room temperature (25 °C). Then the steel container is sealed completely in order to maintain the same conditions for all samples as much as possible.

2.3 PD acoustic measuring system

AE signals are normally captured by piezoelectric sensors. Piezoelectric sensors use the piezoelectric effect, to measure changes in pressure of AE waves by converting them to an electric signal [55]. Determining the exact frequency of the AE waves was in the focus of several contributions [56]. Higher frequency resonance sensors could increase the possibility of detection in terms of environment noise elimination. Due to dependency of the AE frequency to the AE sensors [57], a wide band AE sensor for determining the acoustic wave frequency would be needed. The investigations show that the peak frequency of the AE oscillations generated by PD vary between 100 kHz-200 kHz [59]. Chapter 1.4.4 showed the frequency attenuation dependency of AE signals, the same phenomenon could be seen on AE signal generated by PD at different distances to AE sensors [61]. Fig. 2.6 shows the schematic view of the AE sensor.

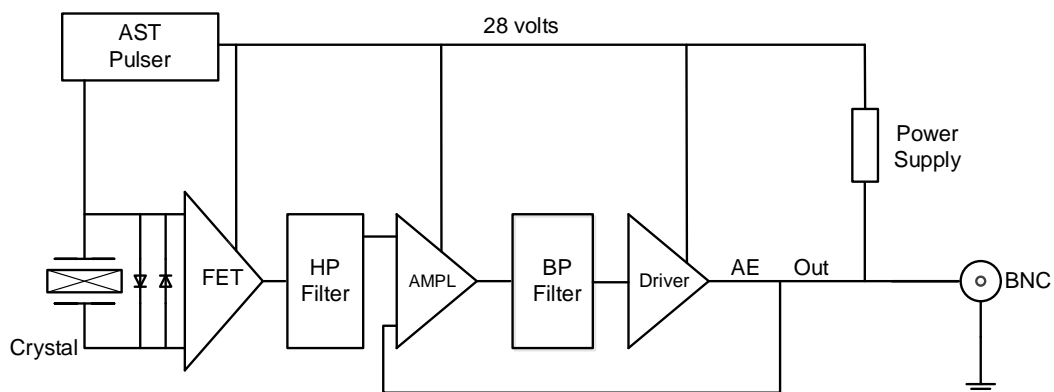


Fig. 2.6: Schematic view of AE sensor [79]

Two main types of AE sensors with peak frequency of the 75 kHz and 150 kHz were used to detect and localized PD inside a power transformer (Fig. 2.7).

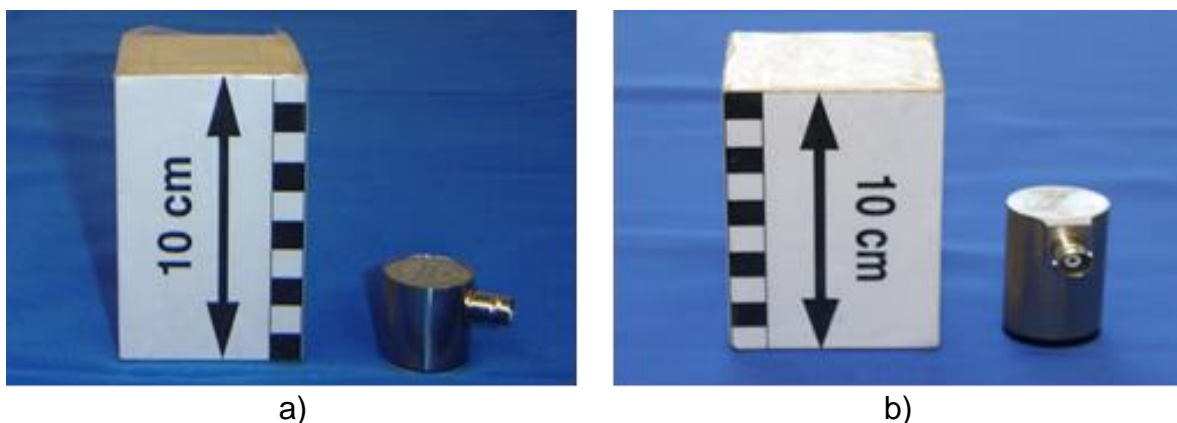


Fig. 2.7: AE Sensors
a) 150 kHz
b) 75 kHz

The integral sensors are completely enclosed in a stainless-steel case and coated to minimize RFI/EMI interference on internal electric circuits. In addition, care has been taken to thermally isolate the critical input stage of the pre-amplifier, to provide excellent temperature stability over the range of -45°C to $+80^{\circ}\text{C}$. Table 2.1 illustrates the specific characteristics of these sensors.

To remove the air from interface between a measurement surface and an AE sensor, silicone grease with more than 3500 times higher acoustic impedance than air has been used. This could increase the sensitivity of AE sensors by connecting them to the oil tank surface.

Fig. 2.8 shows the pencil-lead break calibration method. This test consists of breaking a 0.5 mm (alternatively 0.3mm) diameter pencil lead with 2H hardness approximately 3 mm (± 0.5 mm) from end of guiding to its tip by pressing the lead against the surface of the piece.

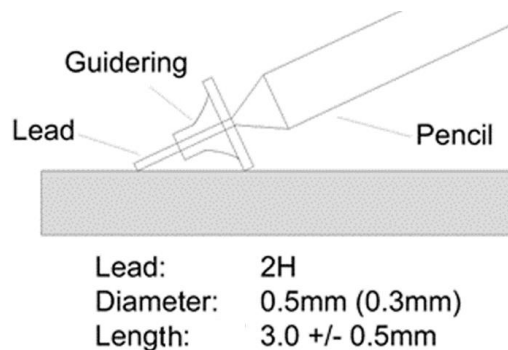


Fig. 2.8: Pencil-lead break calibration method

This generates an intense acoustic signal, quite same as a natural AE source, that the sensors detect as a strong burst. The purpose of this test is twofold. It ensures that the measurement devices work properly and transducers are in good acoustic contact with the part being monitored [62], [63].

Table 2.1: Properties of sensors

Sensor Model	Freq. Range [kHz]	f_{Peak} [kHz]	Size D×H [mm]	Pre-amplifier	Case Material	Wear Plate	Temp. Range [°C]
R15I	70-400	150	29×31	40 dB	Stainless steel	Ceramic	-45 to +80
VS75-SIC	30-120	75	28.6×51.8	40 dB	Stainless steel	Ceramic	-5 to +85

To capture the AE signals, two different measurement methods are used. First, oscilloscope with decoupling method and second digital signal processing (DSP) measurement system.

2.3.1 Oscilloscope decoupling method

To energize the AE sensors and separate AE signals from DC signals for oscilloscope connection, a decoupling circuit has been used (Fig. 2.9).

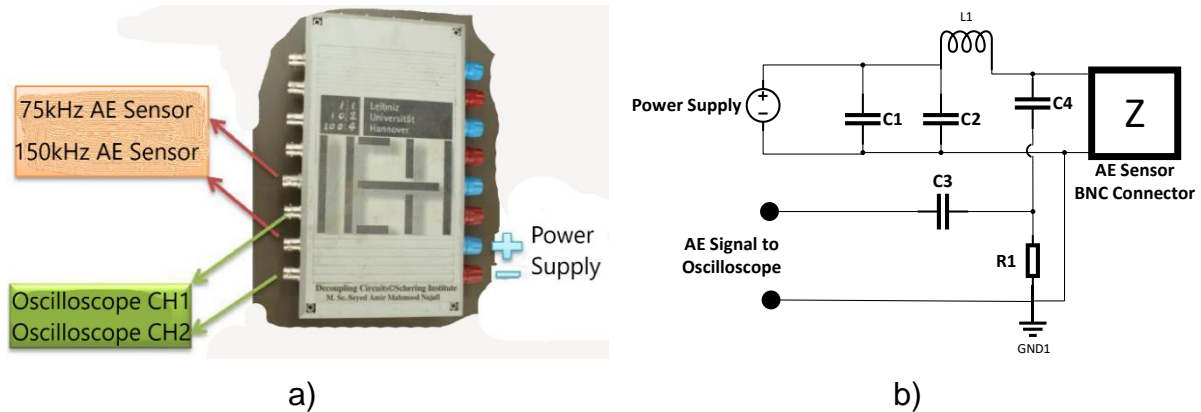


Fig. 2.9: Decoupling circuit
 a) Schematic view
 b) Single diagram circuit

Fig. 2.9 shows the decoupling circuit with the possibility of energizing four AE sensors at the same time.

2.3.2 DSP Measuring device

An 18 bit digital signal processing (DSP) device from Physical Acoustic with a sampling rate of $20 \cdot 10^6$ sample/s was used to analyse AE signals (Fig. 2.10).



Fig. 2.10: Physical Acoustic DSP device with connected acoustic sensor [79]

Thanks to hit definition time (HDT) also known as single channel event time out and hit lockout time (HLT) functions, the reflection of AE signals in DSP was eliminated as much as possible to have more precise comparison of the AE signal maximum amplitudes and numbers [76]. There is no exact information regarding the time delay of HLT and HDT information in Physical Acoustic device, but the investigations show that this should be around 100 microseconds. The HDT parameter specifies the

maximum time between threshold crossings, i.e., if no crossing occurs during this time then the hit has ended. If the HDT is set too high, then the system may consider two or more hits as one. If the HDT is set too low, then the system may not fully capture the AE hit and possibly treat one hit as multiple ones. The HLT parameter specifies time which must pass after a hit has been detected before a new hit can be detected. If the HLT is set too high then the system may not capture the next AE and if it is set too low then the system may capture reflections and late arriving component of the AE as hits. The peak definition time (PDT) parameter specifies the time allowed, after a hit has been detected, to determine the peak value. If the PDT is set too high then false measurements of peak value are more likely to occur. It is recommended that the PDT should be set as low as possible. However, care must be taken not to set it too low because that may result in the true peak not being identified [77]. Fig. 2.11 illustrates the threshold-based hit detection and shows. By crossing the measured area energy from the threshold, the PDT starts and by falling the curve below threshold the HDT delay time starts [78]. It shows that the time required for evaluating an AE burst including HDT and HLT is around 200 microseconds, which is much slower than evaluation of a single electric PD signal. This unmatched limit could lead to underestimation of AE and electric PD numbers at very high PD activities.

Omicron PDL 650 was used to compare the results of Physical Acoustic DSP (Fig. 2.12).

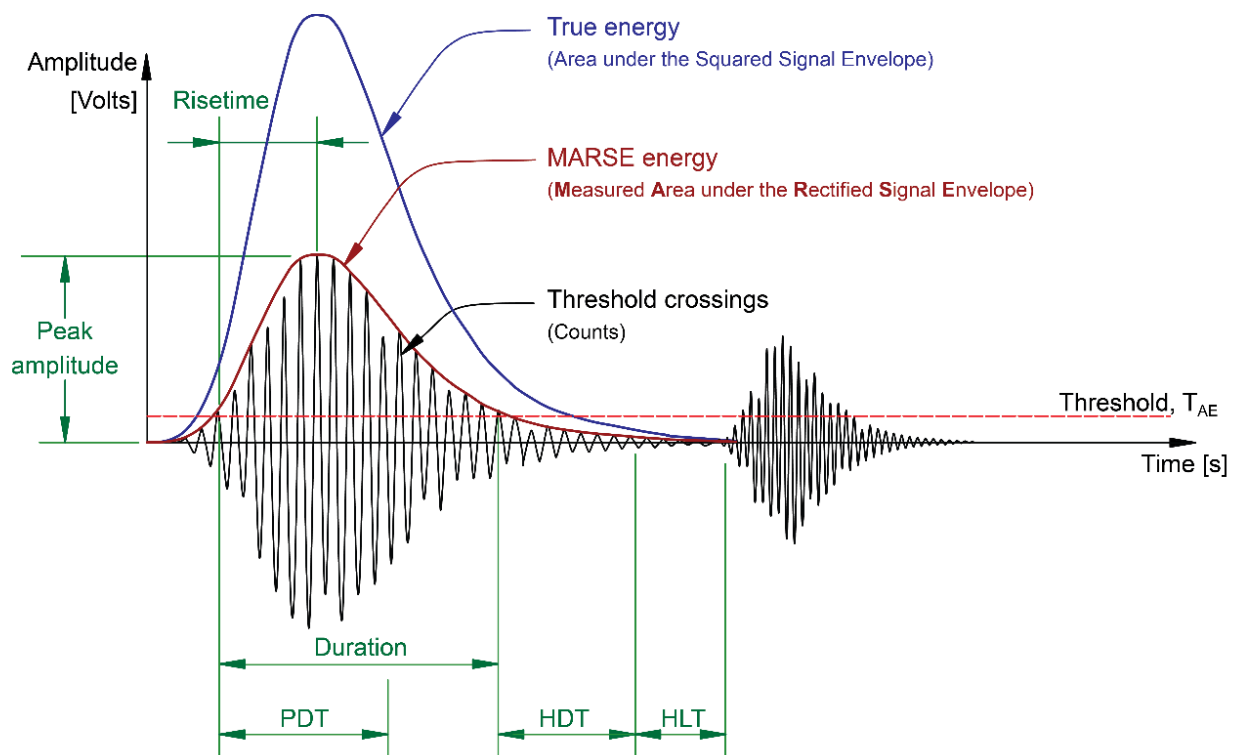


Fig. 2.11: Illustration of the threshold-based hit detection and the AE features extracted from each hit [78]



Fig. 2.12: PDL 650 acoustic measuring device

2.4 Electric PD measuring system

2.4.1 Measuring via coupling capacitor

Measuring principle via coupling capacitor is the same as illustrated in Fig. 1.6. Different measuring devices like ICM (manufactured by “Power Diagnostix Systems”) and MPD 600 (manufactured by “Omicron”) has been used. Fig. 2.13 shows both measurement devices. Omicron MPD 600 should be energized by a battery pack delivered by the device. This has the advantage of noise immunity against noises from power supply, but this makes the measurements limited to the capacity of the battery. ICM device could be connected via BNC cable, which makes this device suitable for measuring electric PD signals from coupling capacitor and measuring acoustic signals by connecting the AE sensors directly from decoupling circuit (Fig. 2.9).

16 bit resolution of MPD 600 compared to 10 bit resolution of ICM makes the MPD 600 a more suitable device for electric PD detection with high range of apparent charge amplitude from 10 pC to 10 nC. Fig. 2.14 shows the PD calibrator device.



a)



b)

Fig. 2.13: Electric partial discharge measurement devices

- a) Power Diagnostix Systems ICM
- b) Omicron MPD 600



Fig. 2.14: Calibrator device

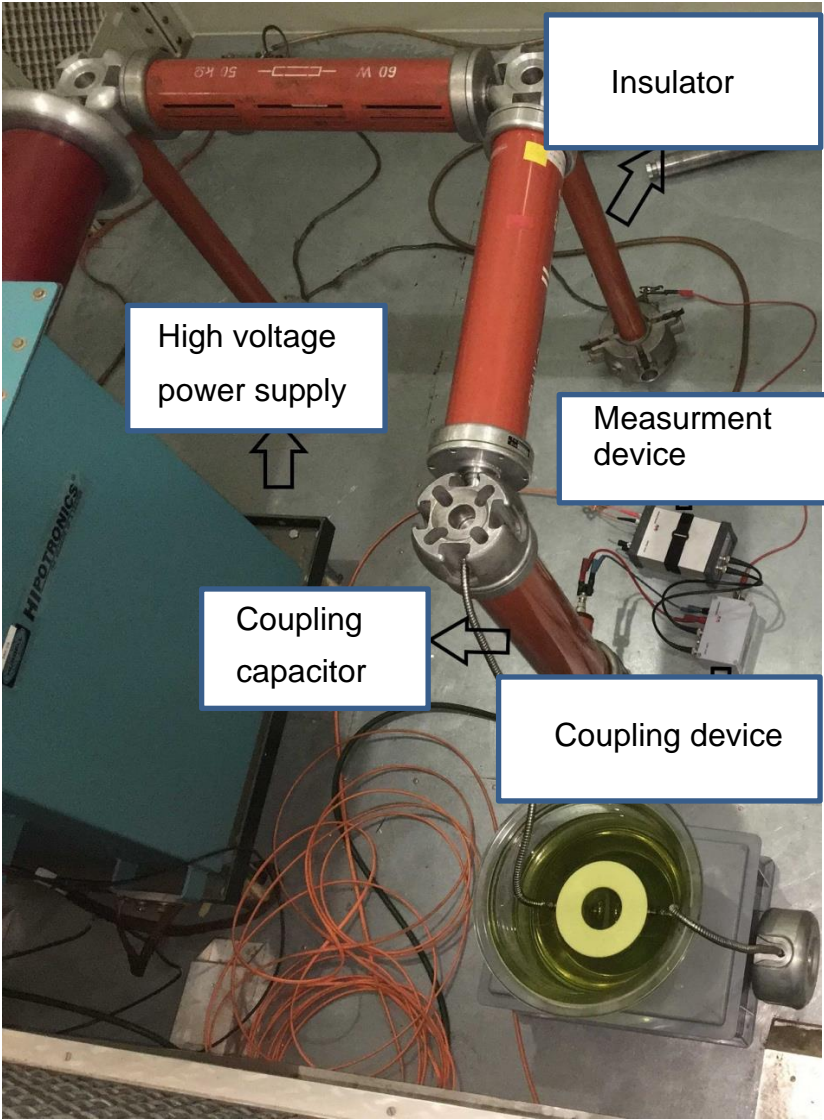


Fig. 2.15: Measurement arrangement for conventional electric PD measurement (Omicron MPD 600)

Fig. 2.15 shows the arrangement of the measuring instrument inside the test field. To measure the PD signals via oscilloscope the ICM device has been used. The calibration has been done before every test.

2.4.2 UHF measurement

UHF sensor has been placed on the most sensitive direction to have the best sensitivity. UHF noise level could be reduced during the measurement (Fig. 3.3) by disconnecting and removing the active elements (like converters) near and inside the open-air test cell. The samples placed carefully inside the tank filled with an insulating oil.

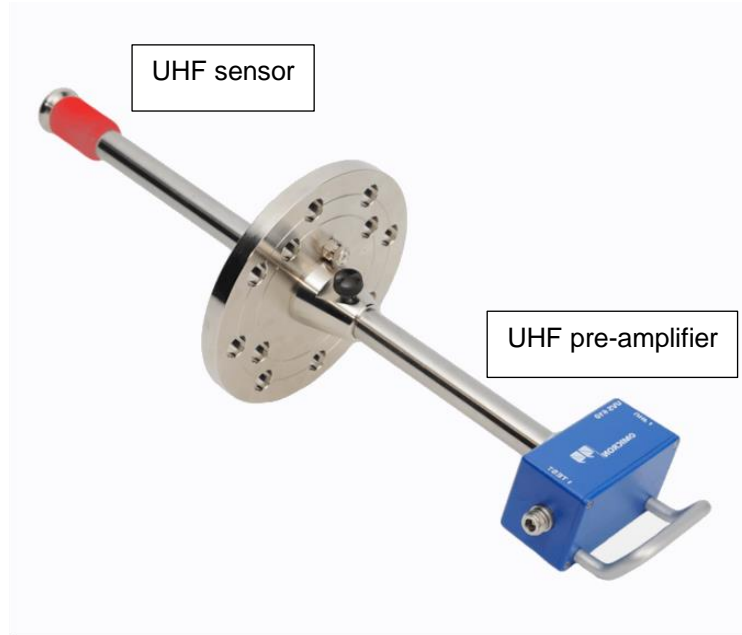


Fig. 2.16: UHF sensor [126]

Depending on the measurement, the UHF sensor has been connected to MPD 600 and UHF 620 (more information in [126]) or oscilloscope.

2.5 Setup for corona in oil

To study the relation between acoustic and electric signals of the PD events a needle as high voltage electrode was placed on top of the pressboard with an oil gap inside the tank with 40 cm × 40 cm × 80 cm dimension (Fig. 2.17). The tank was filled up with transformer insulating oil up to 35 cm. The pressboard was placed on a plane ground electrode 20 cm above the oil tank to produce a barrier between the two electrodes (needle and plane). By placing the pressboard between needle-plane electrode configuration, there would be a better possibility to control the amount of PD discharges. To have a reasonable comparison in terms of acoustic oscillation amplitude recorded from two different AE sensors with 150 kHz and 75 kHz peak frequencies, the AE sensors are mounted on the tank wall about 40 cm from the high voltage needle. Silicone gel has been used between the surface of the AE sensors and the steel tank to increase the sensitivity of the AE sensors to acoustical pressure waves created by PD inside the tank.

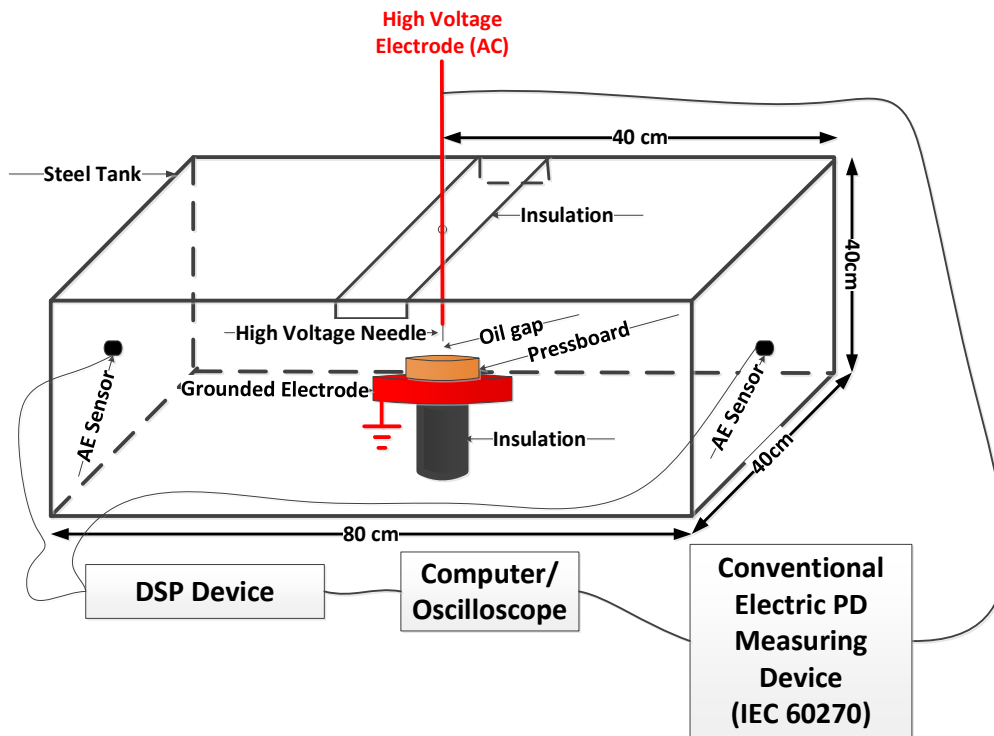


Fig. 2.17: Schematic view of the needle-oil gap-plane arrangement with measuring devices

PD is a random process. The probability of creation PD could be increased by increasing the electric stress. Since the PD creation depending on several different factors the exact prediction of PD would be almost impossible. However, several investigations have been done to make this prediction more reliable [87]. To find the relation of acoustic signals at different electric PD signals different voltage steps has been applied to change the electric field at the tip of the high voltage needle, shown in Fig. 2.17.

2.6 Setup for surface discharge

The needle-plane electrode configuration is like Fig. 2.17, but in this case the high voltage needle is placed on the surface of the aramid pressboard (without oil gap) with adjustable needle diameters to investigate the surface discharges [70].

The tip diameter of the high voltage electrode varies from 4 mm up to 20 mm and in addition two needles with tip diameter of 5 μm and 40 μm has been used (Fig. 2.18). Aramid papers with 0.8 mm thickness, impregnated with ester oil (MIDEL 7131) are used in the tank consisting of 80 l of the same oil, to investigate the PD for long time and the carbonization due to PD activities.

Aramid paper and ester oils are well known for their temperature resistance [75] and Aramid pressboards have been used to have a better insulation material regarding temperature. The R151 AE sensor with the DSP device was used. The voltage was increased for each setup up to the first PD occurred. After reaching steady state discharges, the electric and acoustical signals of PD were measured simultaneously.

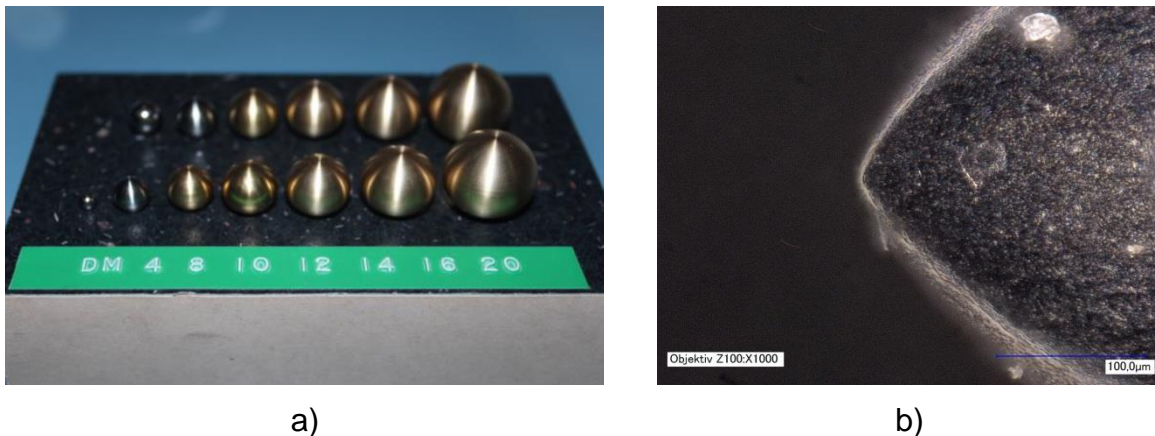


Fig. 2.18: Electrodes with different diameters
 a) Electrode balls from 4 mm up to 20 mm
 b) Needle with about 40 μm tip diameter

2.7 Setup for acoustic and electric PD

Simultaneous measurement means a combination of UHF, electric and acoustic measurement. Fig. 2.19 shows the test setup for measuring electric and UHF signals of PD. Two different acoustic emission (AE) sensors with a peak frequency of 75 kHz and 150 kHz respectively are mounted outside the oil tank to measure the acoustic signals. They are connected to the decoupling circuit with integrated DC power supply and oscilloscope. Technical characteristics of the sensors are illustrated in Table 2.1. UHF and electric signals have been measured simultaneously via ICM, MPD 600, UHF 620 and oscilloscope. Pattern picture of ICM device could capture the signals for very long time without the need for very high data capacity. On the other hands the MPD 600 and UHF 620 devices could communicate together and capture the signal in higher resolution compared to ICM device.

Acoustic signals have been captured via Oscilloscope and ICM device to have short and long term focuses on acoustic signals, since the oscilloscope device could capture the signals in higher sample rates compare to the ICM device. MPD 600 and UHF 620 has been used to capture electric and UHF signals to have a very good resolution of electric and UHF signals in terms of very low and very high magnitudes. The sensors (UHF and Acoustic) were placed inside the Faraday cage to eliminate the electromagnetic interferences during the measurement.

An impregnated aramid pressboard with a thickness of about 0.6 mm was used as an insulating material. A needle with a tip radius of 3 μm was connected to high voltage source and placed vertically to the surface of the pressboard. Since the electric discharges produce high temperature and could melt the tip of normal needles, tungsten needles with capability to withstand very high temperatures were used. High temperature tolerance of these kinds of needles secured the same voltage stresses within the electric discharges.

The entire system has been checked for corona in air and unwanted PD outside the tank. This validation has been done by removing the ground electrode and increasing the input voltage up to 50 kV. PDIV varies from 10 kV up to 30 kV depending on electrode arrangement and electric field stress.

To calculate the sound pressure level (SPL) in dB, the following formula has been used:

$$\text{SPL} = 20 \cdot \log_{10} \left(\frac{V_p}{V_0} \right) \quad (35)$$

Where V_p is the peak voltage output of the AE sensor in volt and V_0 is a constant value of $200 \mu\text{V}$. It means 20 mV on oscilloscope represents 40 dB on DSP device.

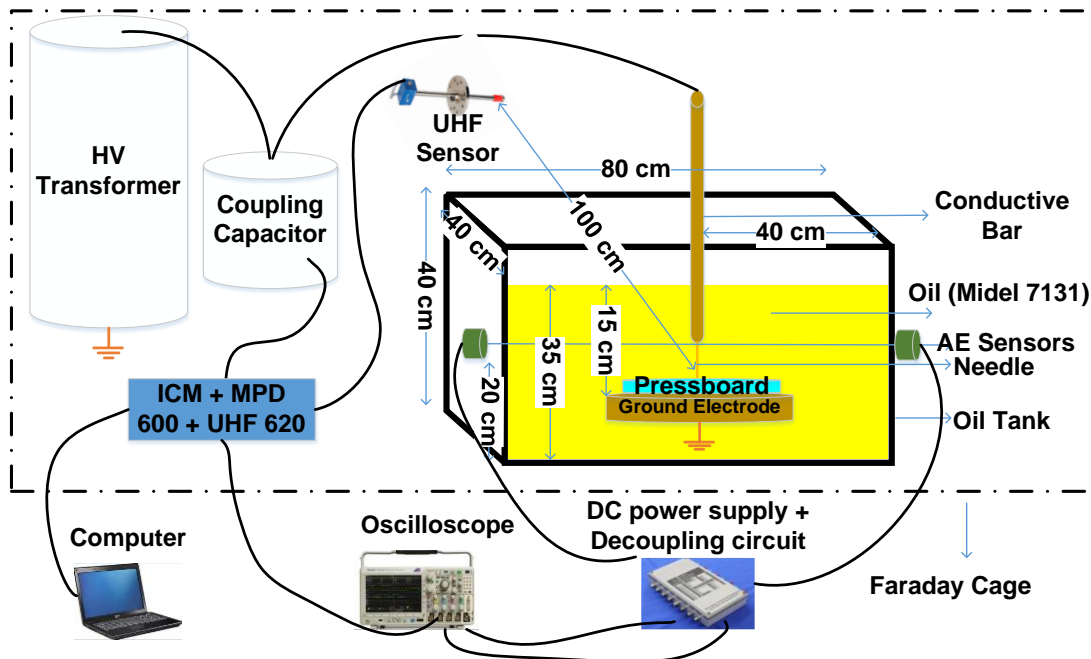


Fig. 2.19: Schematic view of the test setup

3 Basic Examinations

PD is a stochastic phenomenon in terms of exact time and location. Due to this fact to find the relation between electric and acoustic signals, many PD activates should be captured and compared together. To cover different PD categories, different arrangements have been implemented.

Because pressboard and paper cellulose can be simply formed and trimmed, they are commonly used as insulation material in transformers. Oil filled transformers consist mostly of paper, pressboard, and oil as insulation materials. Nowadays some transformers use higher temperature resistive materials like ester oil and aramid papers to decrease the size and increase the reliability of the transformers [64].

Depends on the intensity of electric discharges of the PD activity normal and aramid pressboards have been used during the investigations. Aramid pressboards could increase the time of investigations during PD activity. Aramid papers and pressboards (not natural) are polymers from the group of amides used in the production of fibre and sheets having both high mechanical strength and thermal resistance. Transformer oil also differs from mineral oil to synthetic and natural ester fluids. Ester fluid is well known for their high thermal resistivity and environmentally friendly properties. Depending on the properties of the oil and pressboards, the transformer temperature could be raised to certain level [65].

To study the acoustic signals of different type of PD inside at power transformer, two main categories of PD activity has been investigated. First PD activity in oil and second PD activity in paper/pressboard. To reduce the mechanical attenuation of AE signals, the tank has been constructed without barriers. Also, the PD inside papers/pressboards have been generated very near to the surface of the paper/pressboard (surface discharge).

3.1 Corona in oil

PD is a phenomenon which takes place in gas states (like plasma). Partial discharge processing in transformer oil is a complex process of PD and recombination during which gases are formed and absorbed by the oil. So that damage to a specific point within the system is not necessarily permanent and stationary [66]. However, there are some differences in PD pattern structure of corona in oil and corona in air, but the replacing of affected area by new oil material makes this PD like corona in air. Corona in oil could degrade the electric characteristics such as breakdown voltage and inception PD voltage of the transformer oil [67], [68].

Relation between AE signals and electric signals from corona in oil were examined and discussed. The test sample has been prepared as described in chapter 2.5.

3.1 AE measurement

3.1.1 The effect of overlapping on accuracy

To test the maximum reflections, two different type of AE sensors with 150 kHz and 75 kHz peak frequency were mounted with 20 cm distance to the PD source to have less attenuation compared to 40 cm distance.

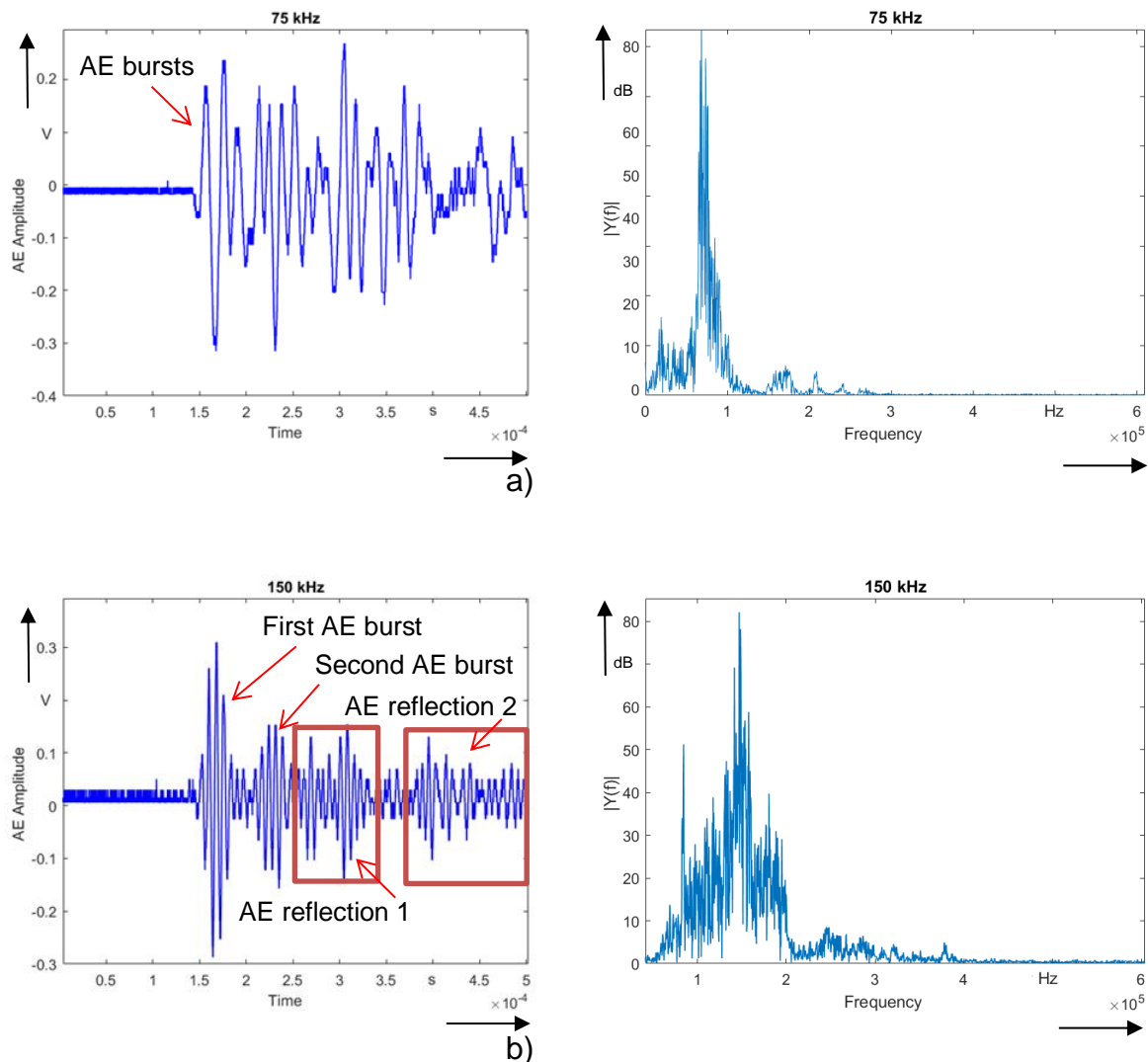


Fig. 3.1: AE signals captured during PD activity at the same distance from PD source with different AE sensors

- a) 75 kHz peak frequency
- b) 150 kHz peak frequency

The lower damping of the lower frequencies compared to the higher frequencies could have an influence on defining the exact responsible electric PD via acoustic method [61], which could cause problem in localization of high number of PDs. Fig. 3.1 shows the AE signals captured by two different AE sensors at the same distance to the PD source. The two different AE bursts at the beginning of the oscillations captured by 150 kHz AE sensor (red arrows in Fig. 3.1b) are very good visible and detectable, while it could not be visible by 75 kHz AE sensor (Fig. 3.1a). In addition to that, the reflections of these two acoustic bursts are also visible by 150 kHz sensor in Fig. 3.1b after the second burst. The reflections could also be not detectable by 75 kHz sensor in Fig. 3.1a. The reflections depend on geometry of the tank. Since the ground electrode was isolated from the oil tank by an insulation material and connected via cable to the ground, it worked as an acoustic barrier to eliminate the reflection from the bottom. Also, the shear waves have very low amplitude compared to the longitudinal waves near to the AE sensors. Because of that, only direct and reflected waves to the sensors could be seen in Fig. 3.1b. Fig. 3.2 shows two reflection possibilities in used geometry. Red arrows in Fig. 3.2 show the reflection from top and sides because of acoustic

impedance differences between air and oil. By considering the distance between 150 kHz AE sensor and PD source about 20 cm, the reflection 1 distance would be about 36 cm and in other word $1.1 \mu\text{s}$ delay (Fig. 3.1b). Reflection 2 (blue arrows in Fig. 3.2) shows the reflections because of oil tank, which create a delay of $2.6 \mu\text{s}$ (Fig. 3.1b). This caused an overlapping effect of lower frequency signals with lower attenuation (details see in chapter 1.4.4). Fig. 3.3 shows the electric UHF signals captured during PD activity with two electric signals with a delay of about $70 \mu\text{s}$.

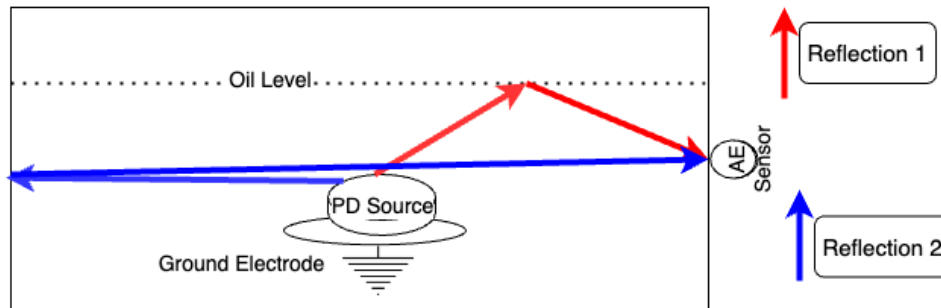


Fig. 3.2: Schematic view of possible reflections in oil tank after PD creation

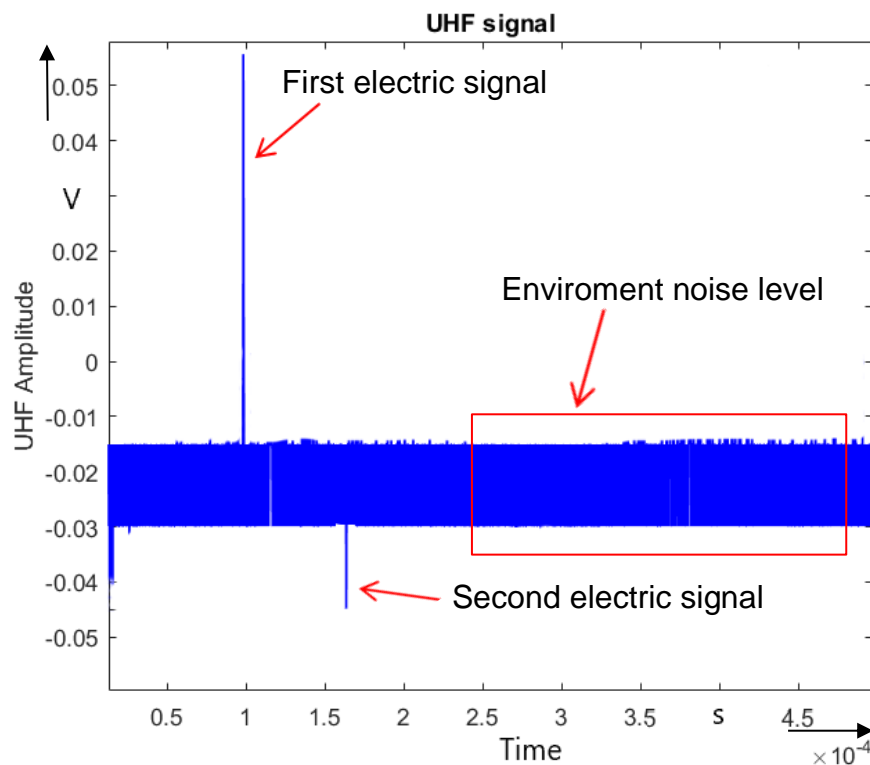
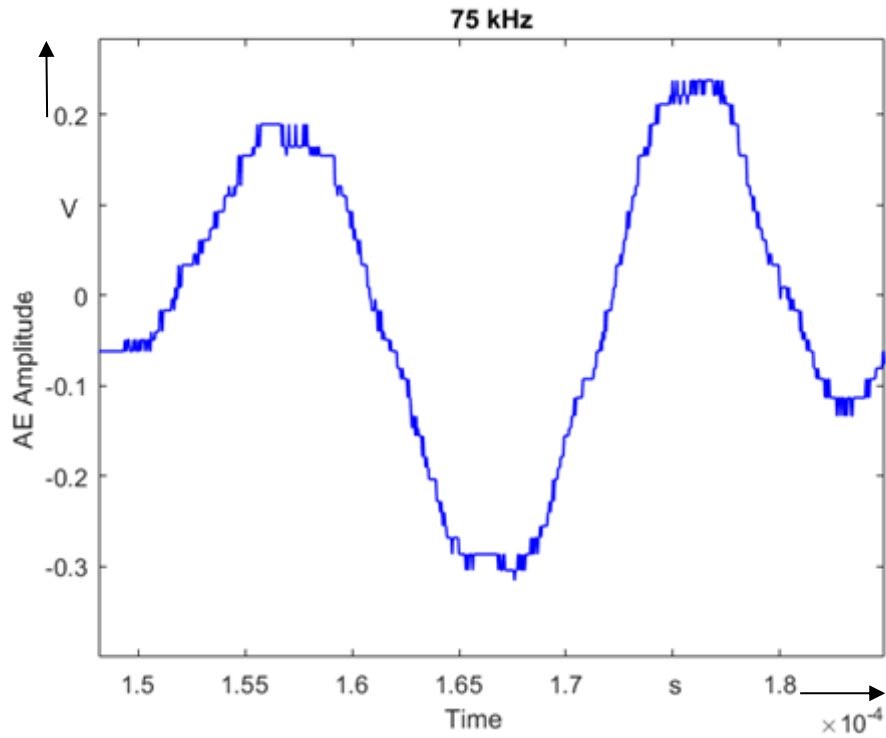


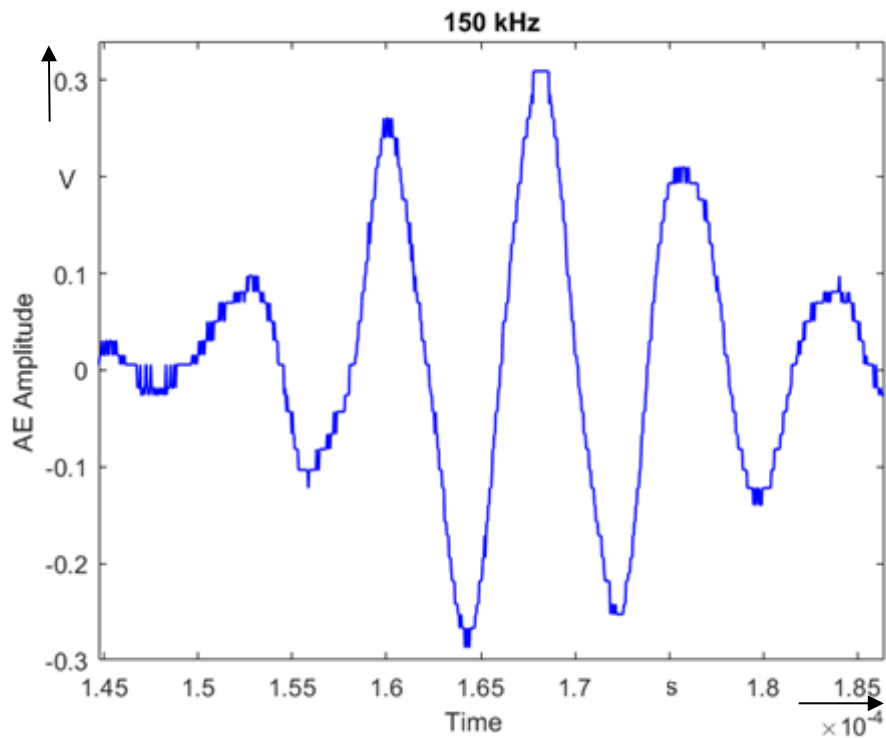
Fig. 3.3: UHF signals of two electric signals captured by oscilloscope

3.1.2 The effect of wavelength on accuracy

The time difference between each acoustic sensor could determine the location of the PD inside the transformer.



a)



b)

Fig. 3.4: Zoomed pictures of single AE burst during a single and same PD activity captured from

- a) 75 kHz AE sensors
- b) 150 kHz AE sensors

The captured oscillations of a single PD event from 75 kHz and 150 kHz peak frequency AE sensors are shown in Fig. 3.4. By considering the traveling speed of acoustic waves inside oil about 1400 m/s, for 150 kHz and 75 kHz AE sensors, respectively. An AE burst from PD signal consists of almost 5 acoustic wave oscillations. This means, higher frequency of AE sensor leads to a higher resolution. Smaller acoustic wavelength means less distance between each oscillation, and this increases the resolution of localization by AE method, respectively.

The effect of overlapping in last chapter shows the effect of lower attenuation of lower frequency parts of AE signals on AE measurement. It could be concluded, by using a combination of both 75 kHz and 150 kHz sensors, lower attenuation of acoustic signals for better detection using 75 kHz sensor and high resolution for localization using 150 kHz sensor could be achievable.

3.1.3 Results

Electric and acoustic signals during PD events have been recorded and arranged in terms of maximum and average acoustic amplitudes from different AE sensors and average and maximum electric signals captured by conventional electrical device.

Table 3.1: Recorded AE signals and electric values from different PD events

Ave PD (pC)	75 kHz peak frequency sensor						150 kHz peak frequency sensor					
	Number of Hits	Max Freq. of AE signal (kHz)	Min Freq. of AE signal (kHz)	Ave Freq. of AE signal (kHz)	Max AE (dB)	Ave AE (dB)	Number of Hits	Max Freq. of AE signal (kHz)	Min Freq. of AE signal (kHz)	Ave Freq. of AE signal (kHz)	Max AE (dB)	Ave AE (dB)
0-50	10	109	23	78	66	54	10	286	15	98	63	52
50-100	5	116	63	100	69	55	4	134	14	75	67	56
100-150	31	115	7	84	78	62	30	286	18	114	80	62
150-200	51	118	7	77	78	68	50	256	18	120	83	67
200-250	599	159	71	97	92	71	600	151	4	129	87	68

To evaluate the acoustic activity of different PD charges, the electric stress on the tip of the needle has been changed by changing the applied voltage after one minute of measurement. By increasing the input voltage (ΔV_a in eq. 11), PD apparent charges would be also increased. Various parameters of acoustic and electric signals have been recorded and evaluated.

Table 3.1 shows the results at different PD charges via changing the applied voltage and measurement for one minute. To increase the PD charges, the applied voltage has been increased. It shows the range of average of PD charges (Ave PD) in pC, number of AE signals (Number of Hits), maximum frequency of the AE signals in kHz (Max Freq. of AE signals), minimum frequency of the AE signals in kHz (Min Freq. of AE signals), average frequency of the AE signals in kHz (Ave Freq. of AE signals), maximum signal of the AE signal in dB (Max AE) and average signal of the AE signal in dB (Ave AE) after one minute of measurement at each voltage level. This procedure has been repeated for five times to gather more information about acoustic and electric signals. This table shows also how the average AE frequency of the electric PD activity varies by using different AE sensors. Table 3.1 shows an increase of maximum and average AE by increasing the average electric PD signals however the high number of hits with low AE dB could decrease the AE signals in average. To have a better understanding of this correlation, the data has been collected and presented in line graph Fig. 3.5.

3.1.4 Discussion

AE sensors with different acoustic peak frequencies could have resonances at different frequencies. That is why each sensor measures the frequency at its own peak frequency (Table 3.1). AE signals could be captured from PD events with 2 pC apparent charge.

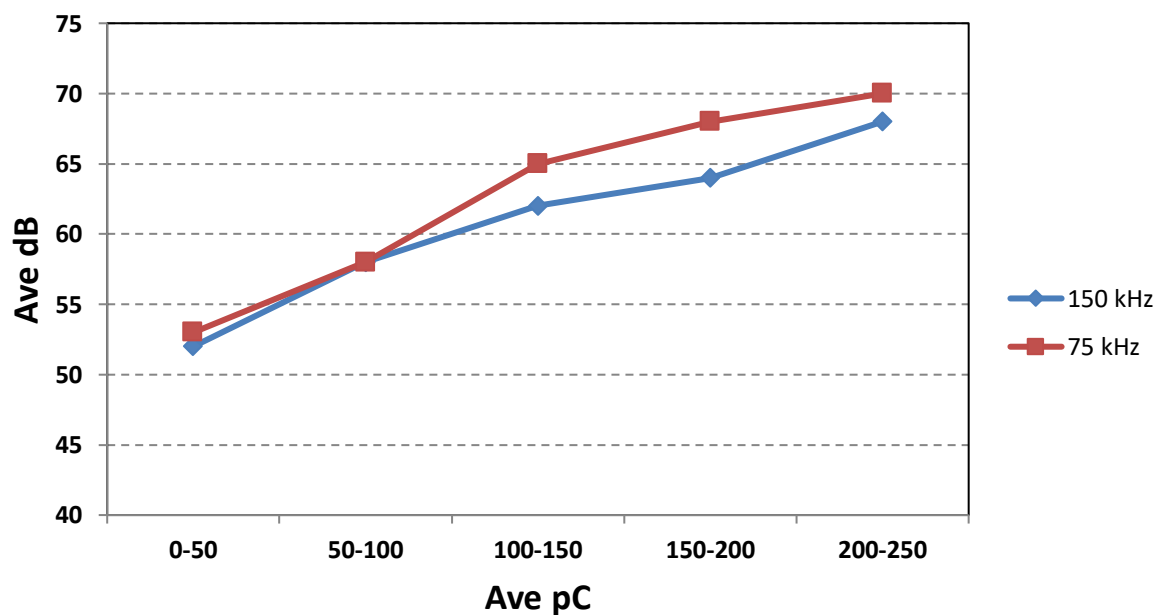


Fig. 3.5: Average AE signals in dB of 75 kHz and 150 kHz sensors as function of the ranges of electrical measured PD in pC

Fig. 3.5 shows a proportional correlation between acoustic amplitudes and electrical measured average apparent charge recorded by both AE sensors at different peak frequencies. The AE signal results in Table 3.1 at given average electric apparent charge range were repeatable. Higher magnitude of the AE signals captured by 75 kHz peak frequency sensor compared to the 150 kHz peak frequency sensor at higher apparent charges could be due to lower attenuation of lower frequencies (Chap. 1.4.4) [57]-[61]. The most probable reason of higher AE signals during the discharges at higher apparent charges could be that more heat energy released by PD and as the result more blast waves are generated (more information about blast waves could be found in Chap. 1.4.5).

3.2 Surface discharge

To create surface discharges the high voltage electrodes are placed on the surface of the aramid pressboard (without oil gap as shown in Fig. 2.19). As it has been described in chapter 1.1.2 contaminations on the surface of the barrier (pressboard), moisture level of the pressboard, the electric field stress etc. could lead to surface discharges on the insulation surfaces and these surface discharges could cause failure in transformers. One of the biggest advantages of investigation of surface discharges would be that no mechanical barrier between PD location and AE sensor exists as it could be seen in Fig. 2.19.

3.2.1 Results

To investigate the surface discharges the test setup as illustrated in chapter 2.6 was used. The acoustic signals were measured and evaluated within one minute with different electrodes at 1.5 nC to 1.7 nC average apparent charges at 40 cm distance between the source and the AE sensor.

Fig. 3.6 shows number of AE bursts, the maximum and average AE amplitude (dB) during a continues discharge activity of about 1.5 nC - 1.7 nC measured with electrical PD measurement system in one minute.

Because of the large number of electric PD charges at each stage, this evaluation could be done independent of the number of PD apparent charges at each electrode arrangement. At very high electric stress (5 μm needle) no AE signal and at high electric stress (40 μm needle) only 14 AE signals in one minute could be detected. The maximum and average amplitude of the acoustic signal is near to the level of the acoustic noise which here considered as 40 dB. By decreasing electric stress (increasing diameter of the electrodes) the number of AE bursts increases. Because of logarithmic figure and DSP limitation (chapter 2.3.2), the changes in number of AE bursts from 8 mm up to 20 mm electric ball is not obvious in Fig. 3.6. Also, the average AE signals shows almost no deviations at different electric stresses, the reason is the high number of AE bursts with low AE amplitude.

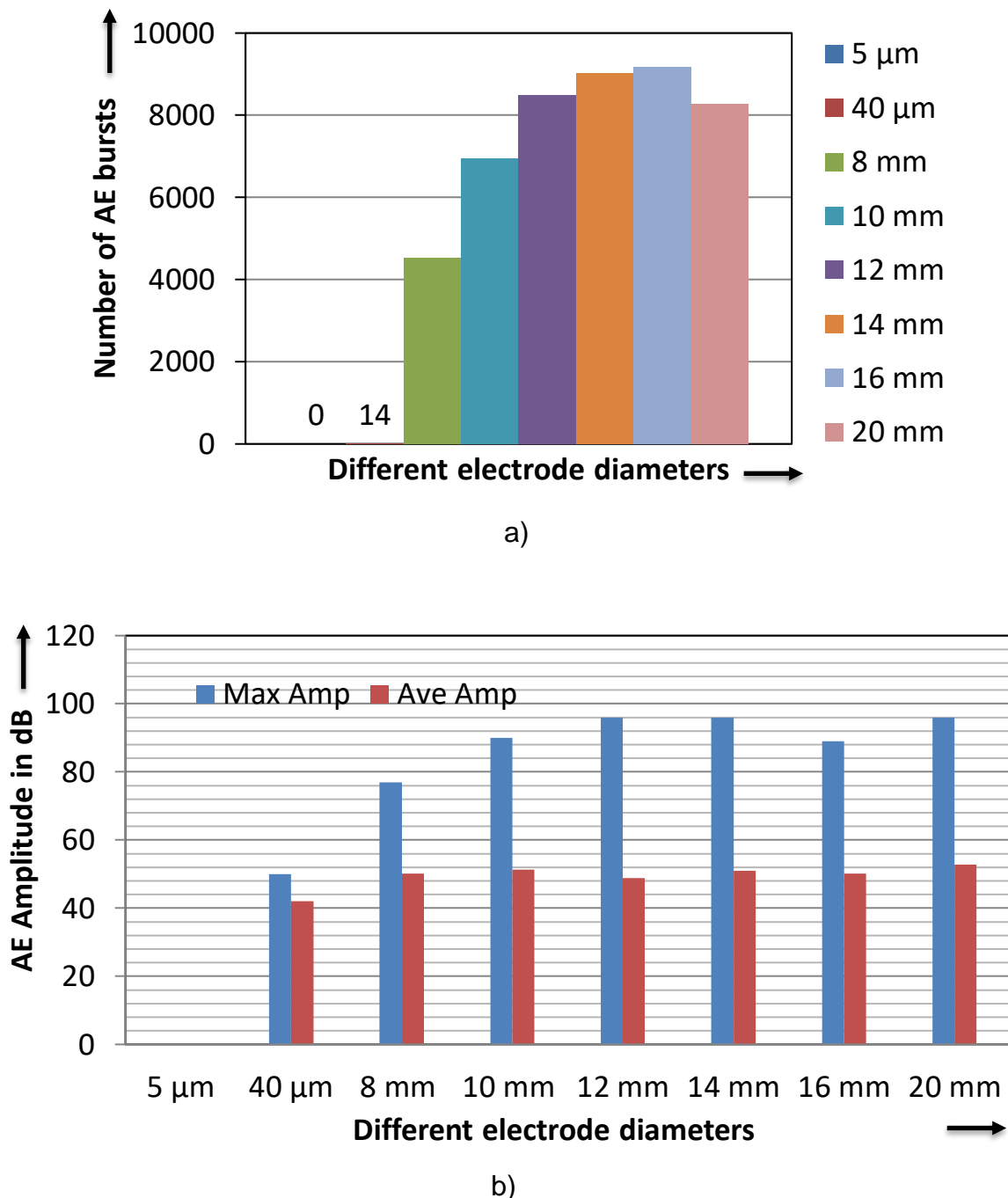


Fig. 3.6: One minute measurement

a) Number of AE bursts

b) AE maximum and average amplitude in dB at 1.5 - 1.7 nC PD apparent charge

Fig. 3.7 shows the electric and acoustic signals captured by oscilloscope during 5 second. The input voltage was constant during the measurement. The dark blue (higher concentration) colour shows more number and light blue (lower concentration) shows less number of the signals. It revealed an increase in electric signals during PD activity, but the AE signals were not followed the same pattern as electric signals. The most probable reason of increasing the electric signals in Fig. 3.7a could be the carbonization. Followed by the same hypothesis, the AE signals could be decreased by increasing the carbonization. The carbonization could increase the conductivity and as the result decrease the temperature generation by electric PD activity. There are also some other hypotheses which could affect the AE signals. First, the PD activity is

deep inside the solid insulation material which could decrease the AE signals due to mechanical attenuation. Second, the high number of PD activity could decrease the AE signals by destructive interferences. Third, is the possibility of creation of dielectric barrier discharge (DBD) during PD activity. All these hypotheses would be investigated and discussed in more detail latter.

3.2.2 Discussion

AE signals created by PD were investigated via two different AE sensors in the frequency range between 30 kHz and 400 kHz at different electric stresses on impregnated pressboard. At very high electric stress the AE amplitude decreased below the noise level (almost no AE signal could be captured). It has been tried to find a name for this phenomenon, which would be simple as possible and illustrate the phenomenon as well. This kind of PDs was denoted as “**silent PD**”. According to these two different categories of PD has been recognized namely **silent** and **non-silent PD**.

With this novel definition of the PD the possibility increases to investigate further the relation between electric and acoustic PD as well as the relation between surface discharges and internal discharges. Decreasing the electric stress by choosing bigger electrode diameters, increases the amplitude of the acoustic emission signals. This investigation shows that, the acoustic emission signals not only depend on the magnitude of the PD apparent charge, but also on the type of PD (silent or non-silent). Due to the higher priority given to the highest sensitivity rather than covering the entire range of electric and acoustic signals, the saturation level of 8 bit or even 10 bit electric measurement devices, such as an oscilloscope, may be reached.

It seems that at high electric stress the possibility of creating silent PD is higher. Then increasing conductivity (σ) could decrease the temperature losses I^2 / σ where I is the PD current and consequently decrease the AE signals generated by temperature. Assuming the direct relation between the carbonization tracks generated by PD activity and electric conductivity (σ), carbonization on the surface could have a direct effect on creation of silent PD. This shows a fundamental difference between electric and acoustic measurement since silent PD could be measured via electric PD measurement and not by AE measuring technics.

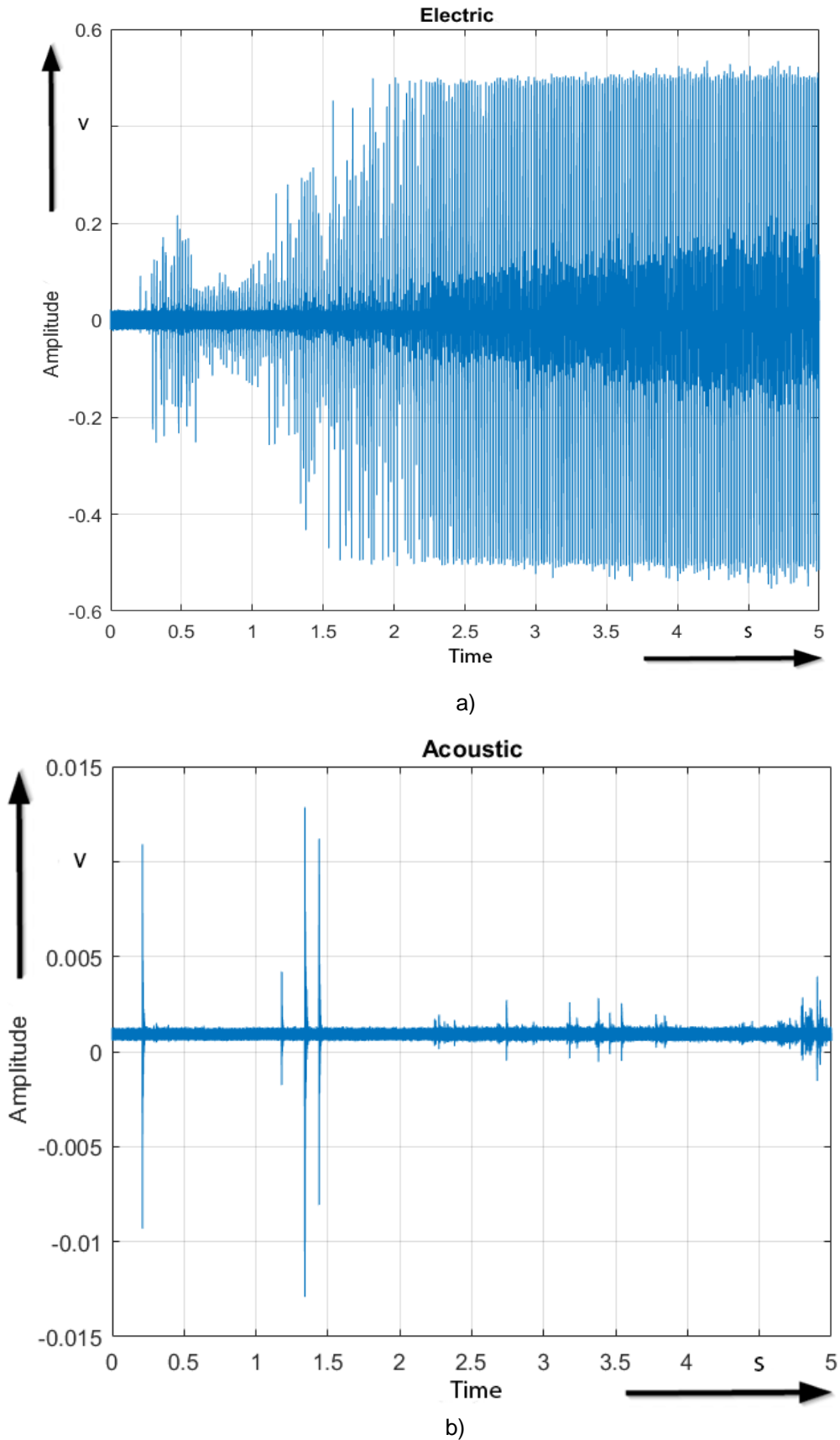


Fig. 3.7: Captured signals during 5 seconds by oscilloscope:
a) Electric Signals
b) Acoustic signals

3.3 Effect of carbonized patterns on AE signals

Existence of the carbonic bond in carbonyl group of cellulose and peptide bond in aramid paper/pressboards can lead to the carbonization at high temperature on paper/pressboard insulation materials. Carbonization could change the resistivity as well as the behaviour of the discharges on insulation materials [74]. To investigate the effect of carbonization after surface discharge on AE generated signals, the same test setup as illustrated in chapter 2.6 was used. This investigation is for detailed understanding of creation of silent and non-silent PD, depending on carbonization effect of electric discharges and for finding the relation between electric and acoustic PD signals.

Carbonized patterns are a random procedure which depends on several electrical and mechanical conditions. Electrons during discharge activity would prefer lower resistivity paths. Due to lower resistivity of the carbonization paths, the first random carbonized paths could determine the paths of the electrons in the following discharges. As it described in Eq. (12), the apparent charge during the discharge is related to the electric field. In addition, the secondary electron emission avalanche, and the release process of absorbed gases in solid insulation are known as two main contributors leading to the development of surface discharge which look like branches. The structure of the branches depends on several factors like the molecular structure of the pressboard and electric field stress. Changing on voltage stress could create different carbonized paths on the surface of the pressboard. This is due to starting probability of carbonization creation. In addition to voltage stress, the number of PD events could influence the creation of tree and branch shape carbonization [71] - [73]. To investigate the effect of different carbonizations on AE signals, different voltage courses is defined.

3.3.1 Voltage courses

Voltage changes on transformers could be generated by switching operation or lightning. To investigate the influence of different voltages on the AE signals created by PD, two different voltage courses on different samples are implemented (Fig. 3.8). PD inception voltage (PDIV) represents a threshold of the electric stress [102]. Fig. 3.8 shows the applied voltage for two different voltage courses. To ensure the existence of the PD activity during each voltage course, the voltage courses start at a voltage above PDIV. The PDIV at all different samples is about 14 kV. The first course represents a stepwise increase of the applied voltage, followed by a decrease and again an increase. Each step lasts five minutes. The shape of the voltage course represents a temporary overvoltage with a short-time reduction of the applied voltage in order to evaluate the PD behaviour under such an overvoltage. The increase of the applied voltage after the reduction should show the behaviour of the PD under electric stress during offline PD measuring procedure on transformer.

Reduction in electric stress could create new branches [72] and carbonization branches increase the conductivity and degradation of the surface [82]. The second voltage course starts with new sample (like first voltage course) and at a voltage level above PDIV and comprises an increase of the applied voltage without a short-time reduction, which eliminate the reduction in electric stress.

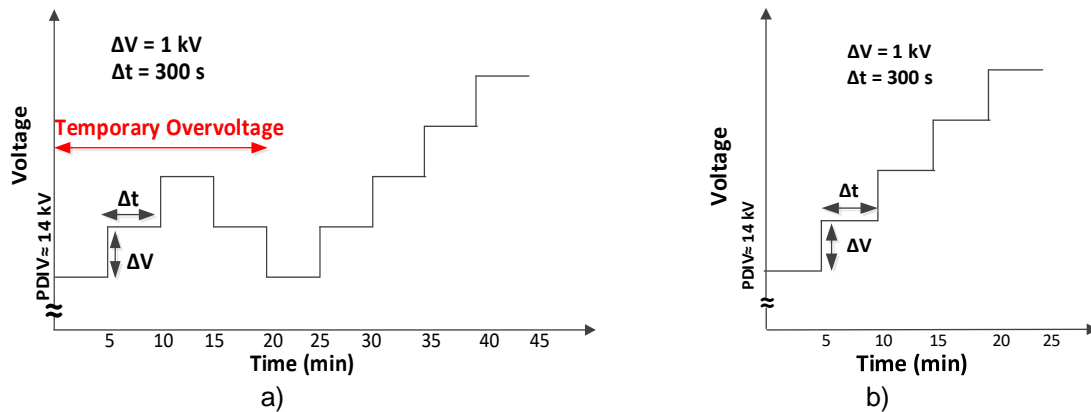


Fig. 3.8: Schematic view
 a) First voltage course
 b) Second voltage course

The results from these two different voltage courses should show the influence of the voltage change on the creation of carbonized patterns as well as on the AE signals. In all voltage courses the applied 50 Hz voltage was increased by 1 kV each 5 minutes. During each voltage level, electric and AE signals from PD were recorded. AE signals were recorded by DSP and electric signals by ICM System Power Diagnostic devices. Furthermore, VHF signals, and AE signals were recorded by digital oscilloscope to investigate the signals in more details.

Finally, the carbonized tracking patterns on the surface of the aramid paper were scanned and compared by using Matlab image processing program (for more information please refer to reference [80]) to evaluate the patterns at silent and non-silent PD, because both types of PDs (silent and non-silent PD) show electric PD signals.

3.3.2 Carbonized patterns

The voltage changes could have some influences on the carbonized surface. Fig. 3.9 shows the surface of the papers after the voltage tests.

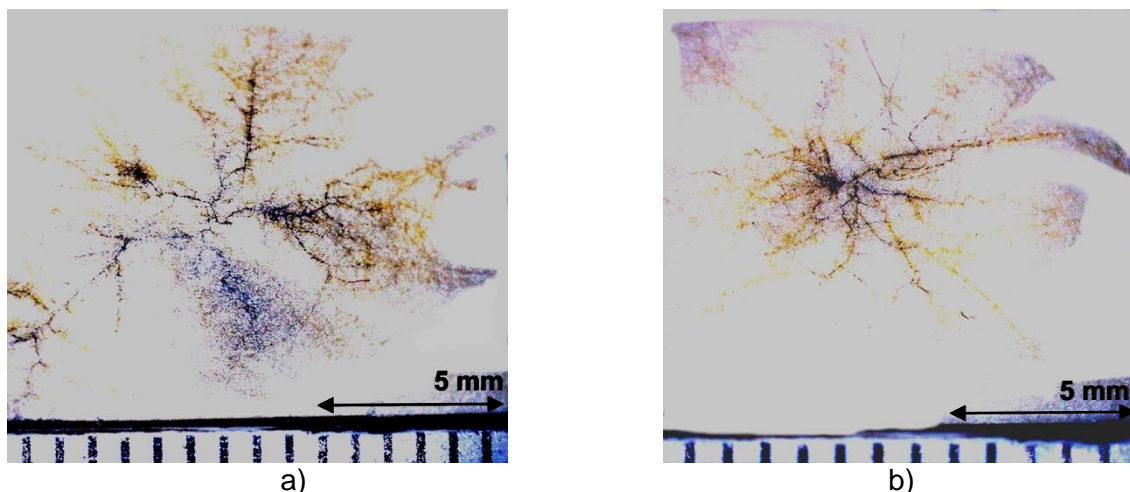


Fig. 3.9: Surface carbonized marks
 a) paper at first voltage course
 b) paper at second voltage course

To compare the carbonized patterns the following technic has been used. The length of carbonization has been measured from the position of the needle by placing a string along the traces (deviation <0.5 mm).

To measure the area of the carbonized tracks, Matlab image processing was used. 1 cm² black area (Fig. 3.10) has been created and measured by Matlab to validate the area calculated by Matlab image processing. The measured value in Matlab was 0.997 cm², which shows less than 1% deviation.



Fig. 3.10: Validation of Matlab Image processing by measuring 1 cm² black area

Table 3.2 shows a summary of the measurements. The area of carbonized tracks is about 167 % larger at the first voltage course compared to the second one and the maximum lengths of carbonization is about 24 % larger for the first voltage course due to longer voltage stress. The dependency of carbonization length on electric stress and branches (area of carbonization) on partial discharges has observed in [73].

However, the material properties and space charges can also influence the creation of different carbonized tracks on the surface [81]. A voltage stress change and a longer duration increase moderately the length of the carbonized tracks but strongly the area of the carbonization, which results in an increase of the conductivity and degradation of the surface [82].

Table 3.2: Results of voltage courses regarding length and area of carbonized tracks

Voltage course	Temporary Overvoltage (minutes)	Overstress (minutes)	Average Maximum Length	Average Area of Carbonization
First voltage course	20	25	7.3 mm	1.15 mm ²
Second voltage course	No	25	5.9 mm	0.43 mm ²

3.3.3 Acoustic emission signals

Because of very random AE values compared to the electric PD values at surface discharge arrangement, only maximum AE signals has been compared with electric signals. The average value of AE signals could be reduced by large number of low AE signals and as result important information about maximum AE values would be missed. Number of Acoustic emission (AE) signals and electric PD events are shown in Fig. 3.11.

The reduction of the applied voltage has no influence on the electric signal of PD because of lower extinction PD voltage compared to PD inception voltage and the later increase of the applied voltage leads to a moderate increase of the number of electric PD signals compared to the increase at the beginning of the test. The characteristic of the AE number is different compared to the number of electric PD as shown in Fig. 3.11.

It should be noted, that superposition could increase the errors and decrease the counting of electric PD pulses depending on the pulse repetition rate of the input pulses [98], superposition could also influence the number of AE signals which discuss in more detail in chapter 4.1. However, overcounting the AE numbers has been eliminated as much as possible by using proper AE sensors and DSP device. HDT and HLT delays of DSP device could eliminate the overcounting (more information in chapter 2.3.2).

The AE number is high at the beginning of the first voltage course test and drops then continuously even if the voltage increases from minute 25 to 45. Only at the highest voltage level at minute 40 the AE number increases again. Second course in Fig. 3.11b shows again a higher number of AE signals at first 5 minutes compared to the second 5 minutes. Since the voltage stress after 25 minutes of first and after 5 minutes of the second voltage courses are the same, the comparison of first and second voltage courses would be done after 25 minutes of first voltage course and 5 minutes of second voltage course.

Fig. 3.12 shows the maximum of the AE signals and the average of electric PD signals. For the first voltage course the electric PD signal follows almost the course of the applied voltage, whereas the AE signals have a peak of the maximum value at the first voltage stress, followed by a decrease of the maximum value. At the following increase of the voltage the maximum value of AE signals remains constant below 65 dB.

Comparing the AE results of first voltage course after 25 minutes and second voltage course shows much lower AE signals at first voltage course even at the same voltage stress and PD numbers compared to second voltage course. This shows the effect of previous stress (carbonization) at first voltage course on AE signals reduction.

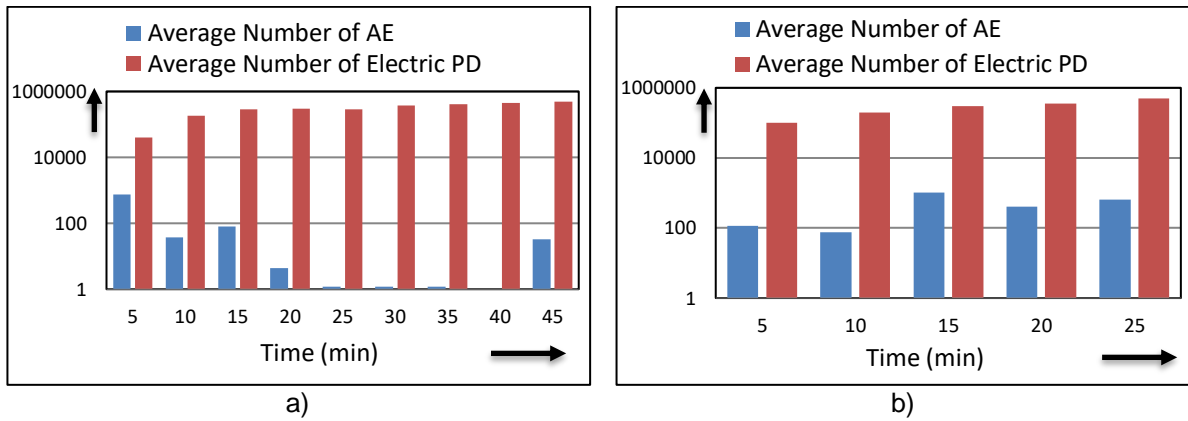


Fig. 3.11: Average number of AE and electric signals (average value of each 5 minutes stage):
 a) first voltage course
 b) second voltage course

Within the second voltage course the electric PD signals increases strongly with increasing voltage, whereas the AE signals show tendentially a linear increase from 63 dB up to 90 dB. Maximum AE shows lower AE values at first voltage course after 25 minutes compared to the second voltage course. Low AE signals with the same magnitude of electric charges, show the non-direct relation between acoustic and electric signals of PD activities. However, the level of carbonization could help to find this relation.

Lower AE numbers and lower maximum AE signals after 25 minutes of first voltage course compared to the second voltage course shows the independency of AE signals to electric PD signals and voltage stress. Lower AE signals could be caused by carbonization during temporary overvoltage; however, the AE signals have been increased at 45 minutes with increasing the input voltage to the highest level. This could be caused by creation new traces of carbonization at high electric stress and not following the old carbonization traces. This shows that the PD signals not always follow the AE signals and prehistory of insulation materials could have influence on AE signal creation.

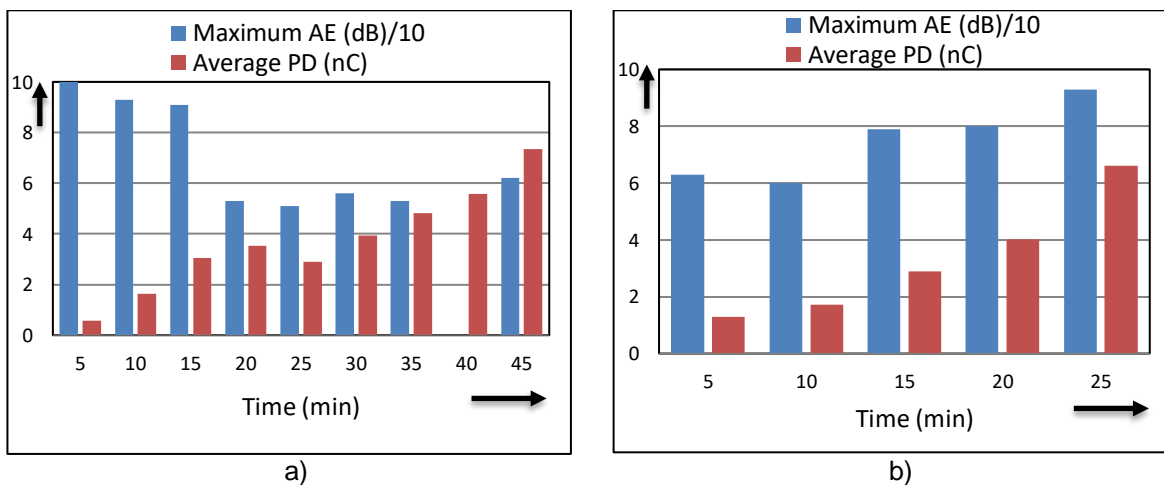


Fig. 3.12: Maximum values of AE signals in dB and average values of electric signals in nC for:
 a) first voltage course
 b) second voltage course

3.4 Summary

In contrast to corona in oil, the surface discharge showed no direct relation between AE and electric PD signals. The acoustic emission and electric signals produced by discharges of a point-plane electrode on the surface (surface discharge) of different oil-impregnated aramid pressboards are measured. AE sensors mounted on the outside of the experimental tank and electric PD measuring system were used to measure the AE and electric PD signals. Numbers, maximum amplitudes and average amplitudes of acoustic bursts and electric signals are measured via a digital signal processor device and ICM device. The tracking patterns on the surface of four different aramid pressboard insulations are compared together by using Matlab image processing program (Table 3.2). By experimental results, tracking patterns on the surface of the bulk impregnated pressboard insulation have different effects on the acoustic emission and electric PD signals.

Acoustic emission signals decrease dramatically on carbonized pressboards and cause so called silent PDs. However, because of the stochastic nature of this process the AE signals did not follow the electric PD and voltage behaviour at some stages of applied voltage. To have almost same voltage stress and electric PD activity, the results of first voltage course after 25 minutes has been compared to the second voltage course from the beginning. Changing the voltage stress have influence on creation of different carbonized patterns and influences the AE signals at different voltage courses. This shows lower AE signals at prestressed situation in first voltage course compared to second voltage course without prestressed situation. Electric apparent charges of the PD followed almost the applied voltage courses at all stages, however this could be increased slightly by carbonization during last stages of first and second voltage courses.

Comparison of the electric and acoustic magnitudes of the two different voltage courses shows that, despite higher AE signal at the beginning of the process, the magnitude of the AE and PD signals varies afterward even at the same voltage. This difference could be caused by different random starting point of carbonized tracking which has an influence on the behaviour of the AE signals. Very large difference between the number of electric and acoustic signals proves the existence of silent PDs during a PD activity.

The importance of this phenomenon is not only for detection of PD by using acoustic method, but also for localization of PD for lifetime estimation of insulation materials.

4 Silent and Non-silent Partial Discharges

The investigations in previous chapter show that in some circumstances, AE amplitudes from PDs went below the acoustic noise level even at very simple test setup without any acoustic barrier.

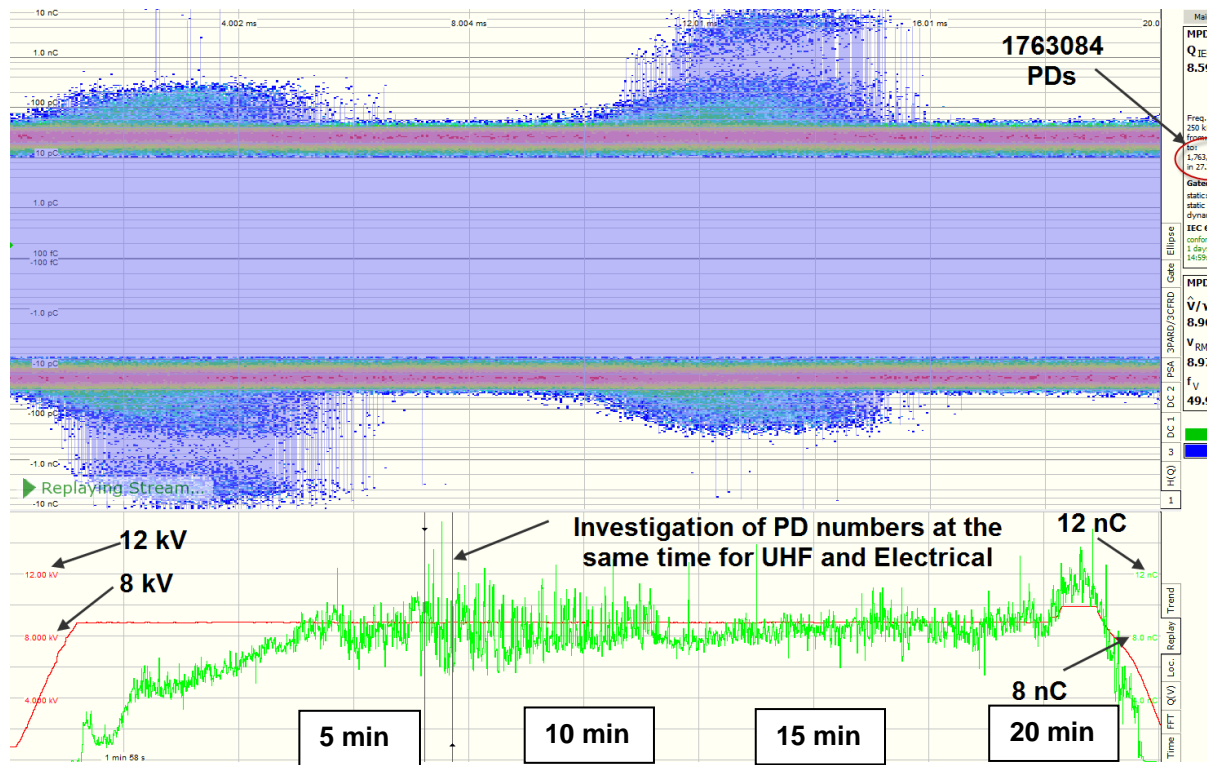
To investigate the silent and non-silent PD situations, a needle-plane arrangement inside a tank has been used. UHF signals and electric signals have been measured with Omicron MPD 600. Acoustic signals have been captured by Omicron PDL 650 (Fig. 2.19).

The input AC high voltage (20% above PD inception voltage) remains constant during the PD activity and PDs were recorded acoustically, UHF and electrically continuously. Fig. 4.1 shows the number of UHF and electric PD (with coupling capacitor) events in a discharge activity without any interruption for 20 minutes. The number of UHF signals is very near to the number of the electric PD signals higher than 10 pC (above 1700000 events), which proves the sensitivity of UHF sensor about 10 pC. Electric PD measurement level set on 10 pC for coupling capacitor and UHF measurements.

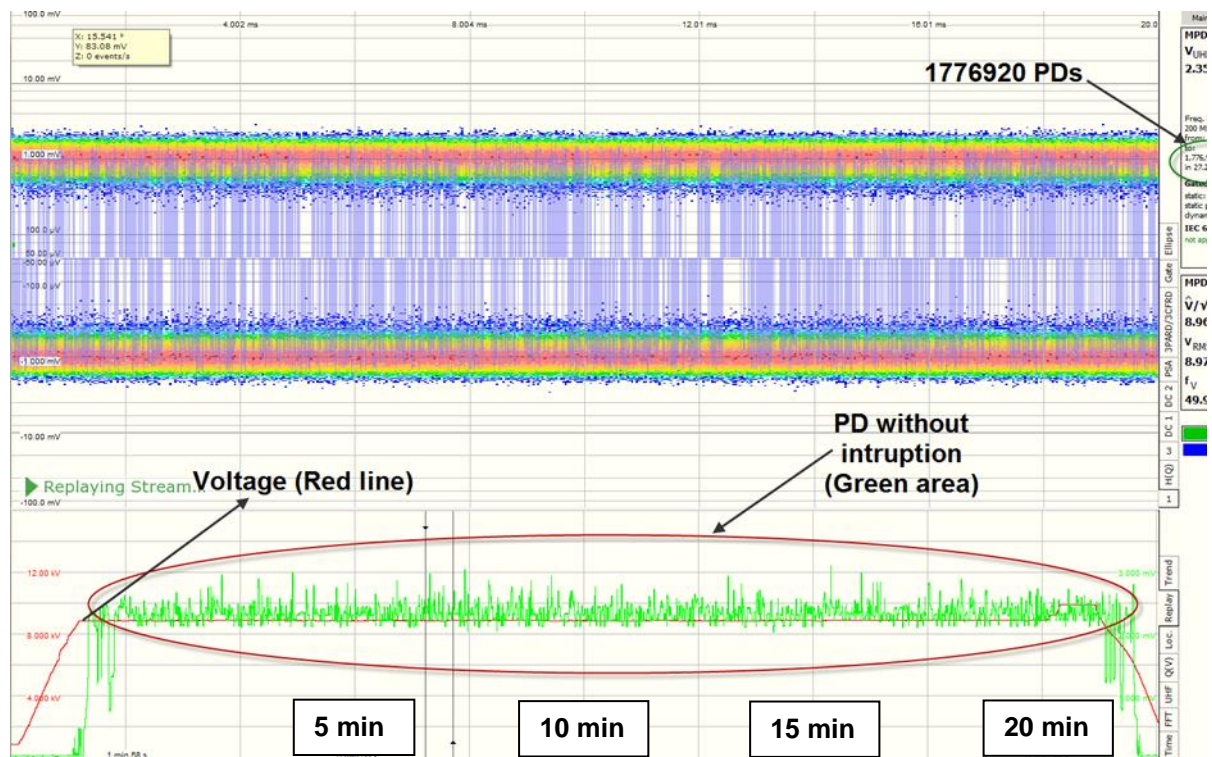
In chapter 1.3 different localization methods as well as acoustic localization were illustrated. Uncertainty in localization could be happened regarding to lack of information in part of the AE sensors due to very low AE amplitudes. However, at transformer site the electromagnetic interferences from high electric activities could also affect the localization, but this issue could be solved by putting the measuring devices in a proper faraday cage (UHF sensors could have the benefit of using transformer oil tank as EMI shield). Electric interferences (surround noises) from outside the test sample have been eliminated during laboratory test by using proper test cell.

Since the Omicron PDL 650 Device is designed specially to localize the PD source by measuring the AE signals, the localization of PD source beside measuring the AE signals are measured. Fig. 4.2 shows the zoomed in picture of AE signals and localization of PDL 650. The AE signals magnitude would be automatically adjusted in mV based on maximum amplitude of the input AE signal and presented in 10 ms intervals. Environment noise level has been measured before measurement (around 10 mV) and the AE trigger has been set on 20 mV. The cone shape structures represent the AE sensor location (Fig. 4.2b). The location of PD would be calculated based on time delay between the AE signals (Fig. 4.2a) captured by AE sensors mounted on the tank (Fig. 4.2b). The colours of AE signals on Fig. 4.2a are the same as the colours of AE sensors on Fig. 4.2b.

The electric PD signals were almost constant during the discharge activity in 20 minutes of time (slightly increasing by the time). Omicron PDL 650 could measure 102 AE events during these PD activities. After measuring over 100 AE events the Omicron PDL 650 stopped measuring new events and started the processing of recorded AE events in terms of evaluation and localization. Fig. 4.3a shows the non-silent PD on the 4th event of 102 measured AE events and Fig. 4.3b silent PD on 12th event of 102 measured AE events which happened after some seconds. The magnitude of the acoustic signals decreased after time (at same voltage and same electric PD activity). One of the biggest advantages of the laboratory investigation is the visible location of the PD. The visible location of the PD in the used tank allows the determination of the uncertainty of the location.



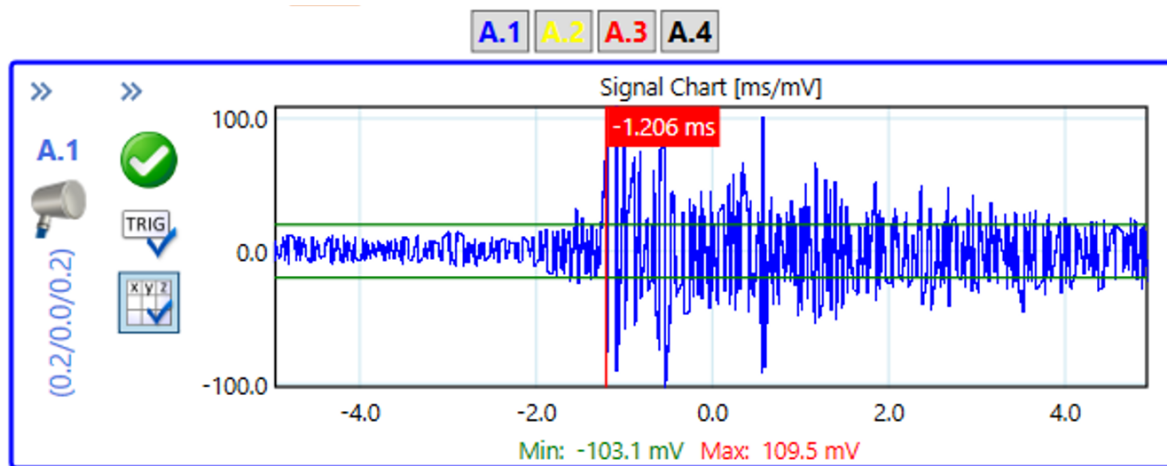
a)



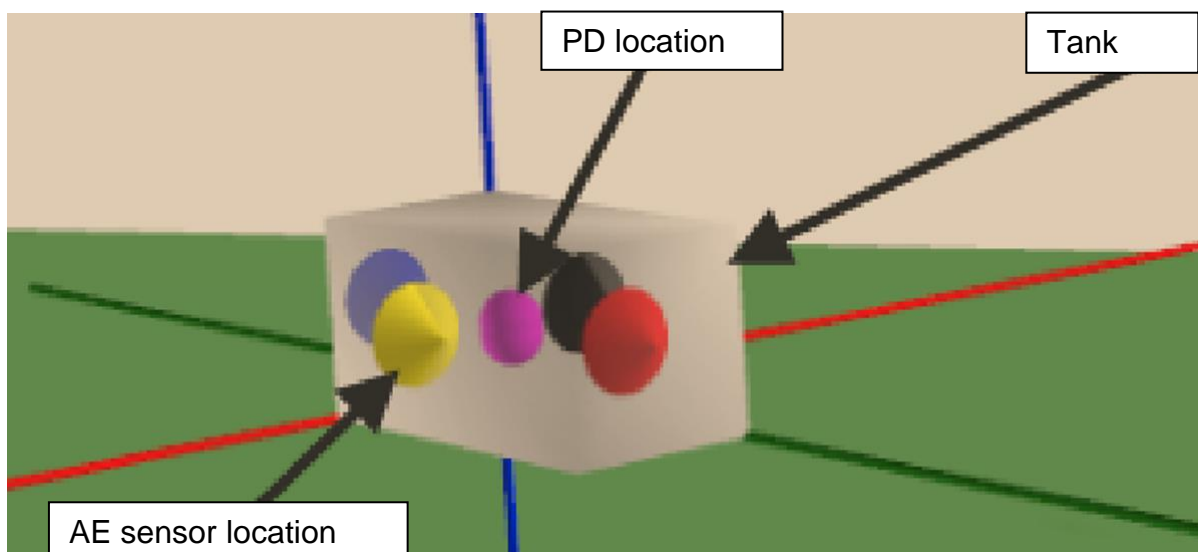
b)

Fig. 4.1: Measuring results of PD activity:

- a) UHF
- b) Electric PD



a)



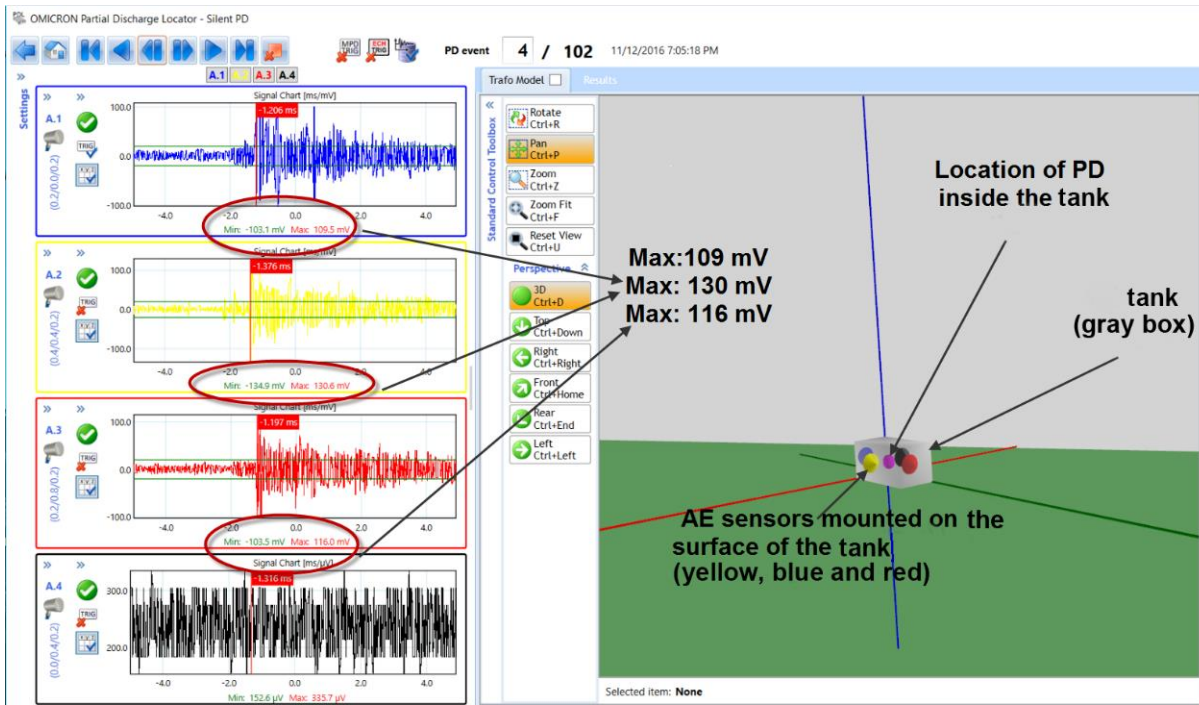
b)

Fig. 4.2: Omicron PDL 650 zoomed in picture

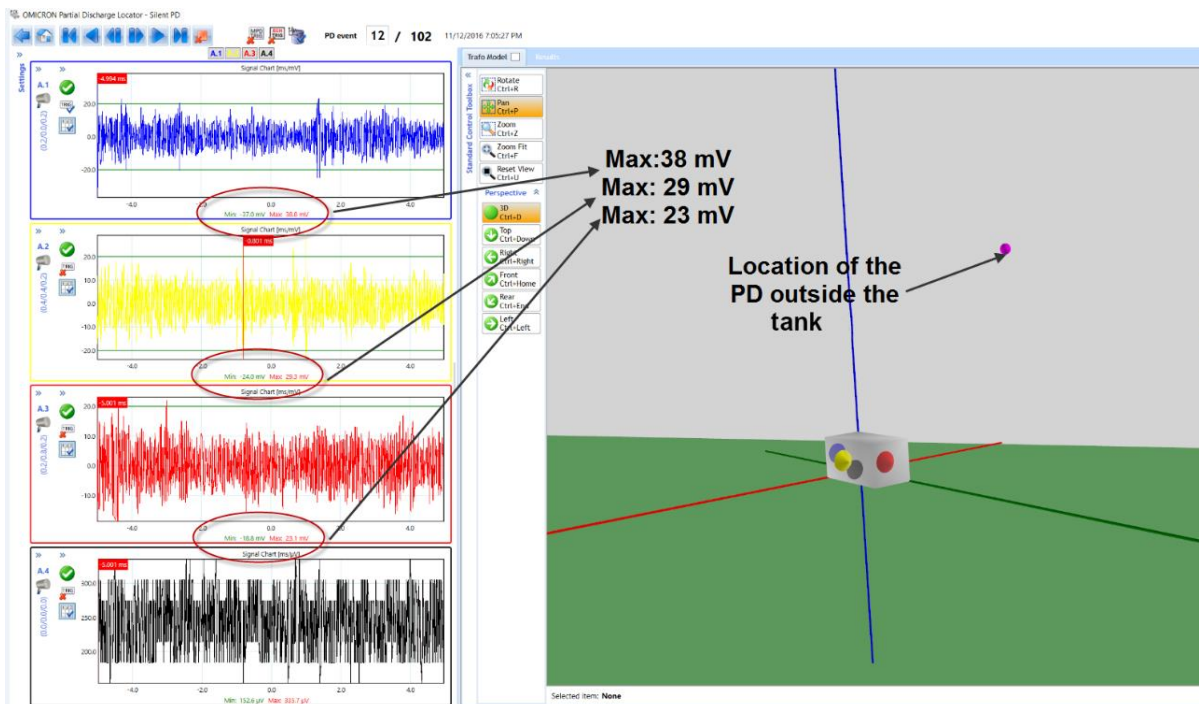
- a) AE signal
- b) Localization

Because of very low magnitude of the AE signals under the noise level (40 mV), the localization error increased dramatically at silent PD situation by showing the PD incident outside the oil tank. Therefore the Fig. 4.3b shows the location outside the tank. Even the nearest AE sensors could detect a very low AE signals (noises) at this situation, which increased the uncertainty in localization. This misleading calculation requires a software update from the manufacturer of Omicron PDL 650 device regarding blocking the silent PD for PD localization.

Fig. 4.3 shows two specific events of 102 events which has been measured during the first 10 minutes of PD activity in Fig. 4.1. The 4th event shows the PD activity inside the oil tank where the actual PD activity has been produced. Closer look on this event shows some minor differences in magnitude of the three different AE sensors mounted on the oil tank. These minor differences are caused by distance differences and slightly differences in characteristic of each AE sensor (however they are all known as 75 kHz sensor).

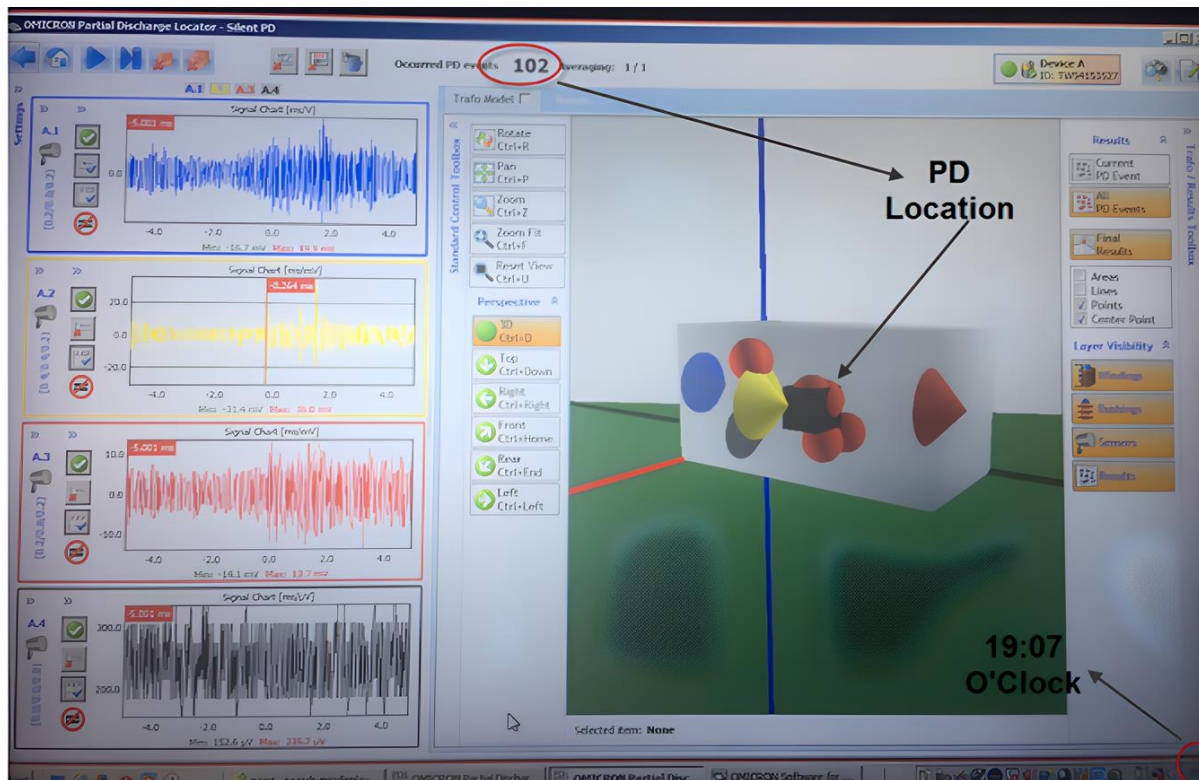


a)

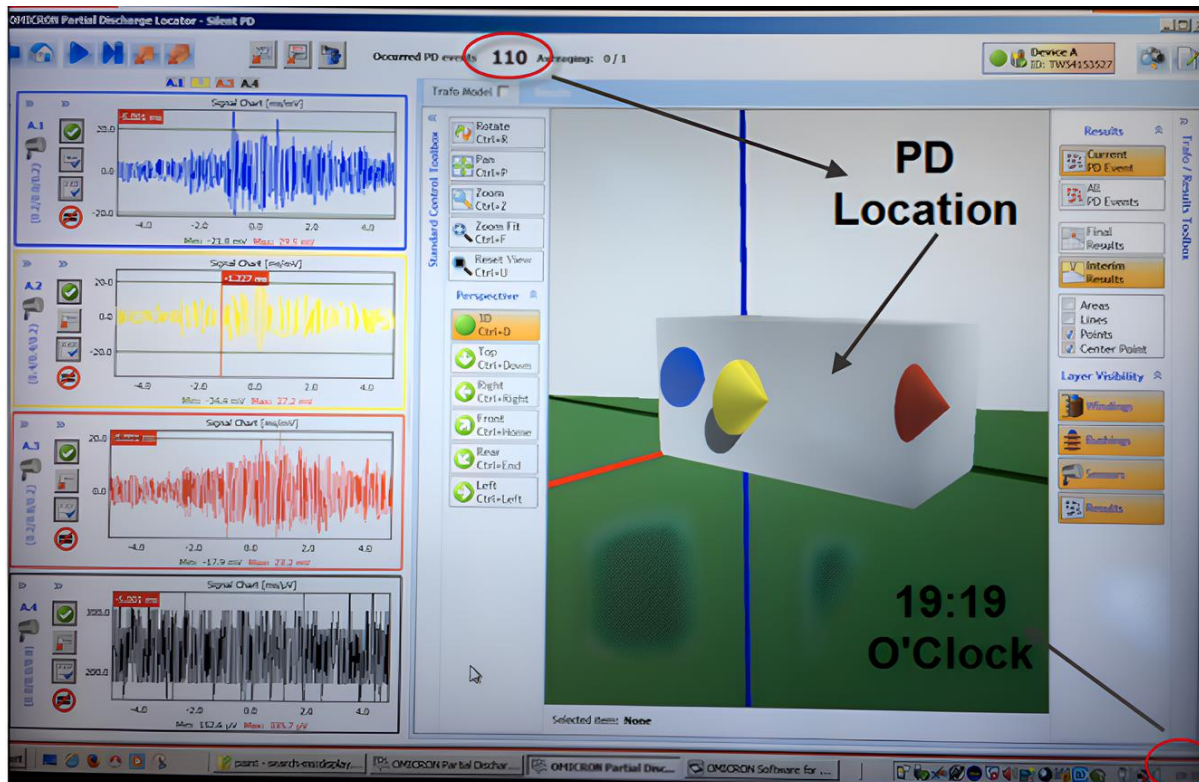


b)

Fig. 4.3: Localization PD inside the tank with Omicron Device
 a) non-silent PD
 b) silent PD



a)



b)

Fig. 4.4: PD localization of PD activity
 a) at first 10 minutes with 102 acoustic PD events
 b) at second 10 minutes with 110 acoustic PD events

In contrast to 4th event, the 12th event shows PD activity outside the oil tank, which was considered as an error caused by not proper calculation of the PD location. This error is caused by very low AE signals on one or two other channels in addition to very high noise level above the trigger level. Comparing the 4th and 12th event shows a decrease in AE signals. In addition to low AE signals, noise level has been also increased. These noises are caused by very high electromagnetic interferences of PD activities. However, the AE measurement is normally robust to EM interferences because the acoustic signals are separated from electric signals generated by EMI, but very high electromagnetic interferences could have influence on some measuring devices (such as oscilloscope and Omicron PDL 650) and AE sensors with active amplifiers.

This reduction in AE signals, could be caused by carbonization, which has been growth during the first PD events. The combination of reduction in AE signal and increasement in electromagnetic interferences could increase the statistic of wrong AE detection, which lead to wrong localization of PD signals. This shows how the silent PDs could cause uncertainty in PD localization.

Fig. 4.4 shows the total AE events during 20 minutes of discharges. The result of first 10 minutes has been presented in Fig. 4.4a and the second 10 minutes in Fig. 4.4b. The PD activity increase to 8 nC after some seconds at a constant level of the voltage (around 8 kV) and remain constant for almost 20 minutes (Fig. 4.1a). Chapter 3.3.2 shows electric PD signal development after carbonization. Fig. 4.1a shows no increasing after 5 minutes on electric PD signals, which could be because of no development in carbonization.

The first PD events normally have the highest probability of AE detection because of carbonization trace creation. This led to a correct PD localization inside the oil tank in Fig. 4.4a. The red spheres show the calculated location of PD signal after each AE signal and the black box indicates the calculated PD location based on the location via average of AE signal. In contrast, Fig. 4.4b shows no red spheres inside the tank, which means wrong localization even after evaluating 110 events. It proves that the AE signals decreased after 10 minutes and are not valid for a localization.

The PD location error has been increased by increasing the time. Fig. 4.4b shows increasing of the localization errors after about 10 minutes, which proves the existence of silent PDs at this stage with very high electromagnetic interferences.

4.1 Acoustic destructive effect

Destructive effects could reduce or even cancel the acoustic signals. In this chapter has been tried to check if silent PD (measured via electric methods) is the results of destructive effect of different AE signals generated by different PDs.

When two waves (transverse or longitudinal) have same frequency with no phase shift, the amplitudes of the waves simply add together (constructive interference). On the other hand, when the two waves with the same frequency have the phase shift of π (Pi), they cancel each other (destructive interference). Constructive and destructive interference is the fundamental behaviour of the waves (Fig. 4.5) [124].

By considering two different sources with the same frequency and same distance (Fig. 4.6), the relation of constructive and destructive interferences could be calculated as follow:

$$\begin{aligned} \text{Phase shift} &= n\lambda ; \text{ constructive interferences} \\ \text{Phase shift} &= n\lambda + \lambda/2 ; \text{ destructive interferences} \end{aligned} \tag{36}$$

Where λ is the wavelength and n is an integer which can take any number.

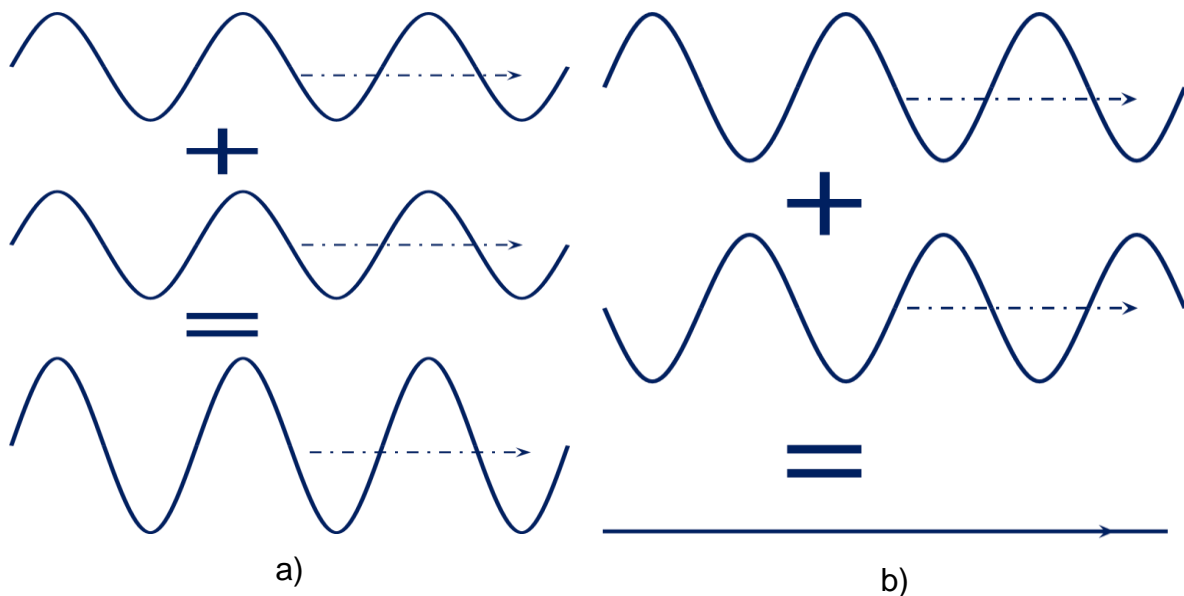


Fig. 4.5: Constructive a) and destructive b) interferences

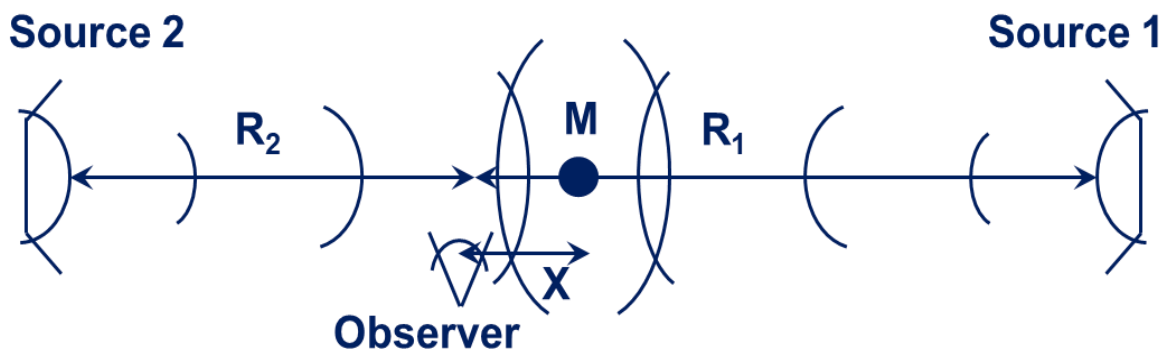


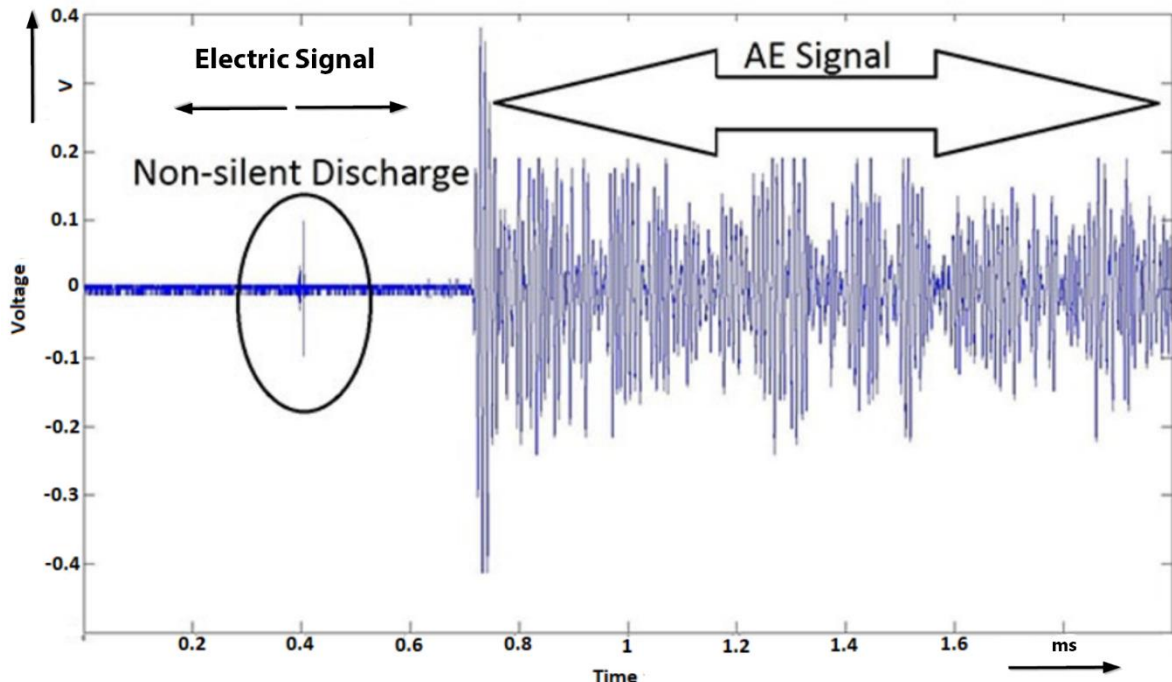
Fig. 4.6: The effect of waves in respect to the observer with a distance X from the middle

Two different examples would illustrate to prove the plausibility of creation silent PD due to destructive interferences.

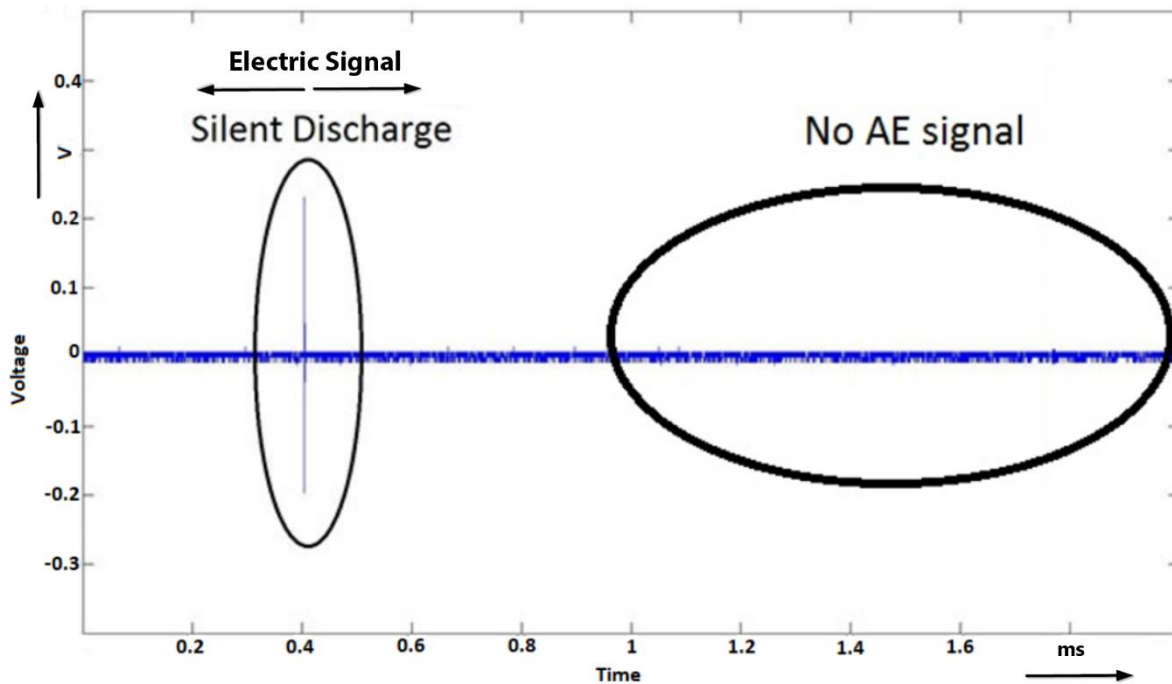
4.1.1 Example 1: Delay between two PD activities

Two sources of acoustic waves with the same frequency and specific distance from acoustic source (here PD) could create a destructive effect. The probability of this example is very low since the PD should have the same acoustic characteristics at two different events with a specific time delay. Due to one source configuration in our test

sample, the only way to have the following scenarios would be two AE signals created by two different PD activities from the same source with specific time delay. It means a time delay of $\Delta t = 1/(2 \cdot T)$ where ($\Delta t = 3 \mu s$ for 150 kHz and $\Delta t = 6 \mu s$ for 75 kHz) between PD activities. This means one PD source with $\Delta t = 3 \mu s$ or $\Delta t = 6 \mu s$ delay between two PD activities.



a)



b)

Fig. 4.7: Electric and acoustic signals
 a) non-silent PD activity
 b) silent PD activity by oscilloscope

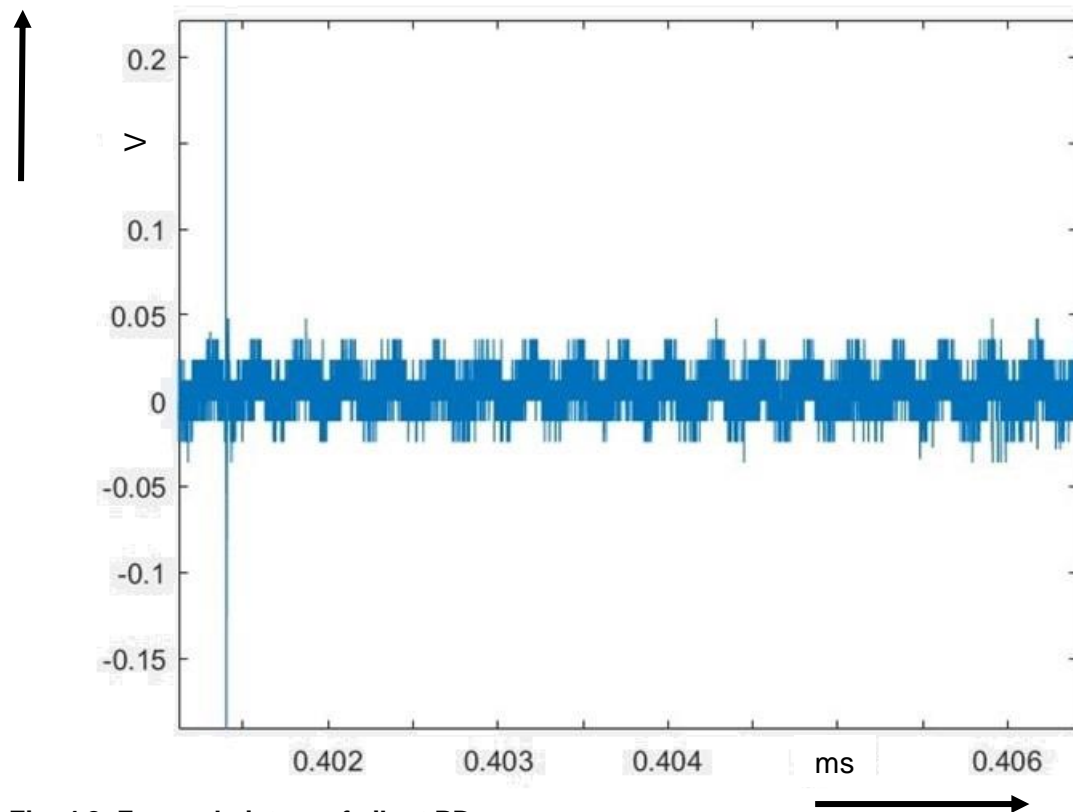


Fig. 4.8: Zoomed picture of silent PD

In addition, almost the same frequency of AE signals created by each PD activity must be also considered. Fig. 4.7 shows electric and AE signals of silent and non-silent PD activity recorded by oscilloscope both with the same time scale. Electric signals have much higher frequency than AE signals, which could be easy to identify. Fig. 4.7a shows the delay between electric and AE signal depending on the distance of the AE sensor to the PD source. Since the PD source is located at the centre of test sample with 40 cm distance to the AE sensor, there exist almost 0.3 ms time delay (1400 m/s acoustic wave speed in oil) between electric and acoustic signals in Fig. 4.7a. In silent PD situation, the same delay shows no AE signal in Fig. 4.7b. Fig. 4.8 shows the zoomed picture of the silent PD.

4.1.2 Example 2: Distance between AE sensor and PD source

AE sensor located at the exact location of $n\lambda + \lambda/2$ from the AE source could have very low amplitude because of zero crossing state (Fig. 4.5). The probability of this example is even lower than the first example since PD sources with the specific distance to AE sensor should have always the same acoustic characteristic. Chapter 3.1.4 shows how the AE sensors could affect the detected frequency of acoustic signals. In other words, AE sensors would detect the AE signals created by PD activity at the frequency range of the sensor. It means the AE sensor with 150 kHz peak frequency would detect AE signals with $\lambda_1 = 9$ mm wave length, which would be the half of the wave length detected by 75 kHz AE sensor ($\lambda_1 = \lambda_2/2$). By placing the two AE sensors (with 75 kHz and 150 kHz peak frequency) at the same distance to the acoustic source (Fig. 4.9), the possibility of creation destructive effect would be eliminated. It proves that the existence of silent PD is not due to the location of AE sensors.

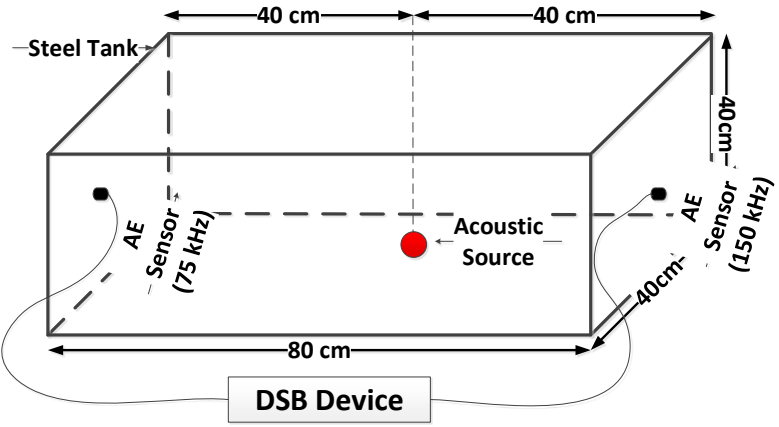


Fig. 4.9: Placing of the AE sensors on the tank

4.2 Material Attenuation

One of the main questions regarding silent and non-silent PD would be the effect of mechanical damping attenuation of the materials on the measurement results. Carbonization traces could be created below the first layers of pressboards and papers which could have influence on the AE signals captured by AE sensors. A change in location of PD inside the material could cause different damping regarding the deepness of the discharges inside the pressboards. Copper has much higher acoustic impedance than paper and oil. This high impedance differences could cause higher reflections, which could be used as sound barrier during the following test (Chapter 1.4.1).

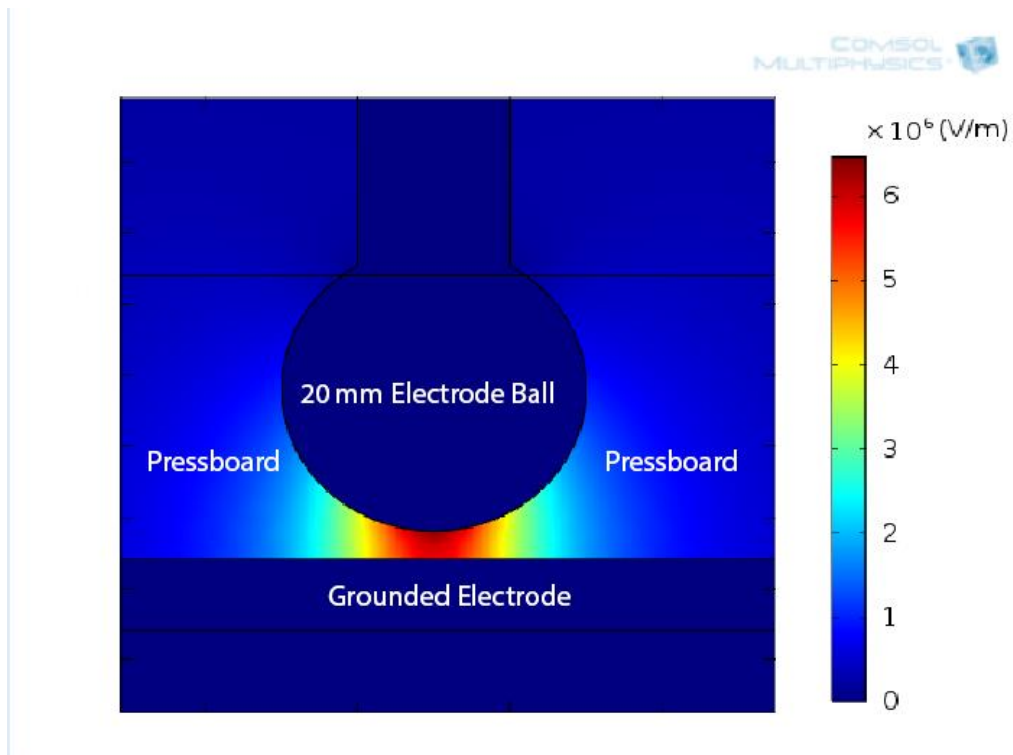


Fig. 4.10: 15 mm thickness pressboard with 20 mm electrode diameter inside the hole at the centre

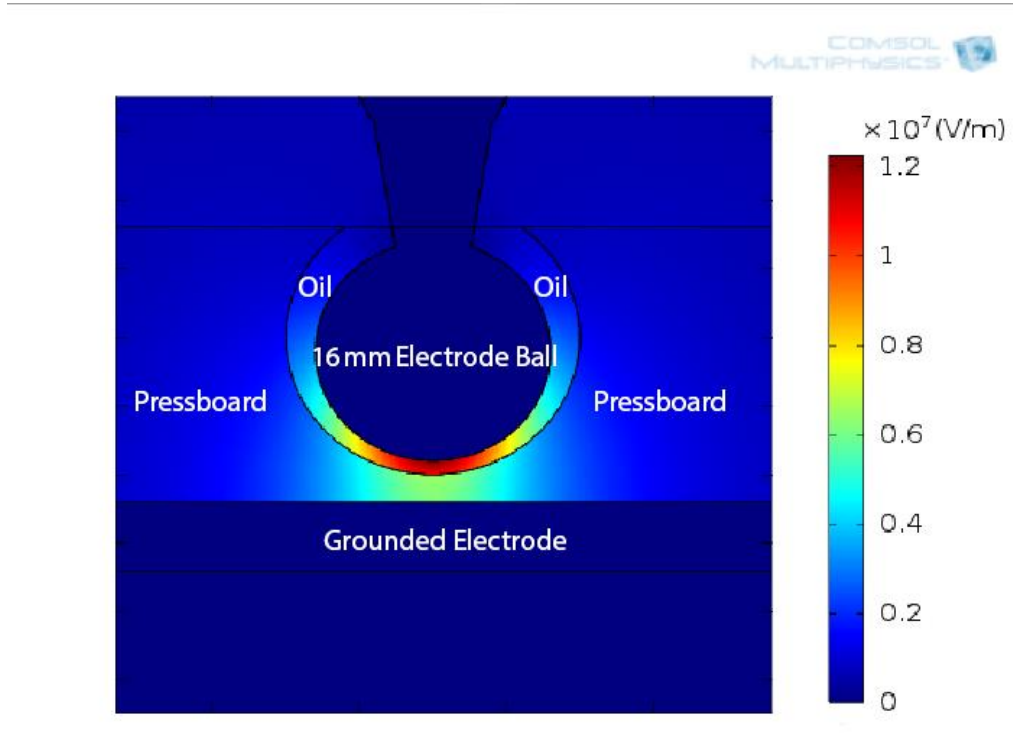
As mentioned in chapter 1.1.1 at homogenous electric field, the possibility of internal discharges due to small air bubbles inside the insulation materials would be increased. To evaluate the material acoustic attenuation, the same setup as Fig. 2.17 has been used. Instead of needle and aramid pressboard a paper pressboard (15 mm thickness) with a hole in the middle (Fig. 4.10) and three different electrodes with 20 mm, 16 mm and 40 μ m diameter (Fig. 2.18) have been used to investigate the discharges at homogenous and inhomogeneous field.

PD signals were measured by ICM system and AE signals via acoustic DSP device. The geometry construction of the 20 mm electrode without oil-gap could force the AE waves to distribute along the thick pressboard and 16 mm electrode with a 1 mm oil gap between the 16 mm electrode and pressboard. The FEM calculation in Fig. 4.11 shows the highest probability of PD activity due to highest electric field on 20 mm and 16 mm configurations both at tip of the electrodes. The travelling of the acoustic wave would be forced to go through the pressboard, because of higher acoustic impedance of copper electrodes compared to paper or pressboard or oil (almost 40 times larger) and therefore the electrodes could work as an acoustic barrier. By comparing the results with oil gap and without oil gap, there would be a possibility to investigate the influence of the AE attenuation during PD activity. If the mechanical attenuation is the main reason of silent discharges, this should be also visible on all these configurations regardless to the type of the discharges.

Electric static field calculation in Fig. 4.11 shows that to have the same electric stress inside pressboard the applied voltage with 16 mm electrode diameter with oil gap should be two-times higher compared to the 20 mm electrode diameter without oil gap.

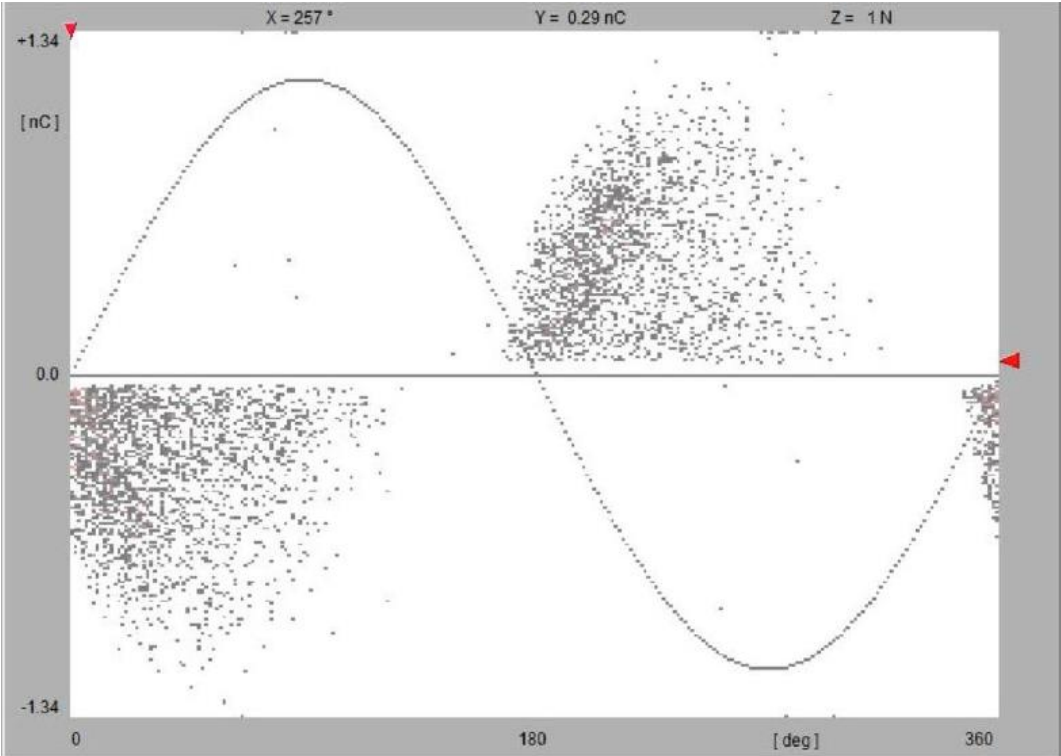


a)

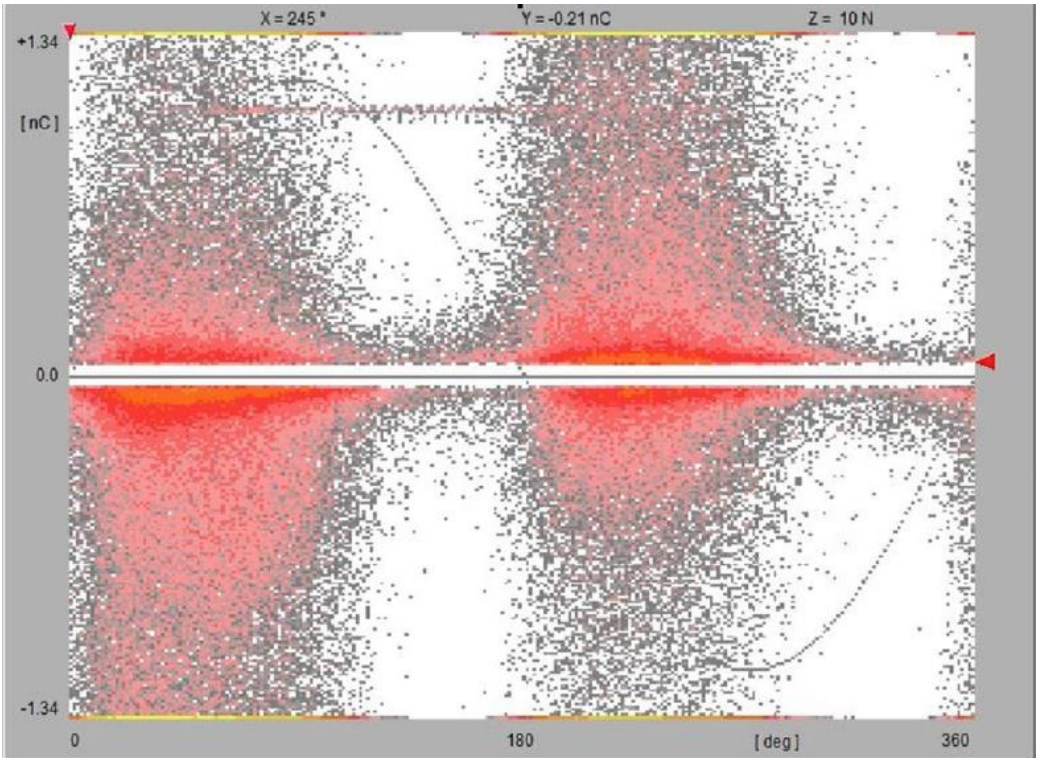


b)

Fig. 4.11: Results of electric field simulation
 a) Sphere electrode-pressboard arrangement with 20 mm diameter electrode at 12 kV
 b) Sphere electrode-oil-pressboard arrangement with 16 mm diameter electrode and 1mm oil-gap at 24 kV



a)



b)

Fig. 4.12: Electrical carbonization process:
a) first stage
b) final stage

The distance between the 16 mm electrode and ground compared to the 20 mm electrode and the lower relative permittivity of oil ($\epsilon_r = 2.2$) compared to the pressboard ($\epsilon_r = 3.5$) reduce the electric stress inside the pressboard. This means that the PDIV of the 16 mm configuration must be more than twice that of the PDIV obtained using the 20 mm configuration to ensure PD is happened within the pressboard.

Since the electric stress has direct relation to the applied voltage, it shows the electric stress at same voltage in oil by using 16 mm electrode is almost the same as in pressboard by using 20 mm electrode. After measuring the PDIV for both configurations, it was realized that the PDIV for 20 mm electrode arrangement without oil-gap was about 34 kV on new pressboard and PDIV for 16 mm electrode with oil-gap arrangement was about 17 kV. Higher PDIV without oil gap compared to the oil gap arrangement confirms that the PD on 16 mm electrode with 1 mm oil-gap arrangement has been happened in oil-gap before it happens inside the pressboard. This shows that the transformer oil has lower dielectric strength compared to the new pressboard. Based on the information in Fig. 4.11, it shows that the oil dielectric strength was lower than pressboard. This study is important to know the exact location of PD during the discharge activity to have better evaluation on AE signals.

To carbonize the pressboards, the voltage has been increased 0.5 kV per minute up to the PDIV and then increased with the rate of 0.1 kV to have more than 100 pC for the configuration with 16 mm and 20 mm electrode arrangement and also needle and sphere electrode. This means one-minute preparing and one-minute measuring time until about 100.000 - 150.000 PD pulses with an average discharge current of about 1.5 μA could be observed. The average discharge current helps to compare the different arrangements at almost the same electric energy released by PD activity. Average discharge current is the absolute discharge current obtained by summing up all charges within a given time and dividing the charge sum by the time [116]. After 100.000 - 150.000 PD pulses, five minutes measuring procedure on the carbonized pressboard has been started. Fig. 4.12 shows two PD patterns at the beginning and final stage of an electrical carbonization process.

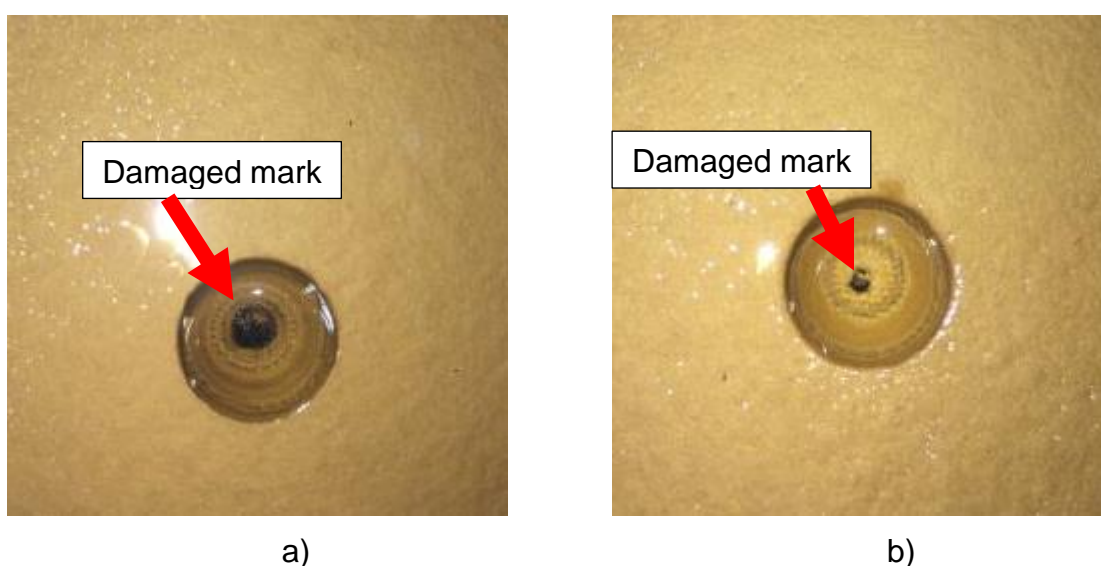


Fig. 4.13: Electrical damaged pressboard for two electrode configurations
a) sphere-plane (20 mm without oil gap)
b) needle-plane (without oil gap)

The average value of two different pressboards at each configuration (with and without oil-gap) and each situation (sphere-plane and needle-plane electrode) has been compared. Fig. 4.13 shows pressboards after electrical carbonization process (damaging process) for needle and sphere electrodes without oil gap. It shows a high concentration of carbonization in the middle of the hole.

Table 4.1 shows the relation between maximum PD apparent charge and maximum AE signal of sphere-plane with 20 mm and 16 mm electrode configurations. It can be figured out that the damaging (carbonization) on pressboard has a strong influence on AE signals generated by PD at configuration without oil-gap. In contrast, carbonization does not have much influence on AE signals in configuration with oil gap. Comparing the new pressboards at both configurations (with oil gap and without oil gap) reveals that, the 20 mm electrode without oil gap has 15 dB less maximum AE compared to the 16 mm electrode with the oil gap. Since the average PD energy released at both arrangements is almost the same and carbonization has not yet been started to effect the AE signals (Chapter 3.3) also the oil-gap to transferred the AE signals have been covered completely by 20 mm electrode, this proved that the thickness of the pressboard could have about 15 dB of mechanical attenuation on AE signals. Fig. 4.13 shows the carbonization tracks created by discharges, which prove the location of discharges between electrode and pressboard.

Table 4.1: Correlation between maximum PD apparent charge and maximum AE amplitude at same electric stress on damaged and new pressboard in sphere-plane configuration

Configuration	Without oil-gap		With oil-gap	
	New	Damaged	New	Damaged
Max PD	2.5 nC	3.5 nC	2.7 nC	3.2 nC
Max AE	85 dB	50 dB	100 dB	100 dB

To compare the results with a situation almost without any mechanical damping attenuation (larger oil gap compared to the electrode size), a needle-plane (40 μm diameter) configuration has been replaced by conductor ball to have an inhomogeneous electric field on the surface of the pressboard. To have a better comparison between AE numbers, electric PD numbers and maximum PD apparent charge during the activity in each step, EA ratio has been calculated. EA ratio is AE numbers divided by electric PD numbers as followed:

$$\text{EA ratio} = (\text{AE number}) / (\text{electric PD number}) \quad (37)$$

This ratio could indicate the behaviour of AE signals during transmission from non-silent to silent PD situation. Higher ration means higher non-silent PD and less silent PD. Fig. 4.14 illustrates the relation between AE numbers and PD numbers as well the relation between EA ratio and maximum PD apparent charges. Fig. 4.14 shows a large difference between AE numbers and electric PD numbers at configurations with and without oil-gap. There is also a large difference between these two configurations (with and without oil-gap) in terms of EA ratio and maximum PD. The main reason of creation higher AE numbers and EA ratios at configuration with oil-gap compared to

configuration without oil-gap is the self-restoring procedure after PD activity in the oil. The same results has been carried out on investigation of corona in oil via needle-plane electrode (chapter 3.1)

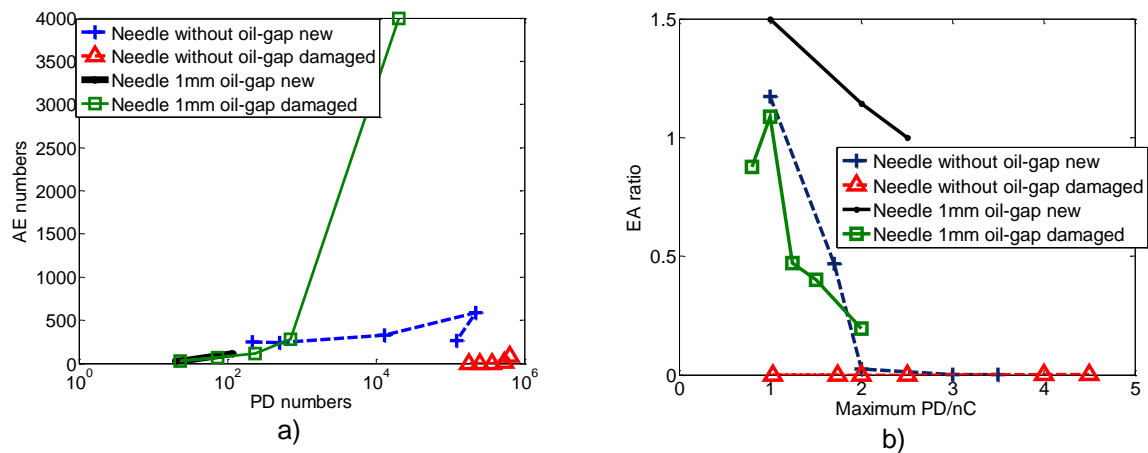


Fig. 4.14: The relation of PD and AE signals at needle-plane electrode configuration measured within one minute for new and carbonized pressboards

- a) AE numbers and PD numbers
b) EA ratio and maximum PD

At needle-plate configuration without oil-gap there is a difference in EA ratio between new and damaged pressboard until about 2 nC PD apparent charge. For PD apparent charge above 2 nC there is no difference in EA ratio for new and damaged pressboard because the discharges damaged the new pressboard during the measurement. After 2 nC apparent charges the new and damaged pressboard shows the same EA ration because the new pressboard is already damaged and not anymore new.

Since the discharges at configuration with oil gap happened in oil gap between the high voltage electrode and pressboard, there exists not much differences between damaged and new pressboards in terms of AE signal. The same phenomenon has been seen on corona in oil (chapter 3.1). Due to self-restoring effect of oil, the AE signals follow the electric PD signals regardless the carbonization or damaging process.

Fig. 4.14 (b) in some cases the EA ratio is higher than 1, which means more acoustic signals than electric PD signals. This could be due to higher sensitivity of AE signals compared to the electric PD measurement at these situations. These situations happened mostly in configuration with oil gap or on new pressboard without oil gap, but they are rare. The reasons can be the reflections of a strong incoming acoustic pulse, which cause an uncertainty in counting of the AE numbers, and AE signals generated from some small electric PD pulses which are not detected with electrical measuring devices (pulseless PDs) [117].

Regarding to Table 4.2 the maximum AE signals at needle electrode without oil-gap arrangement have been decreased sharply on damaged pressboard. However, at needle electrode with oil-gap arrangement there is only 6 dB difference of maximum AE signal between new and damaged pressboards, which shows the corona in oil.

Comparing of without oil gap arrangement on Table 4.1 and Table 4.2 shows that the carbonization with needle electrode arrangement has more influence on AE signals than electrode ball arrangement. This is due to additional partial discharges in oil between the oil gap of high voltage electrode ball and pressboard.

Table 4.2: Relation between maximum PD charges and maximum AE amplitude at damaged and new pressboard in needle configuration

Configuration	Without Oil-Gap		With Oil-Gap	
	New	Damaged	New	Damaged
Max PD	1.8 nC	2.5 nC	1 nC	1.4 nC
Max AE	80 dB	<40 dB (no AE)	90 dB	96 dB

4.3 Electric and UHF characteristic

Electric characteristics of PD has been investigated for several years [87]. In previous chapters, the silent-PD and non-silent PD have been measured via AE sensors and coupling capacitor at homogeneous and inhomogeneous field. In this chapter the UHF characteristics of silent and non-silent PD would be discussed. Fig. 2.19 shows the schematic view of the test setup. Due to lower attenuation of lower frequency signals [61], the AE signals captured by the 75 kHz sensor are presented in the following chapters.

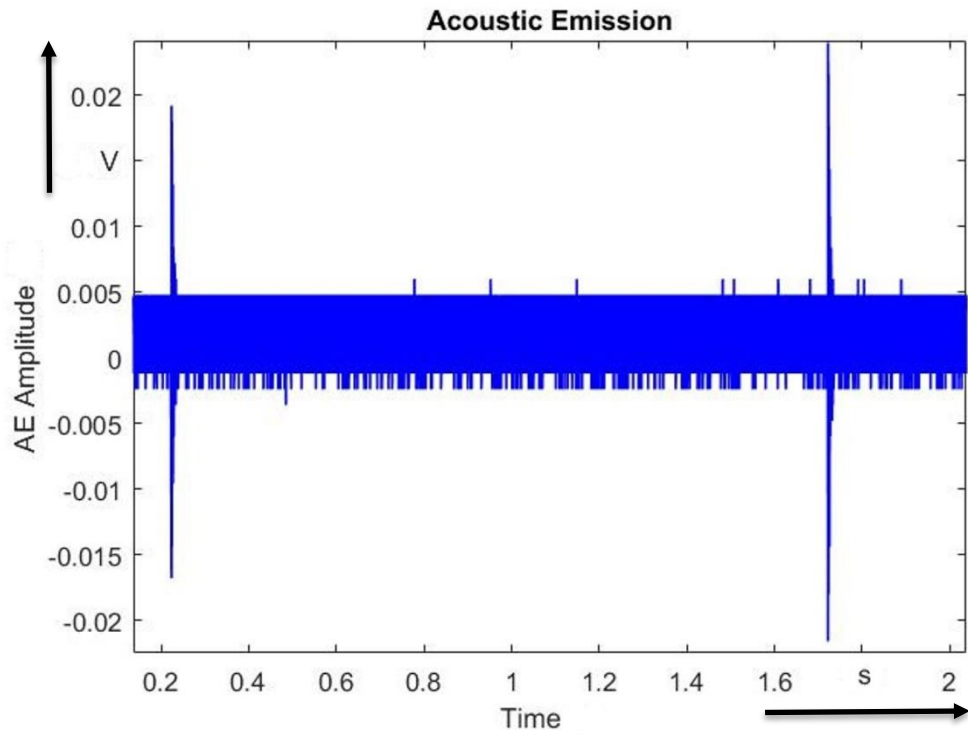
PD detection by UHF method has some practicalities like easy noise immunity and possibility of localization compared to the conventional electrical detection method. Due to the frequency and speed differences of AE signals compared to the electric and UHF signals, various measuring devices have been used to evaluate this correlation at different time scales. These challenges are followed by advantages of the combination of UHF and acoustical measurements [115].

The test setup described in Chapter 2.7 was utilized to simultaneously capture UHF, electric, and acoustic signals from both new and damaged (after carbonization) pressboard. This was achieved by gradually increasing the voltage up to the PDIV and maintaining a constant voltage for several minutes. It is important to note that since the carbonization patterns are located very close to the surface of the pressboard, there is no distinction between the new and carbonized states in terms of the mechanical attenuation of the acoustic signals.

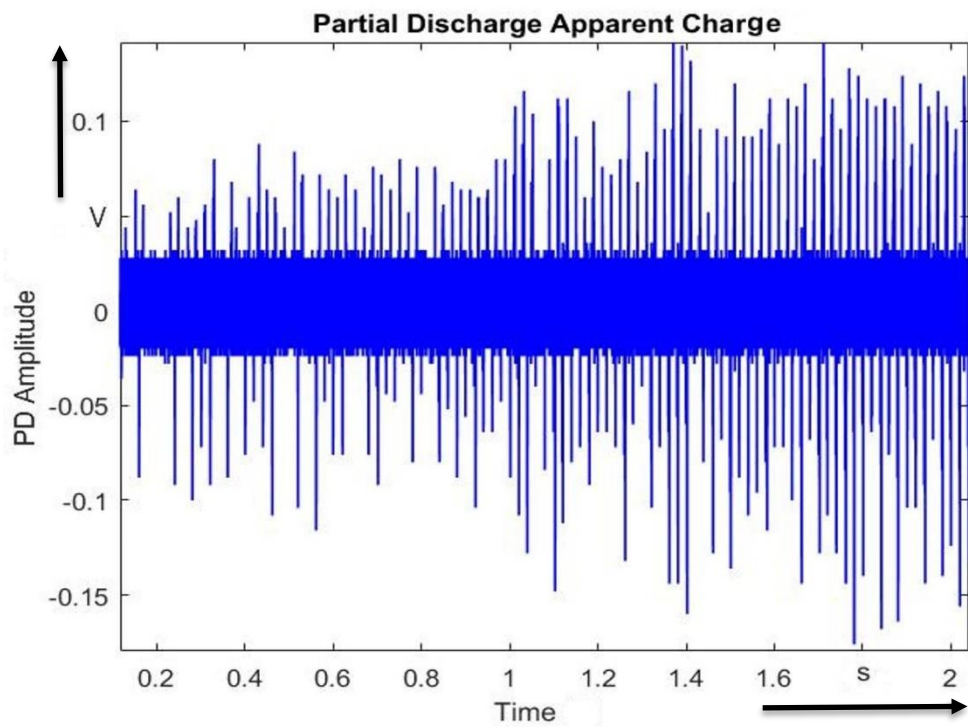
Fig. 4.15 presents a 2-second recording of the PD activity obtained via an oscilloscope at the inception voltage. A comparison between the acoustic and electric signals reveals that the PD activity commences with non-silent PD and is subsequently followed by silent PD. A closer examination of the electric PD apparent charges in Fig. 4.15b demonstrates an increase in PD activity over time at the same voltage stress. This behaviour is consistent with the observations depicted in Fig. 3.7. Additionally, it appears that the rate of increase remains constant after the first second of the PD activity.

Since the location of PD activities at 40 cm from the AE sensors are known (Fig. 2.19), by calculating the traveling time of the acoustic signals, the responsible electric signal for non-silent PD during the PD activity could be found (electric PD signals responsible for the AE signals in Fig. 4.15a). By detecting the non-silent PDs in PD activity, the silent PDs could be also detected. The electric signals of silent and non-silent PD have been shown in Fig. 4.16 in μs . It shows almost no deviation between silent and non-silent PD in terms of shape of the electric signal. Because of recording capacity limitation of the oscilloscope, the long duration measuring procedure have been done by using ICM and MPD 600.

Fig. 4.17 shows 15 minutes of electric PD activity via MPD 600 (coupling capacitor) at different stages in terms of AE activities and constant input high voltage. Acoustic activity is measured via ICM device and categorized in three different levels (high, low and very low AE activity). Fig. 4.17 shows again an increasing of the amplitude of the apparent charge during high acoustic activity.



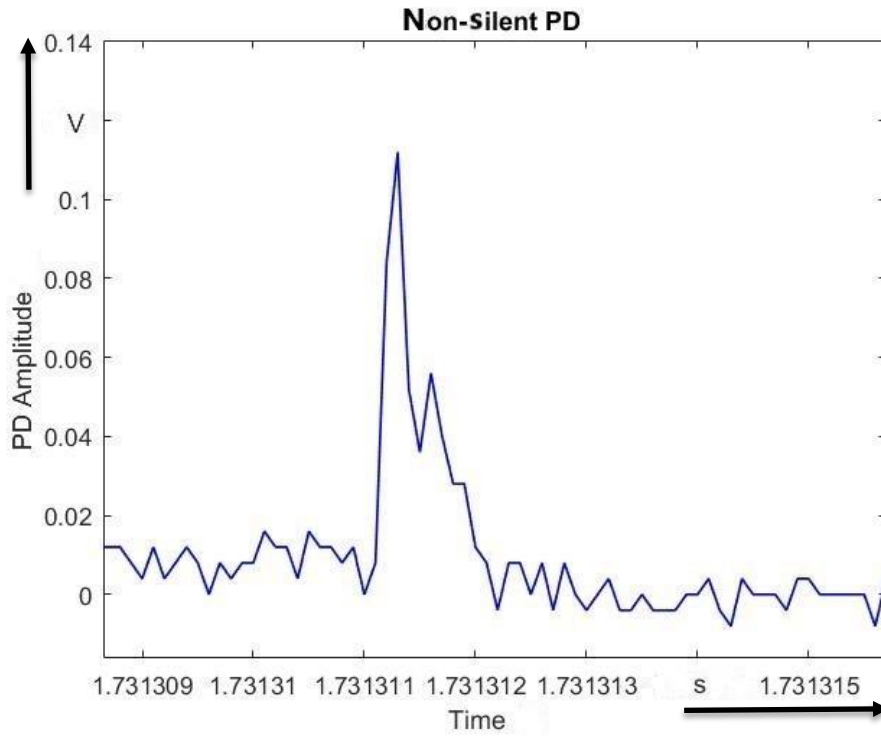
a)



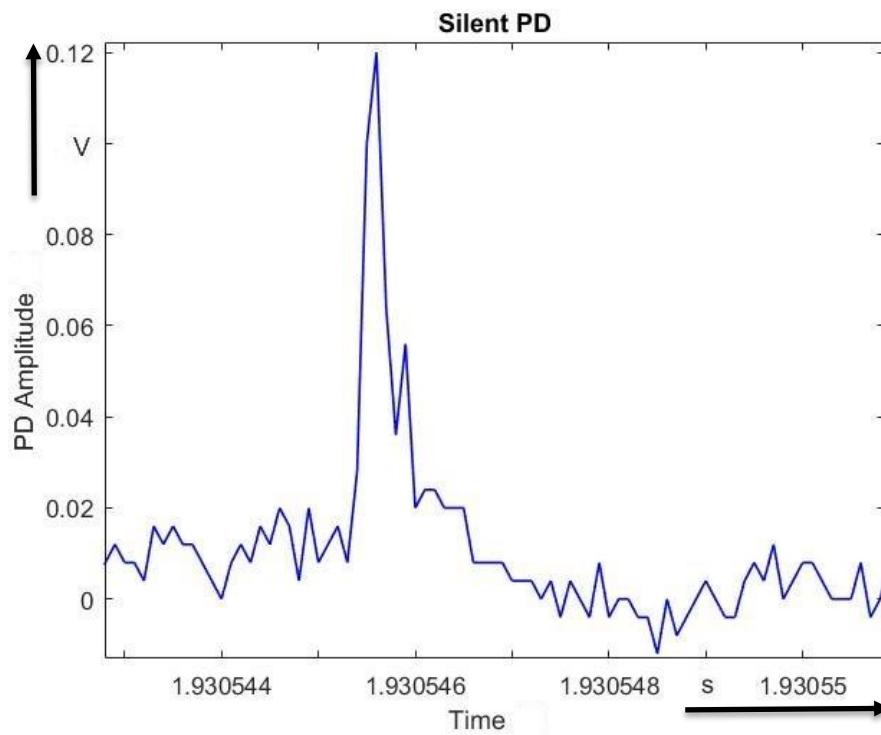
b)

Fig. 4.15: Recorded signals by oscilloscope for 2 seconds during the inception of PD (1 mV represents 1 pC apparent charge)

- a) AE signal
- b) electric PD signal



a)



b)

Fig. 4.16: Zoomed picture of electric signal in Fig. 4.15 representative of (1 mV represents 1 pC apparent charge)

- a) non-silent PD
- b) silent PD

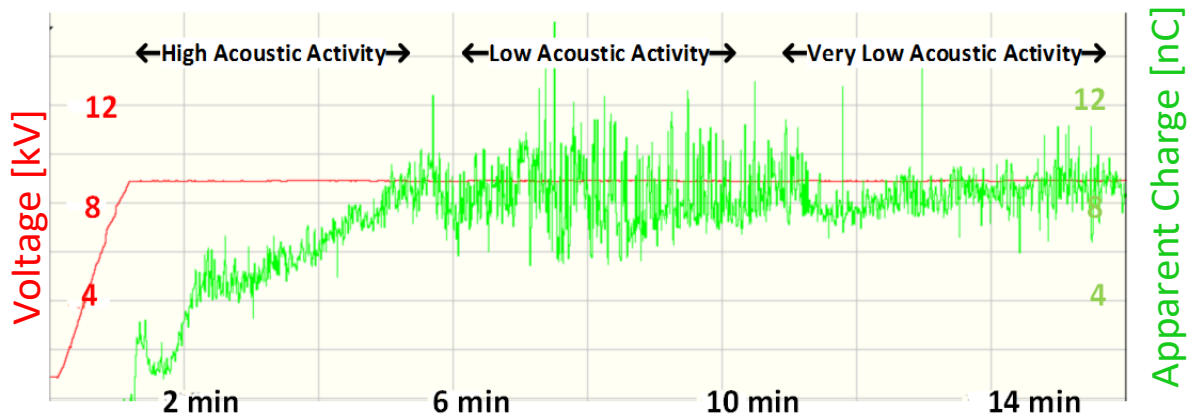


Fig. 4.17: Input voltage and amplitude of the PD apparent charge via coupling capacitor together with information about acoustic activities

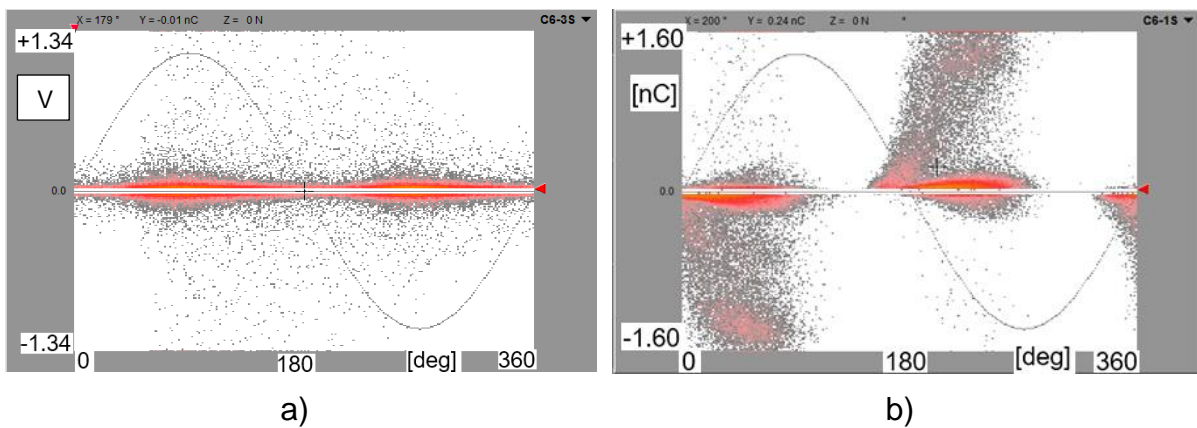


Fig. 4.18: Captured signals by ICM device during first 5 minutes (high acoustic activity)

- a) acoustic
- b) electric

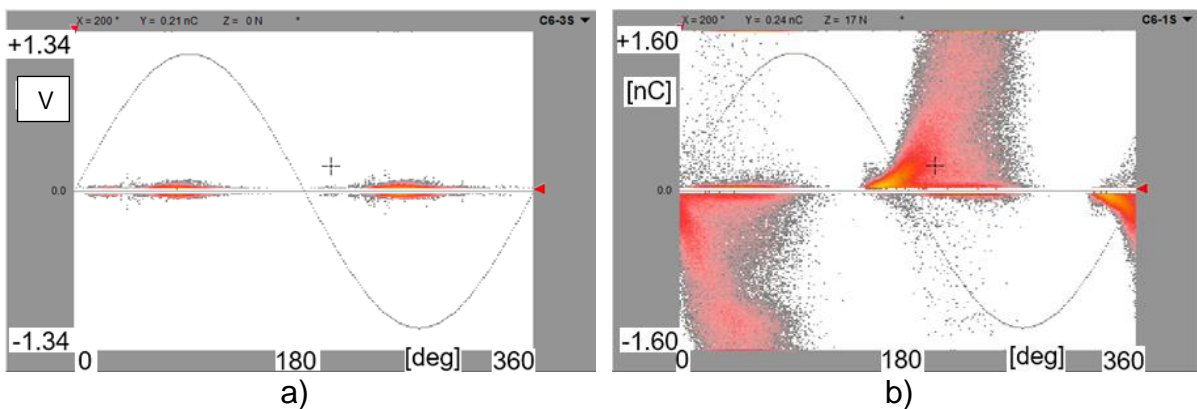
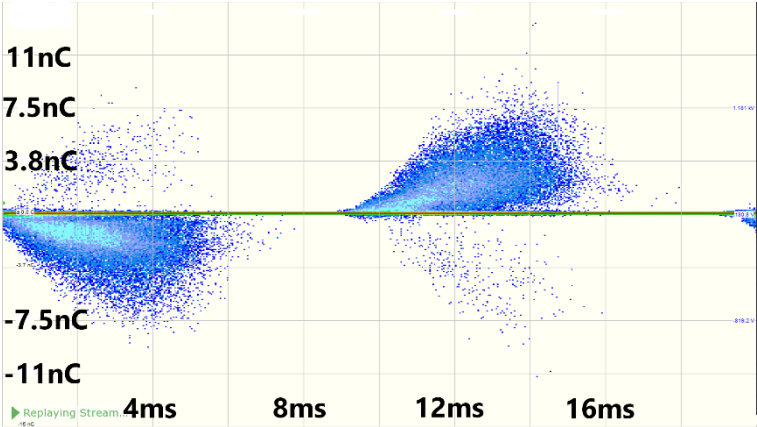
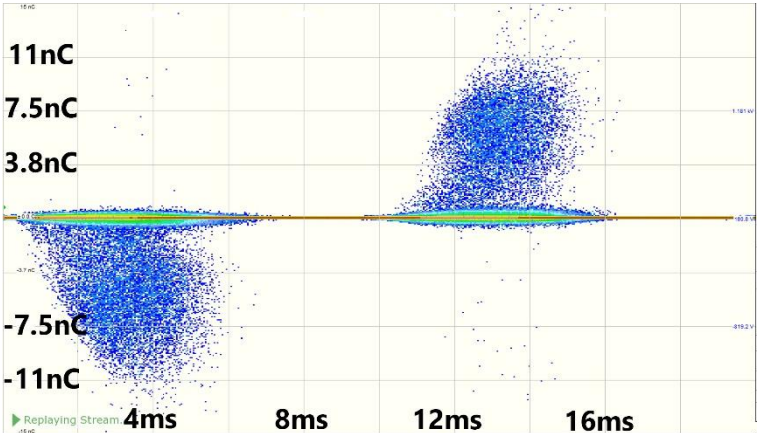


Fig. 4.19: Captured signals by ICM device during second 5 minutes (low acoustic activity)

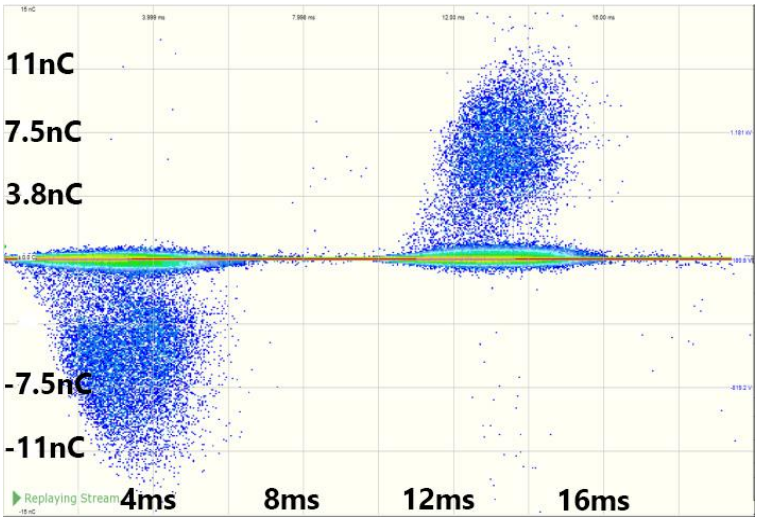
- a) acoustic
- b) electric



(a)



(b)



(c)

Fig. 4.20: Electric PD pattern at
a) high acoustic activity
b) low acoustic activity
c) very low acoustic activity

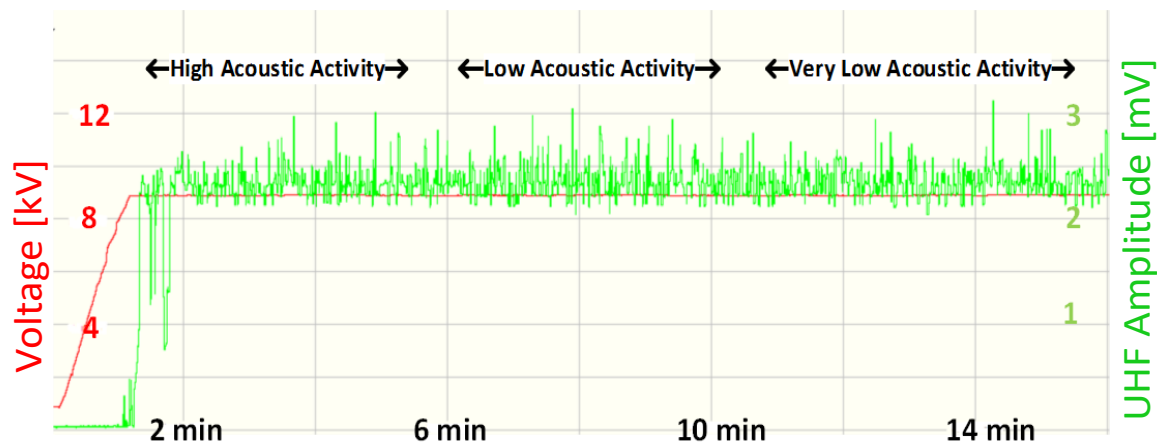


Fig. 4.21: Input voltage and amplitude of the UHF signal at different times together with information about acoustic activities

Fig. 4.18 and Fig. 4.19 show the acoustic and electric captured signals of the discharges after two different period of times each for 5 minutes via ICM system. It shows a very high activity of the acoustic signals during the first 5 minutes of the discharge activity. Second 5 minutes shows a strong reduction of the acoustic activity (low acoustic activity). On the other hand, the electric discharges show totally different scenarios. Electric apparent charges increased in terms of numbers and magnitude after the degradation (carbonization) of aramid pressboard. It could be again concluded that the degradation of aramid pressboard had direct correlation in decreasing the AE signals.

Fig. 4.20 shows the PD patterns of a long duration PD activity during high, low and very low acoustic activities. Electric PD patterns in Fig. 4.20 captured via MPD 600 with 16 bit resolution represents the patterns better than electric PD pattern via 8 bit resolution of ICM device in Fig. 4.18 and Fig. 4.19. Comparing the results of PD patterns at three different steps reveals another fact beside silent and non-silent PD. The first PD pattern at high acoustic activity seems to be totally different compared to the PD pattern during low and very low acoustic activity, even though the electric stress remains the same. Changing in PD pattern could be caused by changing in the test arrangement. Because the voltage (electric stress) remains the same, the only change in PD pattern could be caused by changing within the insulation material, which means carbonization on the surface of the pressboard.

As it is discussed in chapter 1.4.5 the temperature rise could also cause acoustic waves. By considering this fact, it could be concluded, that silent PD takes place at lower temperature compared to non-silent PD. Fig. 4.20 reveals different electric PD patterns at high (first 5 minutes) and low acoustic (second 5 minutes) activity, in contrast a similarity in electric pattern exists during low (second 5 minutes) and very low acoustic activity (third 5 minutes).

Further measurements of acoustic signals in comparison with UHF signals measured with UHF sensor and UHF 620 as shown in test setup (Fig. 2.19) allows a categorization based on maximum magnitude of the acoustic signals in high activity (non-silent PD signals), low activity and very low activity (silent PD signals), which is presented in Fig. 4.21. Fig. 4.21 shows the UHF signals measured by UHF 620 and acoustic activity (Fig. 4.18 and Fig. 4.19) at each stage. The time set for UHF sensor has been set at 0.3 s to record 15% of past data with trigger level higher than 0.025 V (noise level).

Unlike the electric apparent charges in Fig. 4.17, the UHF signals have no deviation during high, low and very low acoustic activities. This could be caused by reaching to saturation level of UHF sensor measurement around nC electric PD activities due to high sensitivity of UHF amplifiers, since the highest sensitivity had higher priority than covering all magnitude of UHF signals.

Fig. 4.22 shows the UHF and acoustic signals for non-silent discharges (environment acoustic noise level is below 20 mV in all measurement). Although the discharges are generated at the same input voltage and distance to AE and UHF sensors, the magnitude of the AE signals are not always following the magnitude of the UHF signals.

Fig. 4.23 shows the UHF and acoustic signals for silent PD signals (acoustic signal below 0.1 V). There is no acoustic signal above the noise level, but UHF signals can be detected, which proves the UHF activity of silent PD signals. The trigger has been set at 0.3 s (to record 15% of past data) like before with trigger level higher than 0.025 V (above the noise level). Therefore, there could exist some other discharge activities even before trigger point below 0.025 V. However, the maximum magnitude of the UHF signals is around 0.05V which is the same as non-silent situation in Fig. 4.22.

High acoustic activity is defined with maximum peak to peak AE signal between 0.75 V up to 3 V (Fig. 4.22), low acoustic activity which is defined with maximum peak to peak AE signal between 0.1 V up to 0.75 V and very low acoustic activity which is defined with maximum peak to peak AE signal below 0.1 V (Fig. 4.23).

The results reveal that the best possible way to classify the silent and non-silent PD is by measuring the acoustic signals together with electric signals. Electric PD signal measurement could ensure the presence of PD activity during silent PD activity. However, the validation of AE sensor location for measurement should be done during non-silent PD activity. It means the acoustic method could not only use for localization of non-silent discharges but also for classification of PD signals in terms of silent and non-silent discharges. As a result, the combined UHF/acoustical PD localization method, which uses advantages of both methods could be very helpful for the classification of PD in power transformers.

The results show less electric PD pattern changes during silent PD compared to the non-silent PD. Since carbonization has direct influence on PD creation, less electric PD pattern changes during silent PD activities could be result of less carbonization. In this regard, the carbonization development during silent and non-silent PD activities would be evaluated. By knowing the carbonization development level at silent and non-silent PD, the lifetime of the insulation material could be better determined.

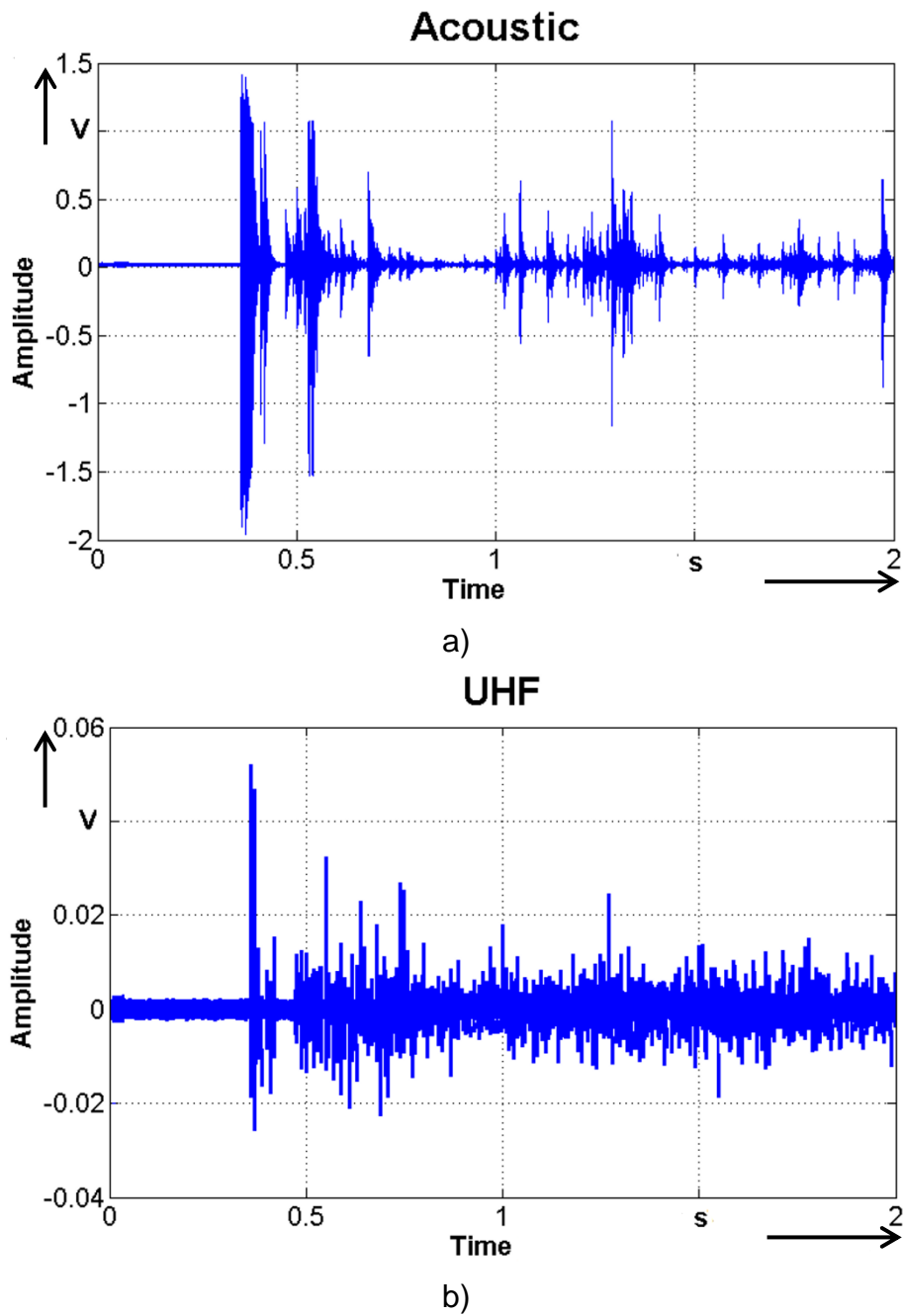


Fig. 4.22: Non-silent PD signals recorded by a digitizer within 2 seconds triggered electrically at 0.3 s

- a) acoustic signals
- b) UHF signals

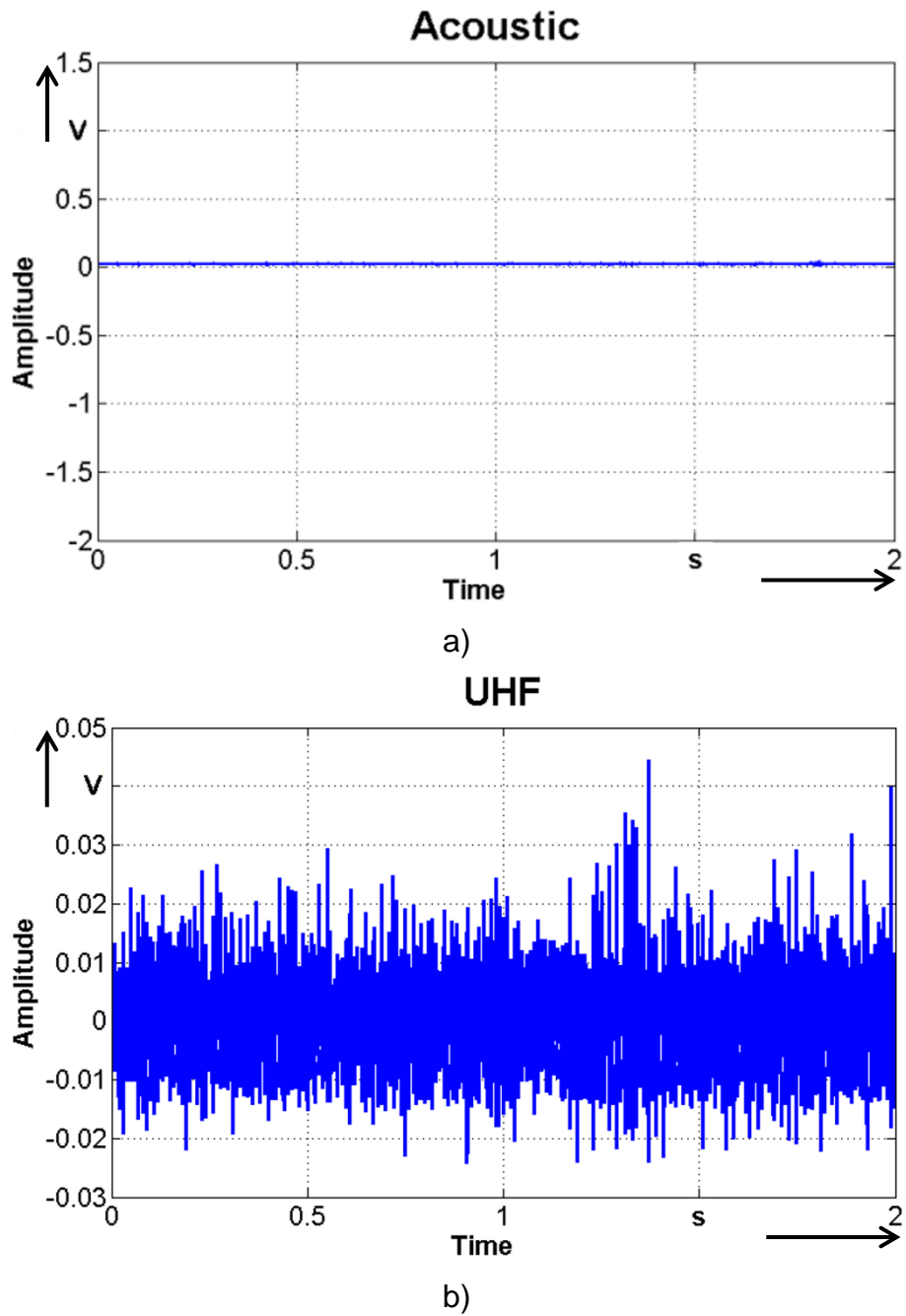


Fig. 4.23: Silent PD signals recorded by a digitizer within 2 seconds triggered electrically at 0.3 s
 a) acoustic signals
 b) UHF signals

4.4 The effect of pressboard material on creation of silent PD

As it has been illustrated in previous chapters, carbonization on the surface of the pressboard seems to have the highest influence on creation silent PD. In this section the focus would be studying the influence of the surface of the pressboard on creation of carbonization and as the results on silent PD. The tip of the needles as well as the moisture content of oil has been measured. Different needle with 3 μm , 5 μm , 20 μm , 50 μm and 100 μm diameter have been used.

The needle-plane electrode is placed on the surface of the aramid pressboard (same configuration as in chapter 2.7). The tip diameter of the needle varies from 3 μm up to 100 μm . Two different types of impregnated aramid pressboard with 1 mm thickness have been tested in a tank consisting of 80 l of MIDEL 7131. Fig. 4.24 depicts the surfaces of these two distinct types of pressboards. High density Nomex® 994 pressboard with a density of 1.2 g/cm^3 and medium density Nomex® 993 pressboard with a density of 0.7 g/cm^3 . Omicron MPD 600 has been used to capture the PD signals within a long time. For short time oscilloscope has been used to capture acoustic and UHF signals from the 75 kHz and 150 kHz AE sensors and UHF antenna respectively. Using oscilloscope has advantages in high sampling rate (giga sample per second) with a high bandwidth and synchronized data of UHF and AE signals, but disadvantages in limited recording time and 8 bit resolution.

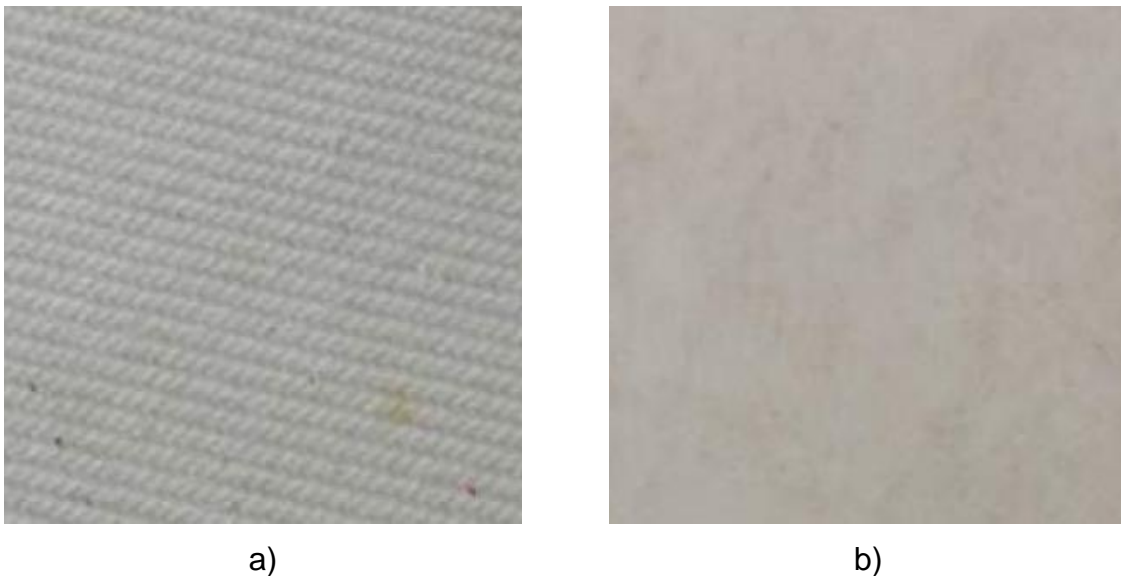


Fig. 4.24: The surface of the aramid pressboard with
a) medium density
b) high density

Karl Fischer titration has been used for measurement of the moisture content of the MIDEL 7131 for impregnation process. The moisture content was 38.5 ppm before and after impregnation. It should be also considered that, MIDEL 7131 has high saturation level of 600 ppm (solubility) at room temperature. The relation of dielectric breakdown voltage of insulating oils is directly proportional to the relative saturation of water in oil rather than the concentration in ppm. The relative saturation level here was 6,4 % (dividing the moisture content in ppm to solubility in ppm) and it shows the level of breakdown was almost independent to water content [118].

Temporary and transient overvoltages in power transformers can reach 1.2 per unit for several minutes and up to 7 per unit for some microseconds [119]. Normally

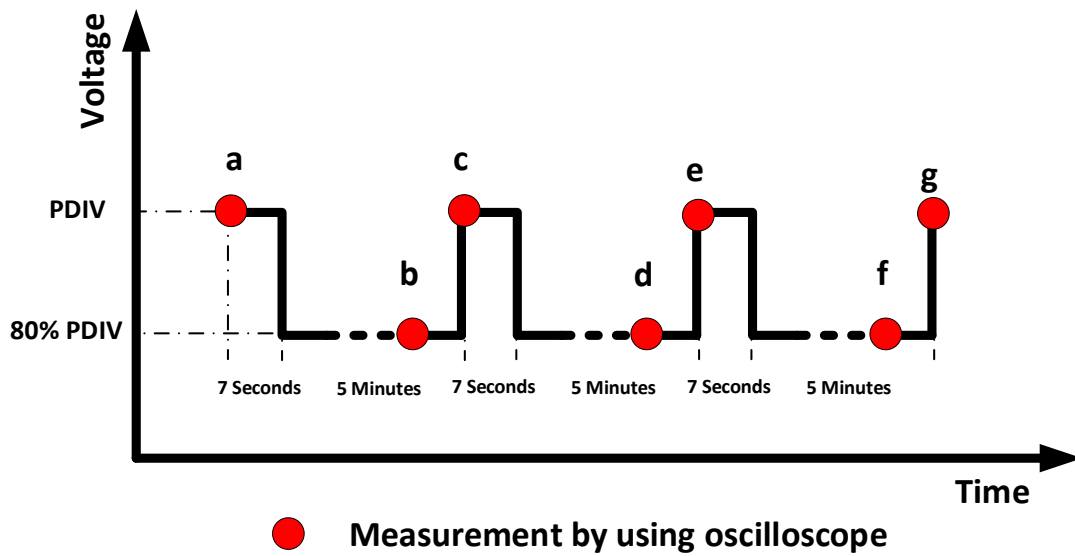
transformers should be able to withstand temporary or transient overvoltages. Regarding to this fact, the voltage level during the PD factory test (offline PD measurement) of a liquid-filled transformer could reach up to 1.8 times of the nominal voltage according to IEC 60076-13 [97].

To investigate the influence of changing electric stress on carbonization, two different voltage courses have been implemented to test the PD behaviour before, during and after damaging process due to the overvoltages on each pressboard and needle variants. The AE signals as well as electric signals of the PD were captured during each voltage courses. Due to the memory limitation of the oscilloscope, two seconds of capturing time has been considered as an optimum measuring time in terms of sampling rate and amount of information for AE and UHF signals.

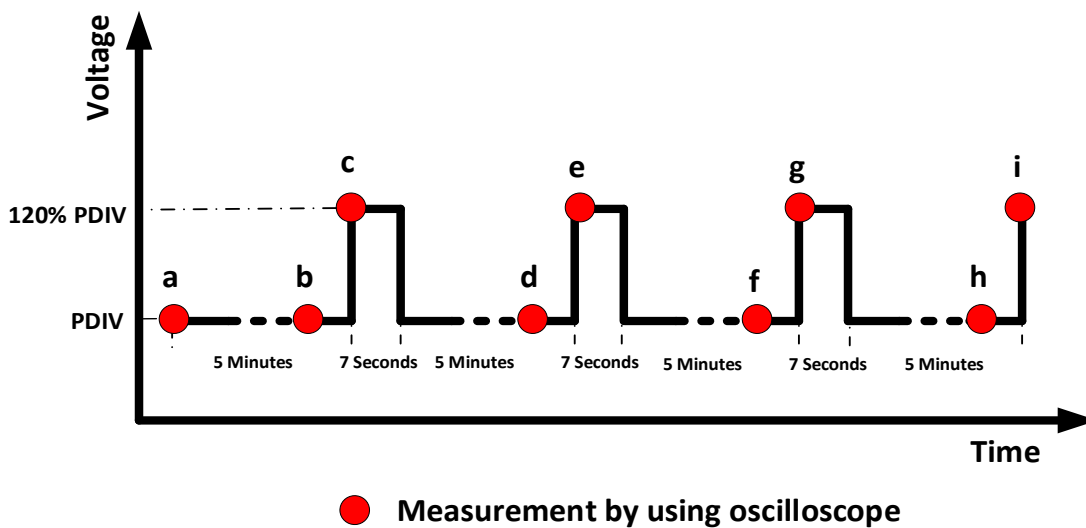
The measuring procedures are shown as red dots in Fig. 4.25. Electric PD measurements has been done during the process without interruption via Omicron MPD 600. The measuring procedure could be done in totally 7 seconds, but saving time needs 2 minutes. This is due to saving data from oscilloscope fast memory to its slower memory (hard drive). In order to have the following produce, the recording time has been done after the changing the voltage (so called resting discharge time).

Fig. 4.25a shows electrical damaging process with lower stress. This voltage course started at PD inception voltage (PDIV), which has been represented as point a in Fig. 4.25a. After 7 seconds of measuring procedure (the lowest possible measuring process), the voltage decreased about 20 % of the inception voltage and at the same time another measuring has been done. After 3 minutes (point b in Fig. 4.25a), the signals were measured again. The voltage was increased again up to PDIV after 5 minutes (3 minutes resting discharge time + 2 minutes recording time) and the signals were measured simultaneously (point c in Fig. 4.25a). This procedure has been done for 4 times. The results at each measuring point a to g are compared.

Fig. 4.25b shows electrical damaging process with higher stress. Like Fig. 4.25a this voltage course also started with PD inception voltage with the measuring procedure (point a in Fig. 4.25b). The voltage remained the same to have another measuring procedure after 3 minutes (point b in Fig. 4.25b). After this measuring procedure, the voltage increased about 20 % of the PDIV and another measuring procedure has been applied (point c in Fig. 4.25b). After about 7 seconds the voltage decreased to PDIV and the measuring procedure started after 5 minutes again (point d in Fig. 4.25b). The same procedure has been done for 4 times.



a)



b)

Fig. 4.25: Voltage courses

- a) first voltage course (low stress)
- b) second voltage course (high stress)

Beside the investigations on high and medium density aramid pressboards with different electrodes, the same test has been applied on a high-density pressboard with a very high humidity at different electrode arrangement to see the influence of the humidity on creation silent PD. To have a pressboard with high humidity, the impregnated pressboard has been kept in air with 85 % of relative humidity for about 4 months. The tests have been repeated 4 different times to have appropriate data.

4.4.1 Effect of different voltage courses on AE signals

Since the PDIV at different arrangements have been used regarding Fig. 4.25, the applied voltage could differ depends on arrangement. Fig. 4.26 shows the results of

PDIV at different configurations. PDIV increased as the needle diameter increased because of decreasing electric stress at the tip of the needle. At the same needle diameter, the medium density aramid pressboard shows slightly higher PDIV compared to the high-density aramid pressboard. This relation could be because of higher probability of small air bubbles during impregnation in high density pressboards compared to medium density pressboards. It could be also seen that, water content inside the pressboard decreased the PDIV, because of very large relative permittivity of the water and consequently higher electric stress of the oil. Higher electric stress increased the probability of PD generation and as the result gas creation at the tip of the needle.

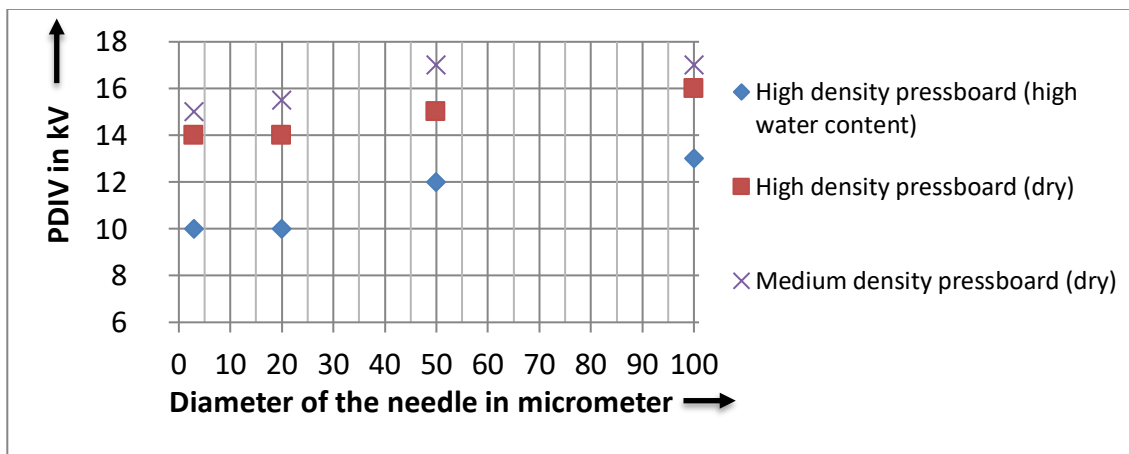


Fig. 4.26: PDIV at different electrode and pressboard configurations

AE and UHF signals has been evaluated by their maximum and average values. Because AE bursts have different oscillations, an intelligent software in MATLAB has been developed to recognize the oscillation of AE signals and analyse the results. Because of the 8 bit resolution limitation of the oscilloscope it would be not possible to record the AE signals above 80 dB. The environment noise level was about 40 dB for all measurements.

UHF signals were used to promise the existence of discharge activity during silent PD. Fig. 4.27 shows the results of maximum UHF and AE signals from 75 kHz and 150 kHz sensors versus different measuring steps during first voltage course. Each different step will be discussed separately to have a better view about different phenomena, which happened during the measurement.

Step "a" shows the results from very beginning of the measurement without any damaging and carbonization process. The maximum AE signal is almost the same for both sensors about 80 dB and the UHF signal about 70 dB at the maximum electric apparent charge about 500 pC.

Step "b" shows the results after decreasing the voltage on 80 % of PDIV. It shows that the AE signals as well as UHF signals dropped down and no PD activity can be detected.

Step "c" shows the data after increasing the voltage up to PDIV. UHF signals increased again up to 78 dB and shows PD activities. Slightly higher UHF signals compared to the step "a" at same level could be observed caused by increasing electric stress at the tips of the conductive carbonized traces, which have been created from beginning

of the discharge phenomena. PD apparent charges showed about 2.5 nC, which is 5 times higher than step “a” due to carbonization.

Step “d” shows again the results after reduction of the voltage to 80 % of the PDIV. Maximum UHF signals decreased slightly from 78 dB down to 72 dB because of lower electric stress. The maximum UHF signal at this stage is still higher than in step “a”, which could be caused by carbonization. AE maximum signal dropped dramatically for both sensors, which can be interpreted as a transition of acoustic signals (non-silent PD) to silent PD, caused by creation of different carbonization patterns and traces on the surface of the pressboard.

Step “e” shows the data after increasing the voltage up to PDIV. No PD activity at this step were observed even if the voltage has been increased. This phenomenon could be happened, when the insulation pressboard at the contact point has been changed or destroyed by carbonization creating a small disconnection and an oil gap in the carbonization traces. The change causes an increase of the PDIV and therefore no PD activities could be observed. It could have two different reasons for not having PD and creation of new traces at this level, first not enough electric field, and second not enough time.

Step “f” shows the data after decreasing the voltage about 20 % of the PDIV. This step also shows no PD activity and as the result no AE and UHF signal.

Step “g” shows again the data after increasing the voltage up to PDIV. AE sensors could detect signals; however, the UHF sensor could not capture any signal. Omicron PD 600 device shows about 300 pC electric apparent discharge during this step. One of the main reasons of low PD activity according acoustic sensors could be starting new PD activities by producing new carbonization traces similar to the results of step “a” or discharges in oil (corona in oil).

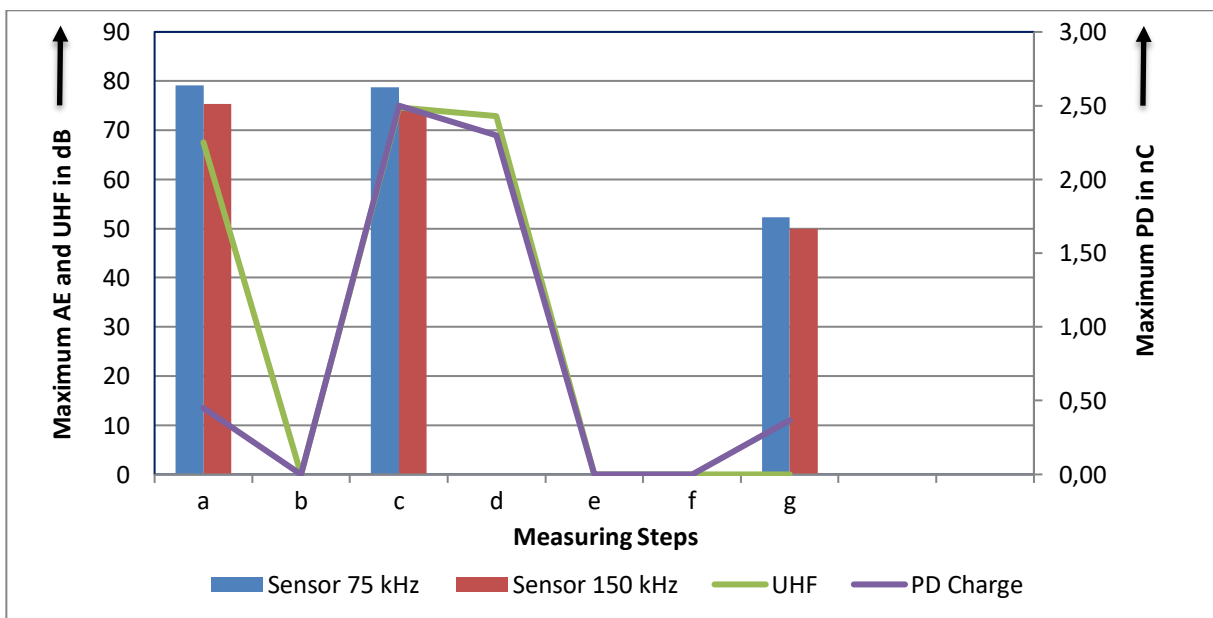


Fig. 4.27: The maximum UHF and AE signals from 75 kHz and 150 kHz sensors versus different measuring steps during first voltage course

Fig. 4.28 shows the results for the second voltage course. To clarify this figure, each step would be discussed separately.

Step “a” shows the results at PDIV at the beginning of the measurement without any damaging and carbonization process. Maximum UHF signal is about 70 dB at 2 nC apparent charge. It shows a very high activity of AE signals (at the level of the saturation of the oscilloscope), which was considered as non-silent PD. AE signal comparison shows that the 75 kHz AE sensor delivered higher signals than 150 kHz AE sensor, caused probably by low attenuation of low frequency AE waves, low frequency of generated AE signals or better mechanical connection of 75 kHz sensor to the tank compared to the 150 kHz sensor. The exact AE peak amplitude difference between the two sensors could be not determined because of the saturation of the oscilloscope (both reach nearly their saturation level).

Step “b” shows the results at PDIV after 3 minutes of PD activity at the same voltage as step “a”. The maximum UHF signal has been increased by about 10 dB, which is probably caused by the carbonization process during the discharge activity. On the other hand, the maximum AE signal has been decreased. This phenomenon has been also seen in Fig. 3.12 and later in Fig. 4.19. This phenomenon happens because of carbonization at the first step of the PD activity. Considering this phenomenon in localization of PD via acoustic method, proves the importance of AE detection at the beginning of the PD activity.

Step “c” shows the data after increasing the voltage over 20 % of the PDIV (for 7 second). Maximum UHF signals decreased slightly to 72 dB despite the voltage has been increased. This could be because of high carbonization, which has been also reported in other investigations [121]. Maximum AE signals decreased even more which makes the capturing from 150 kHz senso impossible due to the noise level of about 40 dB.

Step “d” shows the data after decreasing the voltage down to PDIV (for 3 minutes). No PD at this step could be recorded that means the PD extinction voltage (PDEV) is now above PDIV. As described in step “e” of Fig. 4.27 the carbonization on the contact point could cause damaging process on the pressboard during previous steps and as the result PDIV and PDEV are changed.

Step “e” shows the data after increasing the voltage by 20 % of the PDIV (for 7 second). UHF data shows the PDIV has been reached and the PD activity starts again. PD activity has been increased compared to the step “c” (same level of voltage stress) because UHF results as well as electric PD measuring shows higher maximum value. Acoustic measurements on the other hand show almost the same maximum value at 75 kHz and at 150 kHz PD signals could be recorded. Electric PD charges has been also increased.

Step “f” shows the data after decreasing the voltage down to PDIV (for 3 minutes). UHF data shows the existence of the PD activity during the decreasing of the voltage. The same AE signal values but higher electric activity compared to step “e” are recorded. It seems that lower electric stress has not much influence on electric PD and AE signals at this step.

Step “g” shows the data after increasing the voltage by 20 % of the PDIV (for 7 second). Electric data shows an increase from 3.5 nC at step “e” to 9 nC but the same value as at step “f”. UHF data and AE signals show no change compared to the step “e” and “f”. Again the AE signals are not increasing by increasing of the electric PD activities.

Step “h” shows the data after decreasing the voltage down to PDIV (for 3 minutes). UHF data shows the existence of the PD activity at this stage. The existence of PD activity even at lower electric stress at this stage shows no damaging on carbonization

traces. UHF maximum amplitude decreased about to the level of UHF maximum amplitude at step “a”. AE signals decreased below the noise level and this means, that at this stage silent PD exist. A comparison of the AE signals at this step with step “a” (with same input voltage and same UHF and electric discharges) shows that discharges exist which could be recorded by UHF but nor by acoustic sensors due to silent PD.

Step “i” shows the data after increasing again the voltage by 20 % of the PDIV (for 7 second). It shows about 3 nC apparent charge and small increasing of UHF maximum data. UHF signal shows a small decrease compared to the step “g” and a small increase to step “h”. This was caused by creation new carbonization traces after increasing the electric stress. The acoustic signals have been also increased compared to previous step “h” caused probably by new carbonization path.

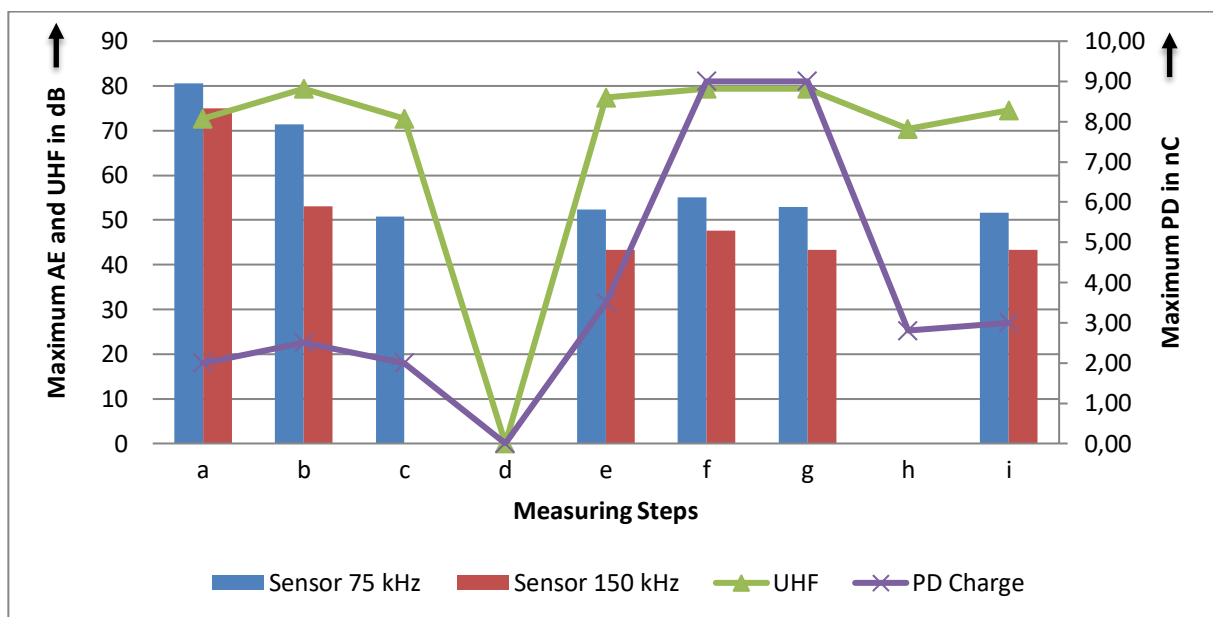


Fig. 4.28: The maximum UHF and AE signals from 75 kHz and 150 kHz sensors versus different measuring steps with during second voltage course

4.4.2 Effect of water content on creation of AE signals

To investigate the influence of the water content on AE and electric signal creation during PD activity, two different pressboards at wet and dry situations by using different electrodes have been used. The pressboard with less than 2 % water content is considered as dry and the pressboards with water content between 2 % and 5 % as wet. Different electric stresses were generated by different size of electrodes. Fig. 4.29 shows the relation of AE number to PD number ratio (EA) at different electrode configuration. The ratio shows a small difference at different electrode diameters before carbonization on both type of pressboards (wet and dry).

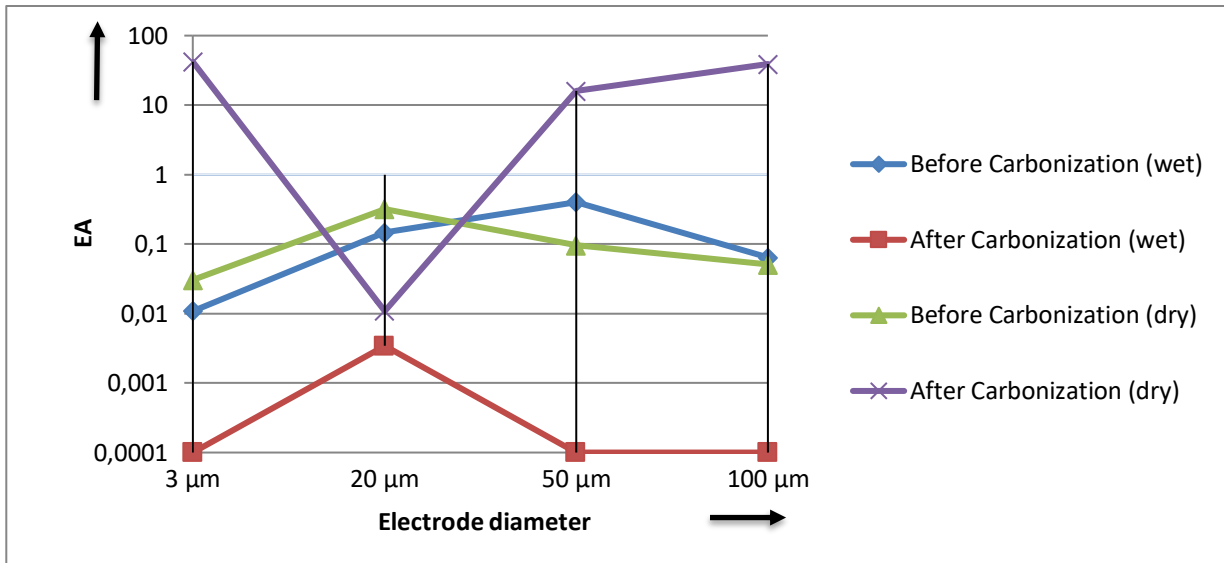


Fig. 4.29: EA at different electrode configuration before and after carbonization on dry and wet aramid pressboards with high density

On carbonized wet pressboard (red line) the ratio has been decreased at all electrode diameters compared to the non-carbonized wet pressboard. At dry type pressboard after carbonization the situation on ration of AE over UHF numbers has been changed in a totally different way (purple line).

To have a better view of the results, the maximum AE signals at different electrode diameters on wet and dry type pressboard before and after carbonization are separately evaluated (Fig. 4.30). Maximum amplitude of the AE signals reveals that the carbonization has decreased the amplitude of the AE signals on wet and dry type pressboards but in a different way for dry and wet pressboards. The AE signals on carbonized wet pressboards (red line) has been decreased more compared to the carbonized dry pressboards (purple line). These results revealed the influence of water content inside the pressboard besides the carbonization. The maximum AE signals before carbonization at wet and dry situation are almost the same at all electrode arrangements (green and blue lines).

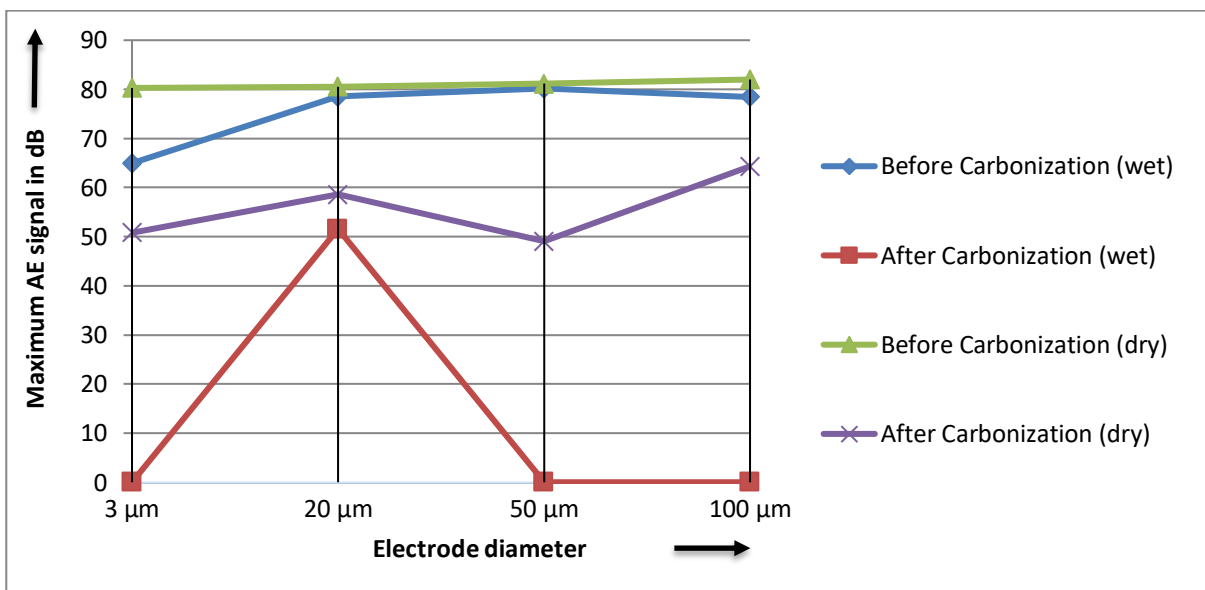


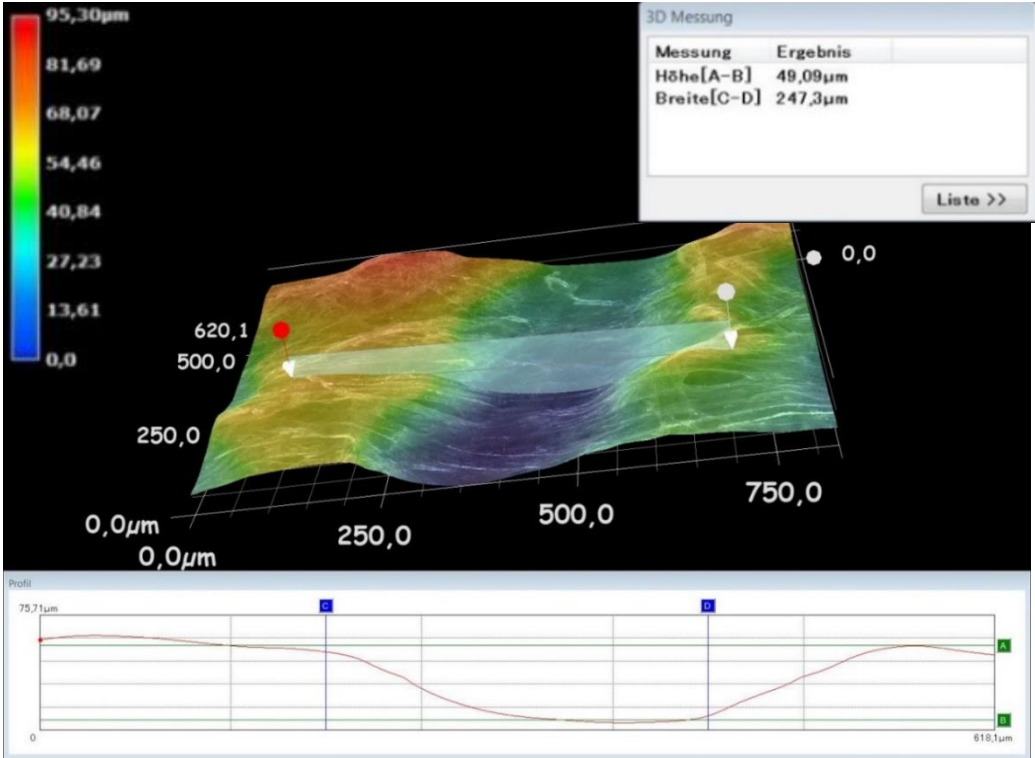
Fig. 4.30: Maximum amplitude of the AE signals at different electrode configurations before and after carbonization on dry and wet aramid pressboard with high density

4.4.3 Gas Generation

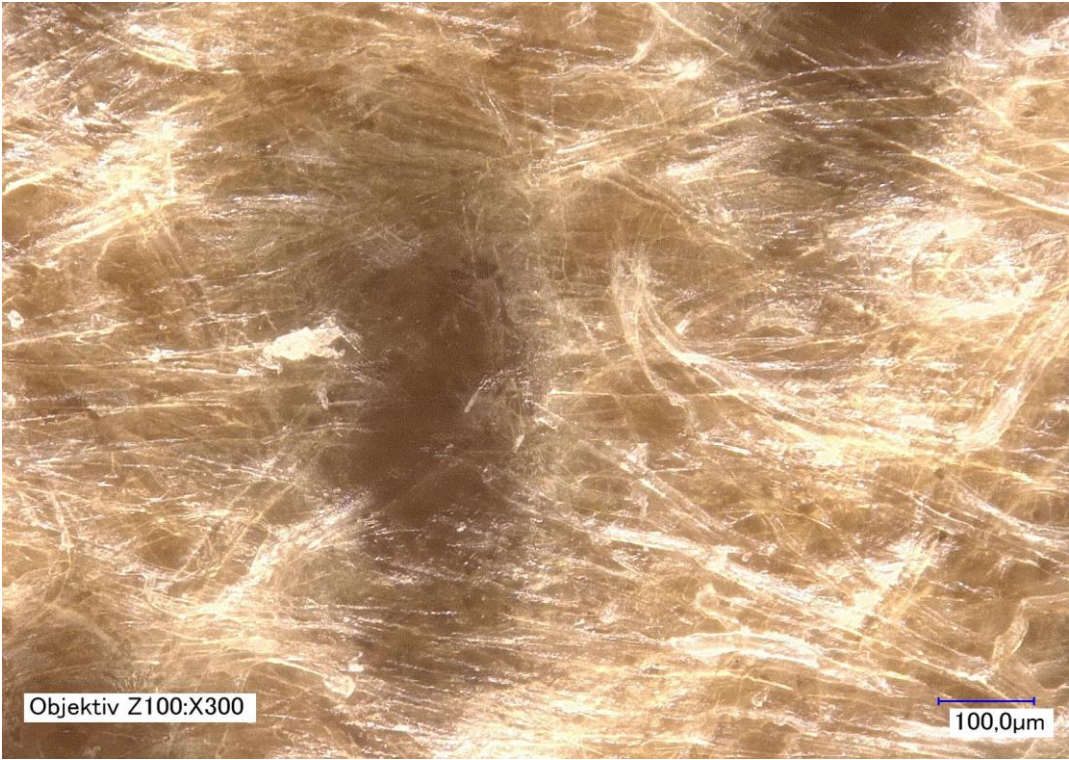
Previous chapter shows the influence of the water content on creation of AE signals during PD activity. In this chapter the probable reason of this phenomenon would be discussed. Fig. 4.31 shows the carbonization under the surface of a pressboard. Keyence Digital-microscope VHX-6000 used (chapter 2.1) a very sensitive focus function to figure out the depth of the carbonized tracks under the surface of the aramid pressboard. The three-dimensional image shows a distance about 50 μm of the carbonized path related to the surface by calculating the difference between point A and B in Fig. 4.31a.

Fig. 4.32 shows the gas generation during very high PD activity on medium density and high-density pressboard. The gas bubble could be seen easily with bare eyes released from the surface of the medium density pressboard, however there are no visible gas bubbles at the high-density pressboard even at 4 times higher electric PD discharge activity. The gas bubbles could be generated by the temperature release of PD activity. Another source of formation of bubbles could be by the drop in pressure created by AE, which is equal or lower than the saturated vapour pressure at a given temperature in a liquid [122].

The holes and lumps on the surface of the medium density pressboard, allow the bubbles to leave the pressboard during PD gas creation inside the pressboard. It means that the gas bubbles are more likely to be trapped under the surface of the high-density pressboard with less holes and lumps (Fig. 4.32).



a)



b)

Fig. 4.31: Microscopic picture of the surface of a carbonized aramid paper:
a) three dimensional
b) two dimensional

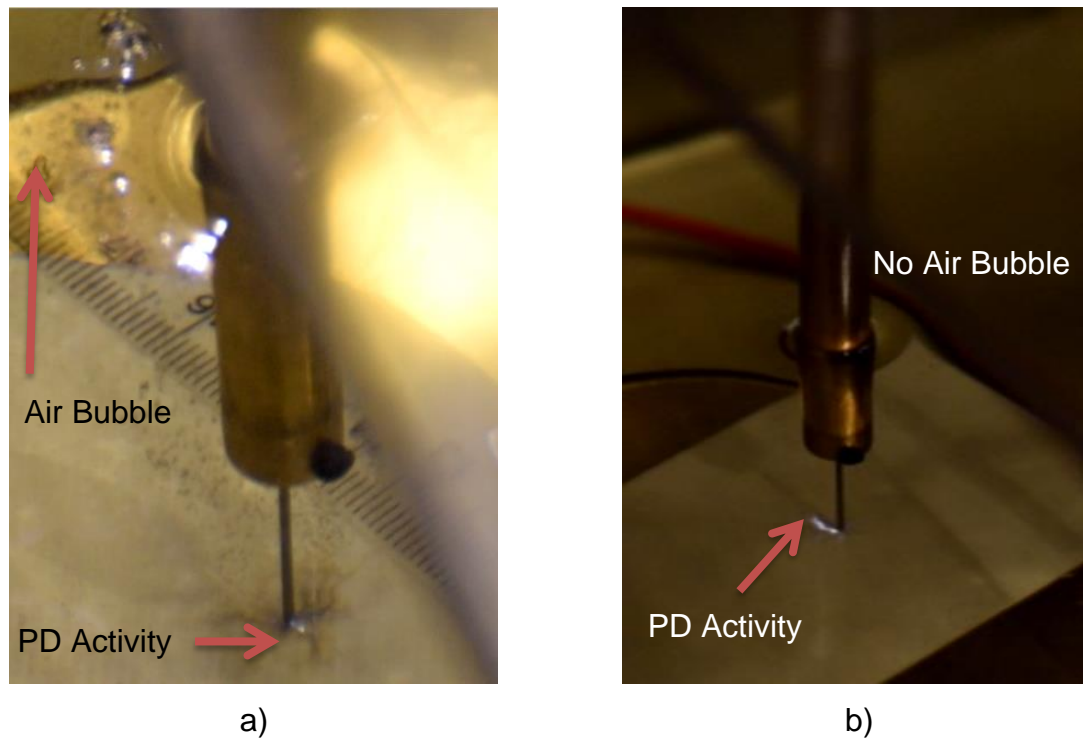


Fig. 4.32: Gas generation during PD activity with 30 nC apparent charge
a) medium density surface aramid pressboard
b) high density surface aramid pressboard

Beside the gas generation by PD, the bonding between oil molecules and dissolved gases inside the oil at the boundary of the electrode could increase the accumulation of gases near to the surface of the electrode. At the phase boundaries the effective surface energy is lower, thus diminishes the free energy barrier and facilitating nucleation. It increases the bonding between oil molecules and decreases the bonding between dissolved gases in oil. The same effect could be seen in water. Fig. 4.33 shows the nucleation of carbon dioxide bubbles around a finger inside the water due to higher hydrogen bonding energy between water molecules and lower bonding energy between dissolved gas.

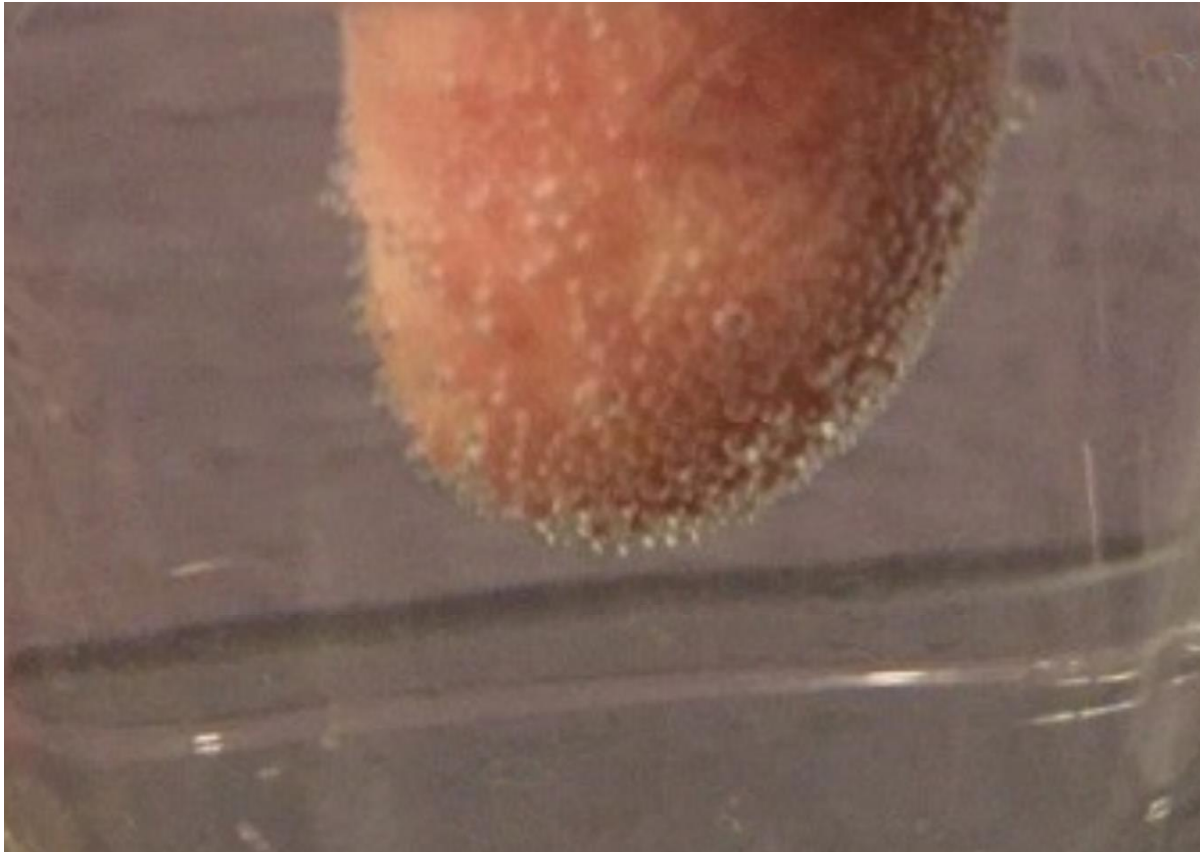


Fig. 4.33: Nucleation of carbon dioxide bubbles around a finger in water

It could be concluded that, trapping gases under the surface of the high-density aramid pressboards are more likely than medium density pressboards. By considering the results of wet pressboards in chapter 4.4.2 and air bubble at different pressboards in this chapter, it could be concluded that the probability of creation silent PD has direct relation to creation and trapping of gas bubbles below the electric discharge location (inside the pressboard).

4.5 Degradation of Silent and non-Silent PD

Fig. 4.34 shows the electric and acoustic signals captured via Omicron MPD 600 and ICM respectively of discharges shown in Fig. 4.32 by using 40 μm electrode arrangement. Higher probability of creation silent PD on the high-density surface of the aramid pressboards could be observed due to very small AE signal in Fig. 4.34b, supported by Fig. 4.32, where a higher probability of trapping air bubbles inside the high-density surface compared to the medium density surface is shown.

One of the most important aspects of the PD analysis is to determine the level of degradation. Closer look at the carbonization development in this chapter could reveal the hypothesis about the level of degradation and carbonization development of pressboard during silent and non-silent discharge activities. This could also reveal the hypothesis about different heat generation of PD at different type of discharges independent to level of electric apparent charge.

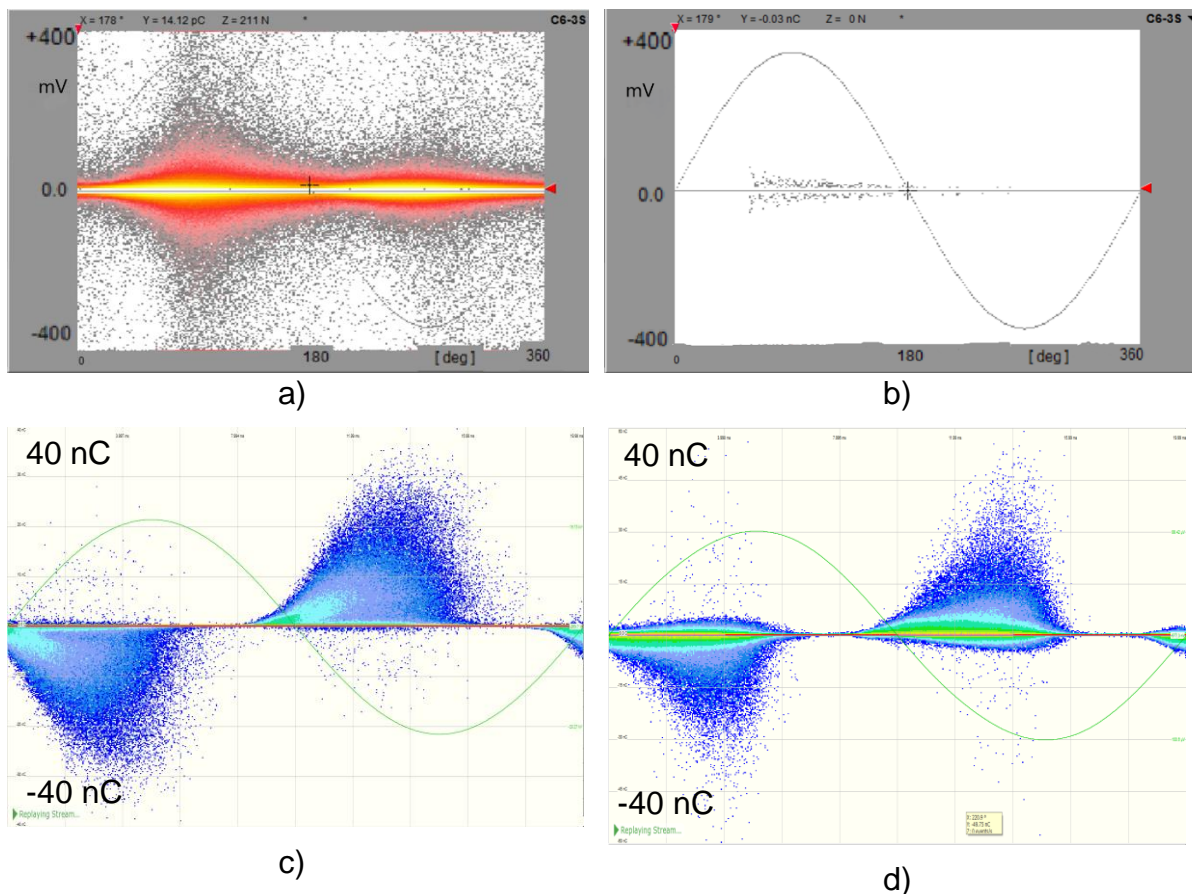


Fig. 4.34: Signals during PD activity with 30 nC apparent charge discharge

- a) AE signals on medium density surface
- b) AE signals on high density surface aramid
- c) electric PD signals on medium density surface
- d) electric PD signals on high density surface aramid

For evaluating the effect of carbonization tracks at different discharges (silent and non-silent) the needle placement during the discharge is important. Any changes in the location of the needle on the surface of the pressboard, create a new situation (chapter 3.2) and should be avoided. The carbonization traces should be evaluated without changing the needle placement. For this purpose, the same test setup as Fig. 2.19 for measuring electric and AE signals generated by discharges has been used.

In addition, a Nikon 5300 Camera with a 300 mm lens to zoom the carbonization tracks from safe distance has been used to capture the carbonization tracks on the surface of the pressboard at different stage of the discharge phenomenon (Fig. 2.2). Also, a ruler has been placed carefully near to the high voltage needle to measure the tracking area. Due to the reflection of the surface of the oil, the pictures have been taken at different directions and the best has been chosen.

The voltage course in Fig. 4.35 has been used to investigate the carbonization traces (taking picture of carbonization patterns) on the surface of the pressboard after 15 minutes of PD activity at same level of electric stress. The voltage increased with 300 V/s slope up to 1 kV higher than PDIV. PDIV has been investigated acoustically and electrically via ICM and Omicron devices respectively. 10 minutes resting time during each step has been considered for taking picture without changing the location of the needle during each step of the voltage course.

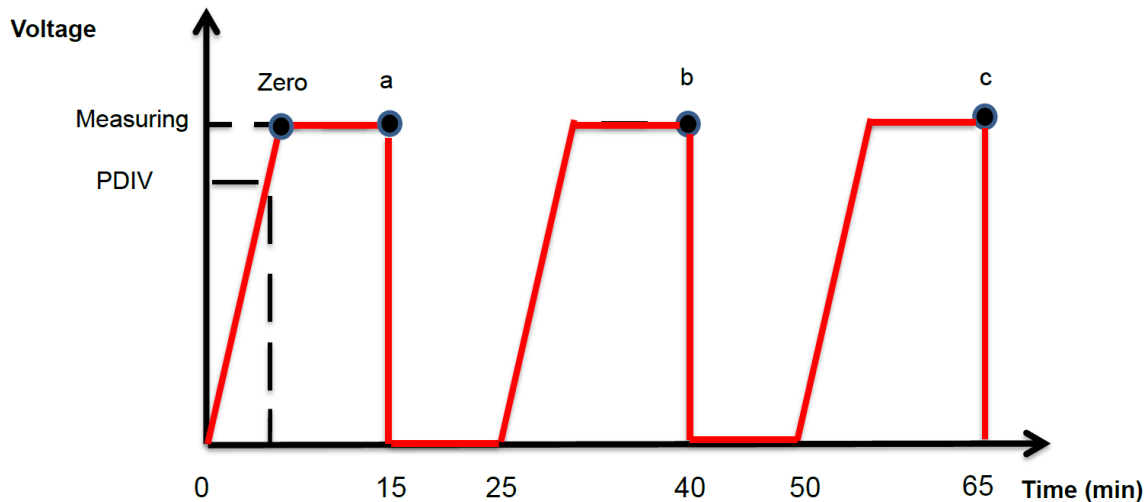


Fig. 4.35: The voltage course for investigating carbonized tracks on the surface of the aramid pressboard

Changing the needle position on the same pressboard deliver new and independent results. After changing the location and pressboard after each voltage course for more than 20 times, four different scenarios have been reached. By using ICM as AE measuring device acoustic activity could be divided in three different categories (High, Low and Silent PD).

4.5.1 Scenario 1

The electric PD signals increased up to 10 nC and AE activities decreased until silent PD. Fig. 4.36 shows “zero” point (before discharge) to “a” with 4 nC average apparent charge and 13.5 kV applied voltage in high acoustic activity (non-silent PD) situation.

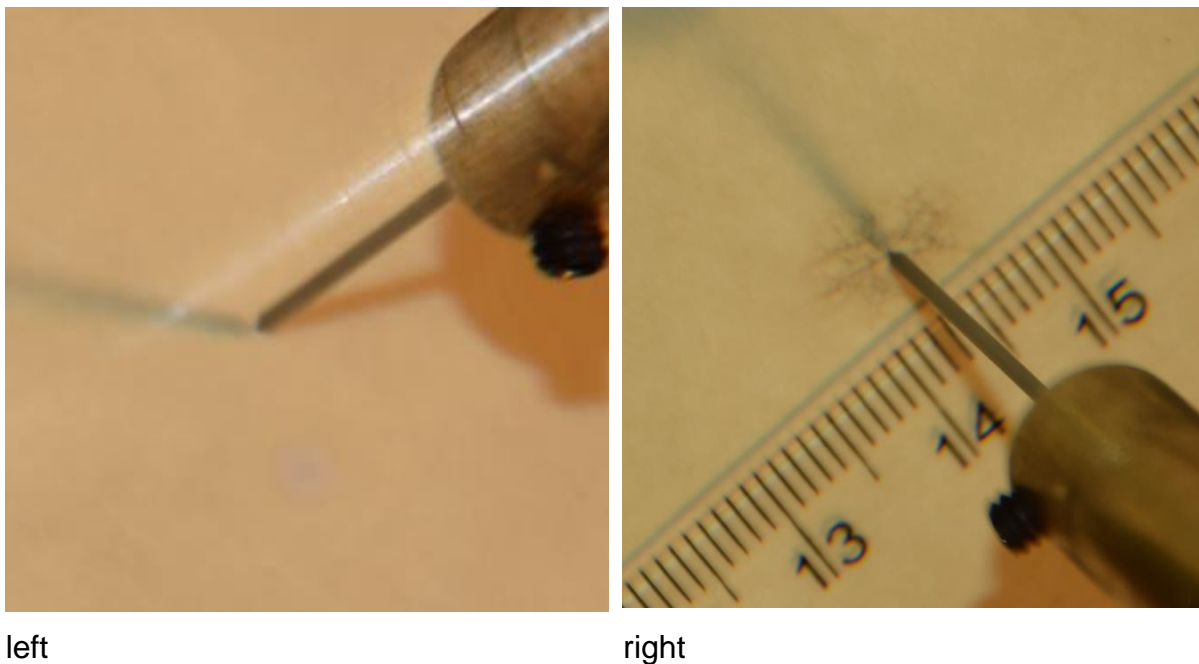
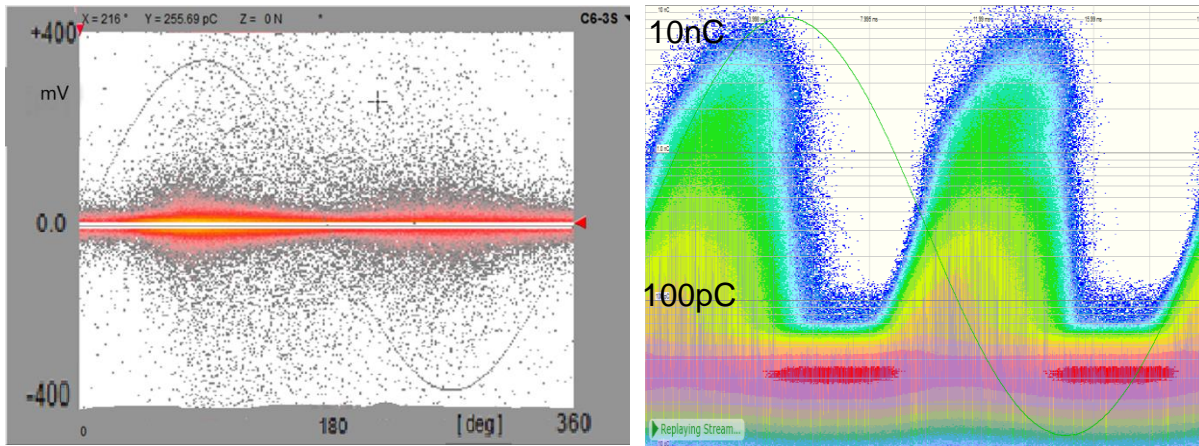
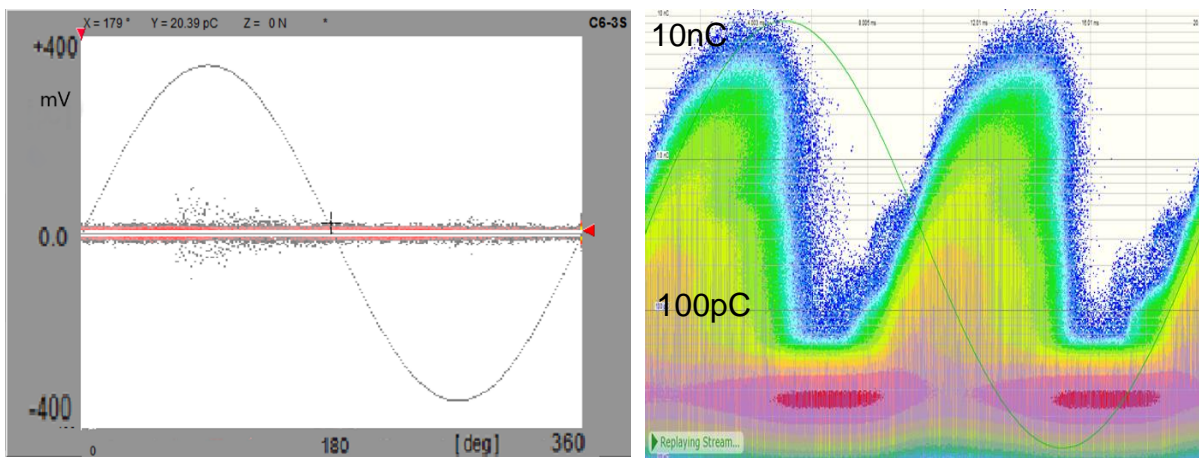


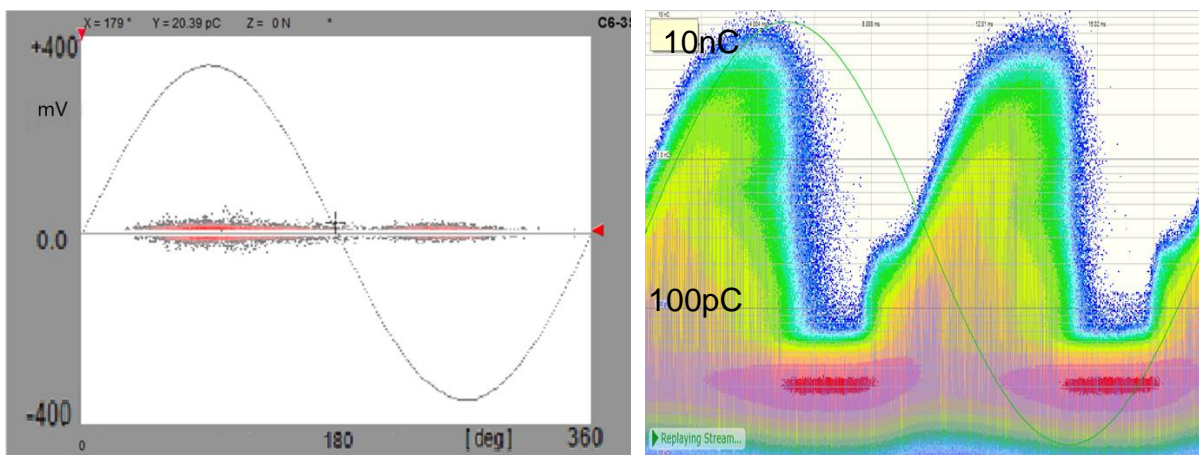
Fig. 4.36: Carbonization at the surface of the pressboard at zero (left) and after “a” (right)



a)



b)



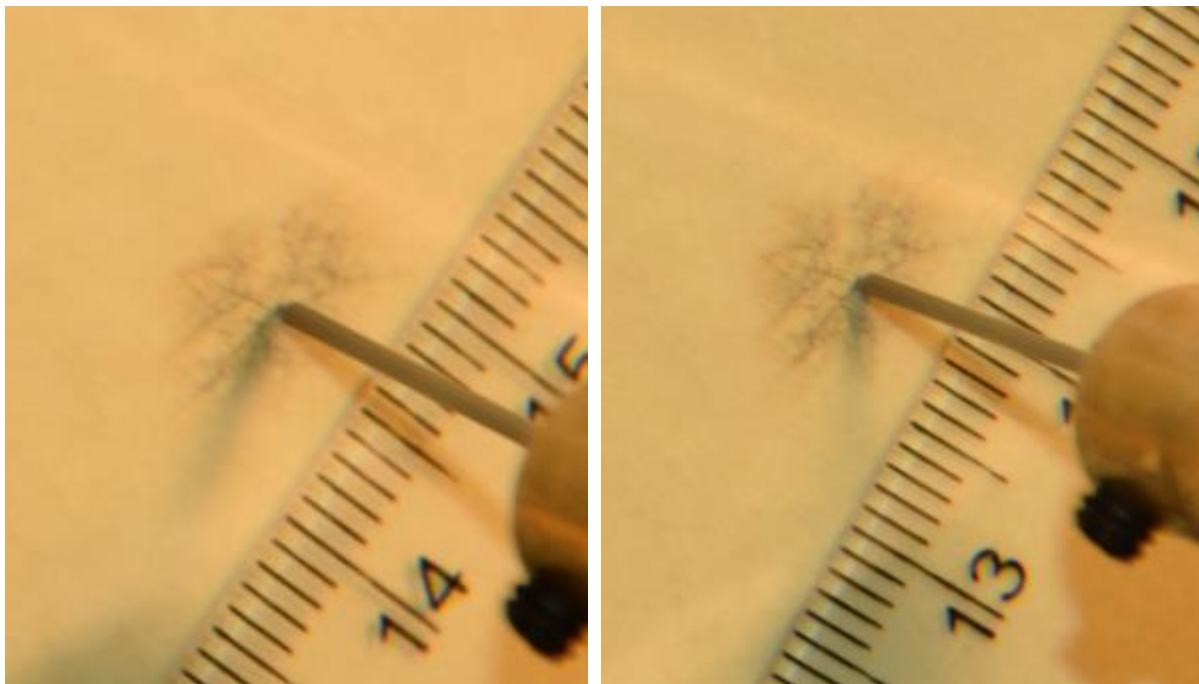
c)

Fig. 4.37: AE and electric PD activity during 10 nC PD apparent charge
 a) step a (AE signals left and electric signals right)
 b) step b (AE signals left and electric signals right)
 c) step c (AE signals left and electric signals right)

Fig. 4.37 shows AE activity at each step. In this scenario the electric PD activity changed not much, and the PD activity reach 10 nC maximum apparent charge and 4 nC apparent average charge during all steps. It shows a decrease in AE signals from step “a” to step “c”. At step c the AE signals reached its lowest level.

Fig. 4.38 shows carbonization after “b” and “c” for about 15 minutes at the same voltage (13.5 kV) in silent PD (very low acoustic activity) situation during “b” to “c”.

By comparing the Fig. 4.36 and Fig. 4.38 it reveals that, carbonization development from nothing (zero) to something in “a” in terms of length and number of traces is more than carbonization development from “b” to “c”. The electric discharges show not much differences in terms of average apparent charge from “b” to “c”. By comparing the AE signals measured at these two different stages (from “a” to “b” and from “b” to “c”), it could be concluded that silent PD have less destructive effects (from “b” to “c”) compared to the non-silent PDs (from “a” to “b”) at the same level of the apparent charges.



left

right

Fig. 4.38: Carbonization at the surface of the pressboard after “b” (left) and after “c” (right)

4.5.2 Scenario 2

The electric PD activities decreased, and AE signals increased over the time. Fig. 4.39 shows AE activity on pressboard at step b and c. AE signals has been increased at step c compared to step b, but on the other hand the electric PD signals decreased.

Fig. 4.40 shows carbonization after “a” and “b” in 15 minutes at 1.4 nC average apparent charges (max 5.8 nC) and 17.5 kV applied voltage with low acoustic activity during “a” to “b” (zero position is not shown because it shows the healthy pressboard without carbonization).

Fig. 4.41 shows carbonization after “b” and “c” 15 minutes at 473 pC average apparent charge (max 1.4 nC) and 17.5 kV applied voltage with high acoustic activity from “b” to “c”.

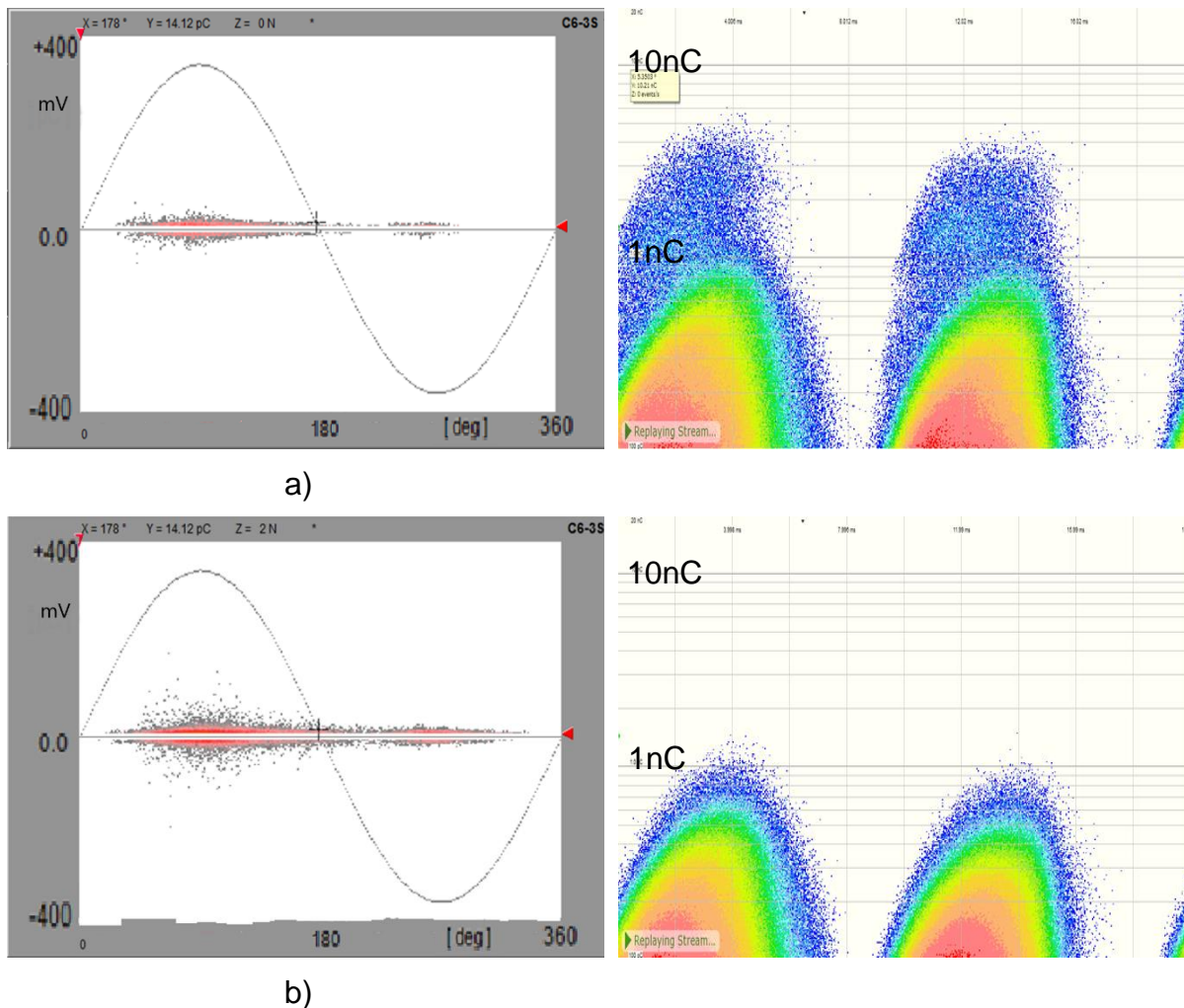
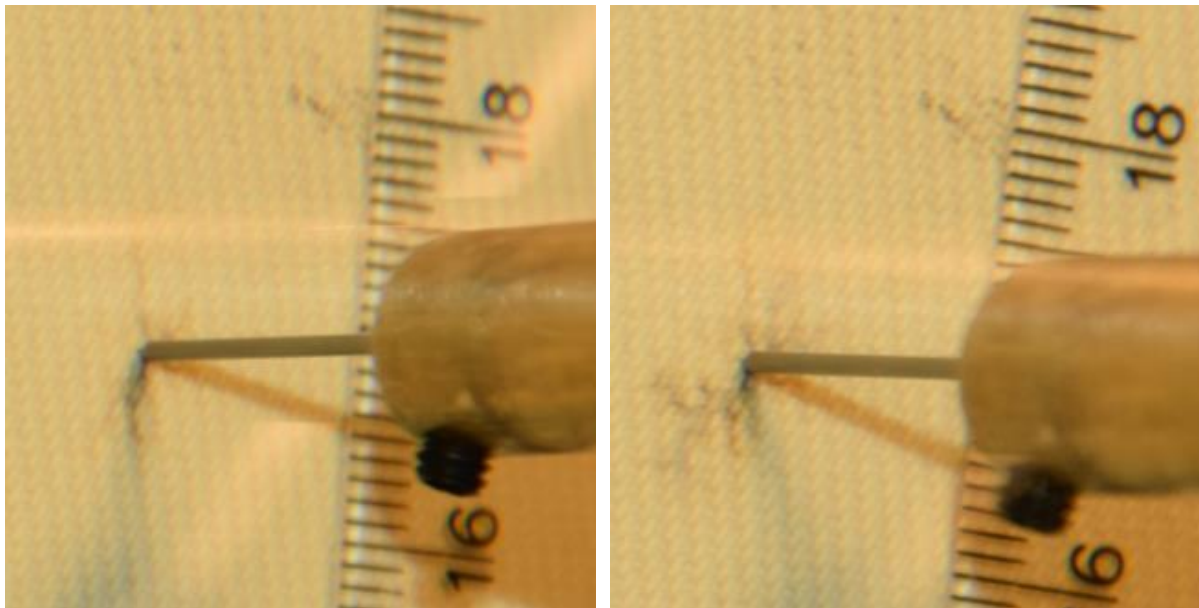


Fig. 4.39: 15 minutes AE and electric PD activity

- a) Between step a and b (AE signals left and electric signals right) with 1.4 nC average and maximum 5.8 nC apparent charge
- b) Between step b and c (AE signals left and electric signals right) with 473 pC average and maximum 1.4 nC apparent charge

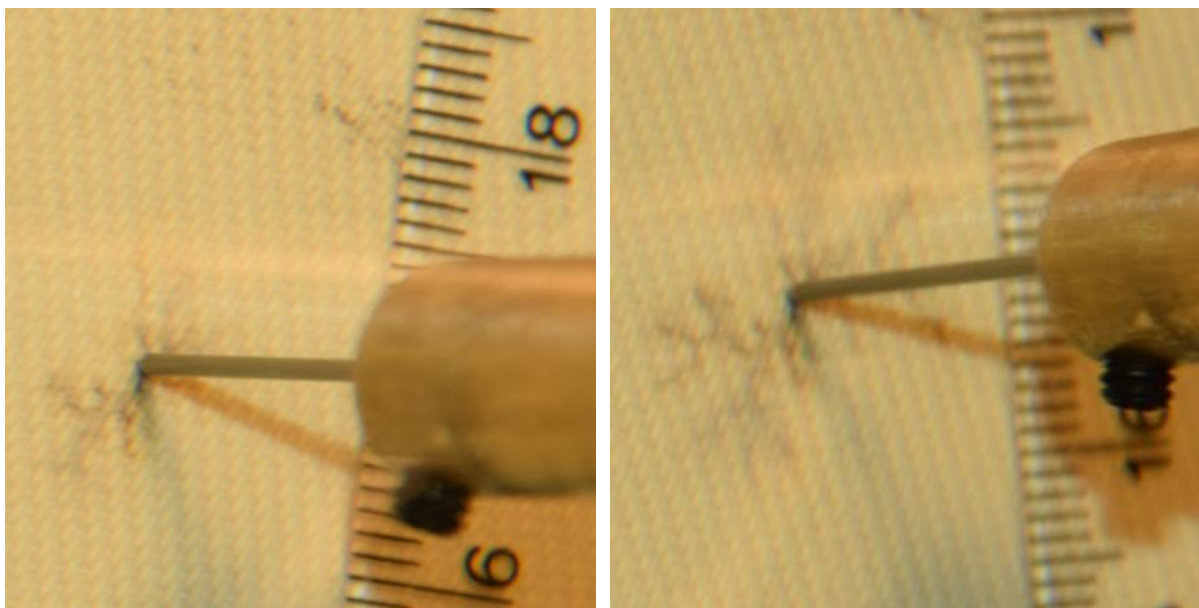
By comparing the Fig. 4.40 and Fig. 4.41 it reveals, that carbonization development from stand “a” to “b” shows lower values in terms of length and number of traces compared to carbonization development from “b” to “c”. However, the reduction of electric apparent discharges was less from “a” to “b” compared to from “b” to “c”. In contrast, AE signals increase from step “b” to “c” compared to step from “a” to “b”. The direct relation between AE signals and development level of carbonization shows that the AE signals give us more information regarding to the carbonization behaviour.



left

right

Fig. 4.40: Carbonization at the surface of the pressboard after “a” (left) and after “b” (right)



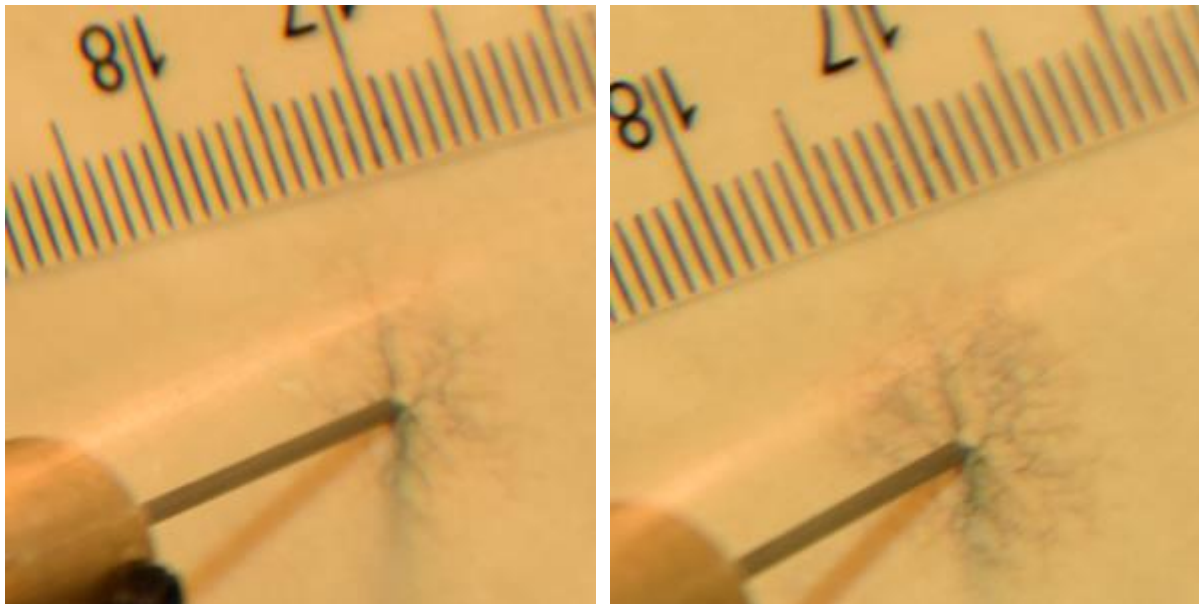
left

right

Fig. 4.41: Carbonization at the surface of the pressboard after “b” (left) and after “c” (right)

4.5.3 Scenario 3

The electric PD signals have been increased up to 47 nC (very high electric apparent charge) and the AE signals decreased until silent PD. Fig. 4.42 shows carbonization from “a” to “b” during 15 minutes at 17.2 nC average apparent charges (max 41 nC) and 13.5 kV applied voltage with low acoustic activity during discharges between “a” and “b” (acoustic activity very similar to Fig. 4.39b).

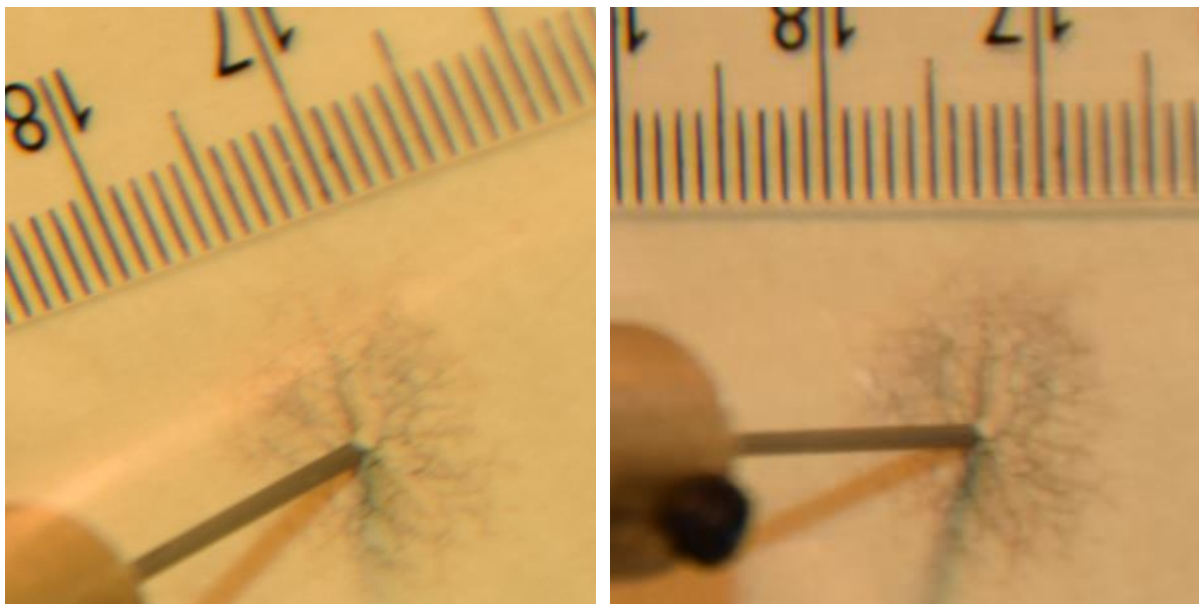


left

right

Fig. 4.42: Carbonization at the surface of the pressboard at “a” (left) and after “b” (right)

Fig. 4.43 shows carbonization between “b” and “c” in 15 minutes at 17.9 nC average apparent charges (max 47.24 nC) and 13.5 kV applied voltage in silent PD situation (no acoustic activity).



left

right

Fig. 4.43: Carbonization at the surface of the pressboard after “b” (left) and after “c” (right)

Fig. 4.42 shows by existing AE signals beside PD activity, the carbonization developed from “a” to “b”. The length of the carbonized traces has been not grown from “b” to “c” in Fig. 4.43, but the density of traces shows a small increase at very low acoustic activity (silent PD) and very high electric activity.

4.5.4 Scenario 4

In this scenario two different pressboards with two different AE and electric PD signal behaviour after the whole process (from “a” to “d”) are compared.

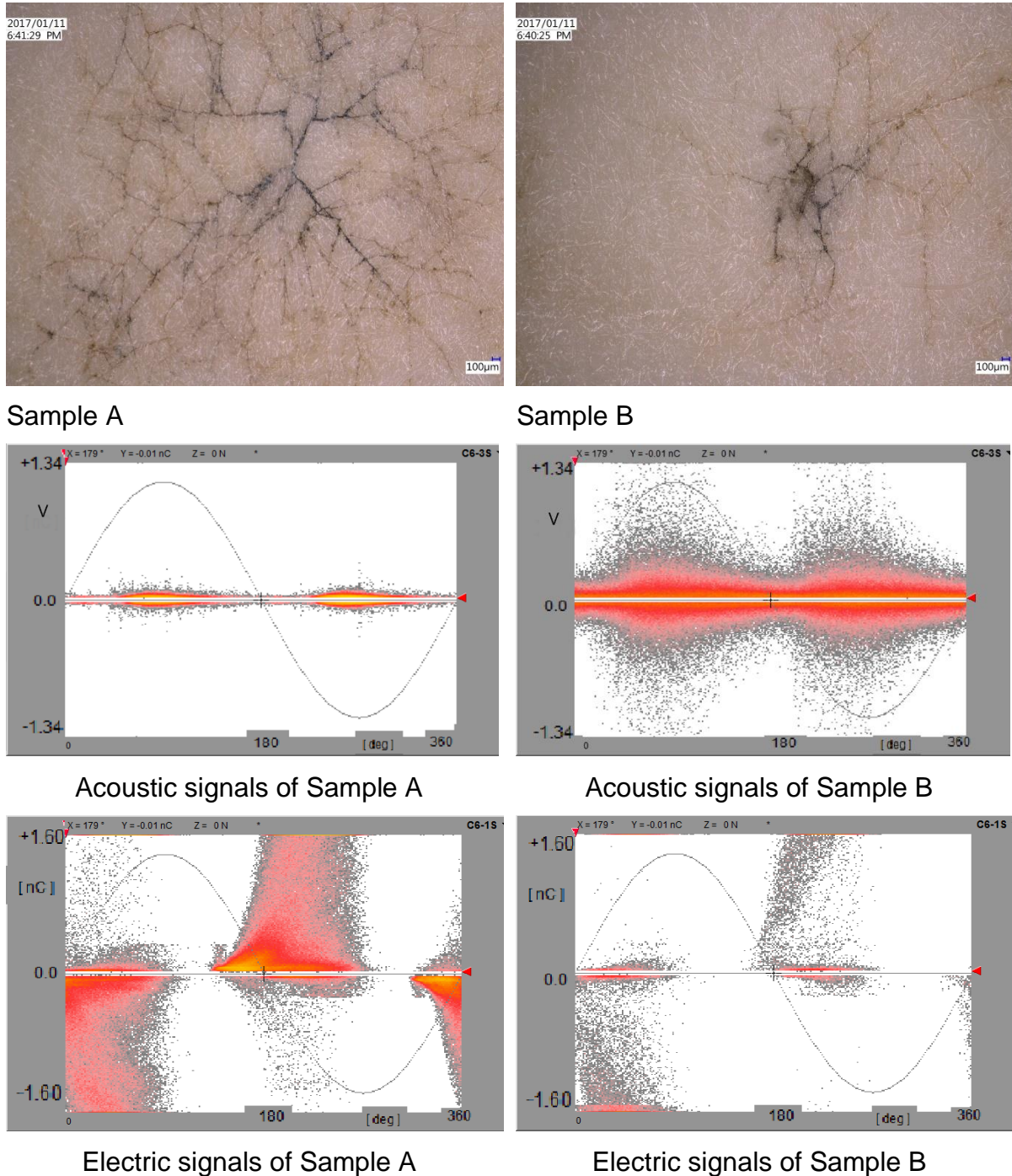


Fig. 4.44: Electric and acoustic signals measured by ICM during PD activity

Fig. 4.44 shows the electric and acoustic measurement of two different samples of a same pressboard (namely A and B) measured via ICM device at the same electric stress with the same PDIV and pressboard type (different location on the same pressboard). Sample A could tolerate a very high electric PD activity even after 65 minutes (after step “c”), while sample B could not and had a breakdown. However, the electric PD signals show less apparent charges on sample B before breakdown

compared to sample A. In contrast, the AE signals were higher on sample B compared to the sample A. These results show with same inception voltage and even lower PD apparent charges, the level deterioration could be higher. This proves the possibility of detection the level of carbonization and deterioration by comparing the AE signals. At non-silent activities the carbonization developed stronger than silent PD activities. Especially the length of the carbonization traces which had increased during non-silent PD. At PD activities even with very high apparent charges (above 30 nC), there were almost no changes in carbonization and in consequence silent PD activities.

4.5.5 Energy of silent PD

Less carbonization of silent PDs compared to non-silent PDs proves, that silent PDs won't produce much heat as non-silent PDs at the same amount of electric discharge.

Discharges emitte different light frequencies depending on the gas the discharges passing through, for example in air this turn to blue with the wavelength around 460 nm (Fig. 4.32). A photon is a quantum electromagnetic (EM) radiation. The energy of photon at each frequency is given by $E = hf$ where, f is the frequency and $h = 4.14 \cdot 10^{-15} \text{ eV.s}$ ($6.663 \cdot 10^{-34} \text{ J.s}$) is Plank constant. By considering the frequency of the blue light is about $0.6 \cdot 10^{13} \text{ Hz}$ there need to be an energy amount of $E = 3.9 \cdot 10^{-21} \text{ J}$ to release one photon.

To compare the light brightness of a PD light, an 80 W light bulb with 10% efficiency as an example would be considered. There would be $2.4 \cdot 10^{19}$ photons per second emitted for a 10 % efficiency of 80 W light bulb with visible light frequency of $5 \cdot 10^{14}$ [127]. More efficient lamp like fluorescent and LED lamps would generate the same number of photons with less energy, which would lead to much lower heat generation [128].

By considering a time difference of $\Delta t = 200 \mu\text{s}$ between two PD events (5° grades) around zero crossing of sinusoidal voltage (the most probable position of PD) with a peak voltage of 15 kV (inception voltage), the voltage difference between two PD events would be $\Delta V = 900 \text{ V}$. By considering a 2 nC discharge activity the number of photons released for 100 % efficiency (without any temperature losses) would calculate as follow:

$$J = \Delta V \cdot q = 900 \cdot 2 \cdot 10^{-9} = 1.8 \cdot 10^{-6} \text{ J} \quad (38)$$

$$\frac{\text{Total energy of one PD}}{\text{Energy of one Photon}} = \frac{1.8 \cdot 10^{-6}}{3.9 \cdot 10^{-21}} = 4.5 \cdot 10^{14} \text{ number of photons} \quad (39)$$

$4.5 \cdot 10^{14}$ number of photons are much less than number of photons emitted from a 80 W light bulb with 10% efficiency ($2.4 \cdot 10^{19}$ number of photons). This results to a very low light emission of 100 % discharge efficiency of PD activity compared to the 80 W light bubble with 10 % efficiency. The real picture of PD activities during silent discharge (Fig. 4.32) also showed blue light emission, which could transfer the discharge energy mostly to light emission with very low heat generation.

4.6 Summery

High number of electric PD activities could cause some constructive and destructive effect on AE waves created by PD. There could be some doubts about creation silent PD in result of destructive effects caused by high number of PD activities at a very

short time. To answer this question, two different examples have been discussed. The examples prove that silent PD is not caused by any destructive effects. In addition, the investigation on 20 mm and 16 mm electrode balls showed that, the mechanical attenuation could be not the main root cause of creation silent partial discharges. Microscopic picture of carbonization revealed the carbonization traces of surface discharges very near to the surface (Fig. 4.31). The results of chapter 4.2 show that electrical damaging process, has a significant influence on creation silent PD at different electrodes without oil gap. It could be understood that oil-gap distance between the electrodes and pressboards increases the possibility of detection AE signals generated by electric discharges (non-silent PD) even at carbonized situation.

The main advantage of UHF method against acoustic method is the detection of silent PD. The creation of silent PD on different insulation materials has been tested. The results showed lower degradation of silent PD compared to non-silent PD. Very low AE signals of the silent PD show a similarity to dielectric barrier discharge. But to have dielectric barrier discharge some essential conditions should exist, namely gas creation between solid insulation and high voltage electrode.

By assuming the heat generation of PD activity, the heat generation during silent and non-silent PD has been compared by comparing the carbonization traces at each stage. This could be seen by comparing the electric PD and AE signals in Fig. 4.37 with carbonize traces in Fig. 4.36 and Fig. 4.38. It proved the lower temperature generation during silent PD compared to the non-silent PD.

Conclusion

Comparative evaluation of acoustic and electric partial discharge (PD) signals requires investigation on typical arrangements in order to evaluate the consequences of discharge activities inside insulation materials such as oil, paper and pressboards on acoustic emission (AE) signals. Therefore, investigations were done on different arrangements.

Needle-plane arrangement with oil gap was used to generate PD in oil (corona in oil). Electric PDs were measured via coupling capacitor and AE signals via acoustic DSP device. Corona in oil showed repeatable results with a proportional relation between average PD apparent charge and AE signal, where 50 pC average electric PD apparent charge produced around 53 dB average AE signal and 250 pC average electric PD apparent charge around 70 dB average AE signal. This relation is caused by a higher thermal energy release from higher magnitude of the electric PD event (apparent charge), which led to higher AE signal. AE captured frequencies from PD actives were directly related to the AE sensor peak frequencies (75 kHz and 150 kHz).

To generate the PD in pressboard without mechanical acoustic barrier, surface discharges via needle-plane arrangement without oil gap has been chosen. Investigation on surface discharges showed the uncorrelated behaviour of the AE and electric PD signals. Surface discharge by needle-plane arrangement (without oil gap) showed lower AE signals compared to same arrangement with oil gap. During the surface discharges, some electric PD signals without AE signals could be captured via coupling capacitor measurement. In this regards, two different categories in terms of acoustic measurements have been named (silent and non-silent PD), which silent PD defined for PDs with AE signals below the acoustic noise level and non-silent PD for PDs with AE signals above the acoustic noise level.

Carbonization on the surface of the pressboard was assumed as the main reason of creation of silent PD. Random process of creation of carbonization was influenced by changing voltage peak and as the result on creation of silent PDs. Image processing results of carbonization after discharge activity showed a higher impact of the carbonization area compared to the carbonization length on creation the silent PD. At beginning of PD activity, carbonization started always by non-silent PD activities. Noticeable reduction of AE amplitudes after some discharges were measured after each test due to the carbonization. In contrast to AE signals, carbonization normally increased the electric PD signals in terms of amplitude and numbers.

The silent PDs have been investigated via two different AE sensors with 75 kHz and 150 kHz peak frequency. By arranging the PD source in the middle of the tank, the acoustic destructive superimposition effects caused by delay between two PD activities and same acoustic wave travel distance to AE sensors has been investigated. The results proved the existence of the silent PDs are not due to the acoustic destructive effect.

To investigate the acoustic damping inside the pressboards, PD activity during internal discharges via ball electrode arrangements have been used. To eliminate the corona in oil discharges around the ball electrode, a paper pressboard (15 mm thickness) with a hole in the middle has been used (Fig. 4.10). The results showed 15 dB AE reduction from the PD inside the pressboard compared to the surface discharge before carbonization due to the acoustic attenuation. Noticeable reduction of AE amplitudes

(silent PD) after carbonization has been realized at the same electrical signals. This proves the existence of silent PD due to the carbonization and not acoustic damping.

Digital signal process (DSP), high speed oscilloscope and ultra-high frequency (UHF) sensor in addition to AE sensor have been used to measure the UHF signals of the silent PD at different resolution and sample rates. The results showed that silent PDs could be captured by UHF sensors. There exists also no difference in terms of electric UHF signal characteristic between silent and non-silent PD.

Deep investigation on electric PD pattern via coupling capacitor measurement in parallel to AE measurement showed, that PD pattern changed after some minutes of non-silent PD, but the pattern did not change during silent PD activity at same level of apparent charge and time slot (10 minutes of PD activity). This is due to lower temperature generation of silent PD compared to non-silent PD.

To investigate the carbonization development rate, the carbonization at silent and non-silent PD activities on wet and dry type low density and high-density pressboards have been studied. The study admitted higher probability of creation non-silent PD on the surface of dry low-density pressboard compared to the wet high-density pressboard. The nucleation of dissolved gases inside the oil around the solid materials beside the creation of discharge some micrometres below the surface of the pressboard creates a perfect situation for dielectric barrier discharge. Dielectric barrier discharges generate electric PD signals with very low temperature and as the result lower carbonization and AE signals compared to other PD activities will be observed.

Study the level of deterioration by comparing the pictures of carbonizations during different PD events on pressboards proved the higher carbonization of non-silent PD compared to the silent PD at same electric charge. This evidence showed the lower temperature of the silent PD versus non-silent PD. Also, very high carbonization in some cases even during PD activity with low AE signals destroyed the pressboard at contact point and created an oil gap. The oil gap increased the possibility of generating corona in oil and non-silent PD. This normally led to a break down after some non-silent PD activities (Fig. 4.44).

The possibility of conversion the energy release of silent PD to visible light instead of heat energy has been illustrated. This study proved the possibility of transforming high amount of PD energy into light (lower thermal energy). Carbonization detail experiments also showed lower AE activity during slow carbonization process and high acoustic activities during fast carbonization process of the pressboards.

However electric PD measurement has the advantage of detecting PD regardless of silent or non-silent type, but classification of these two types of PD via AE measuring system could determine the level of carbonization. The carbonization at the beginning generates high electric and AE signals and latter with no progress in carbonization, no AE signals could be detected and therefore availability of the signal information from the beginning of PD activity plays a very important roll. If non-silent PD happened after a period silent PD activity this shows a sign of a strong progressive carbonization and damaging of the insulation materials. These results could be used to improve lifetime estimation of insulation materials by measuring the AE and electric PD signals. This feature is an advantage of combination electric and acoustic method versus all other measuring technics.

References

- [1] V. Y. Ushakov, V. J. Ušakov, V. Y. Ushakov, V. I. Ushakov, "Insulation of high-voltage equipment", Springer Science & Business Media (2004).
- [2] W. Ziomek, "Transformer electrical insulation", IEEE Transactions on Dielectrics and Electrical Insulation, 19.6 (2012): 1841-1842.
- [3] Y. Z. Lv, "Recent progress in nanofluids based on transformer oil: preparation and electrical insulation properties", IEEE Electrical Insulation Magazine 30.5 (2014): 23-32.
- [4] M. Kohtoh, "Aging effect on electrical characteristics of insulating oil in field transformer", IEEE Transactions on Dielectrics and Electrical Insulation, 16.6 (2009): 1698-1706.
- [5] D. S. C. Verma, P. Singh, "Effects on tensile strength of transformer insulation paper under accelerated thermal and electrical stress" Annual Report-Conference on Electrical Insulation and Dielectric Phenomena IEEE, (2007).
- [6] H. M. Ryan, "High voltage engineering and testing", No. 32. Iet, (2001).
- [7] R. James, Qi Su, "Condition assessment of high voltage insulation in power system equipment" Vol. 53. IET, (2008).
- [8] A. Küchler High Voltage Engineering: Fundamentals-Technology-Applications. Springer, (2017).
- [9] S. Tenbohlen, J. Jagers, F. Vahidi, "Standardized survey of transformer reliability: On behalf of CIGRE WG A2.37", 2017 International Symposium on Electrical Insulating Materials (ISEIM), Toyohashi, Japan, (2017): 593-596.
- [10] G. Winsor, S. Buncombe, "Repair/Replace Decision Making Practices," ICOMS Asset Management Conference, Melbourne, Australia, (2007)
- [11] X. Zhang, E. Gockenbach. "Age-dependent maintenance strategies of medium-voltage circuit-breakers and transformers", Electric power systems research 81.8 (2011): 1709-1714.
- [12] D. Martin, "Investigation into modeling Australian power transformer failure and retirement statistics", IEEE Transactions on Power Delivery 33.4 (2018): 2011-2019.
- [13] D. Shipp, "Transformer failure due to circuit-breaker-induced switching transients", IEEE Transactions on Industry Applications 47.2 (2010): 707-718.
- [14] M. KornATKA, "Analysis of the exploitation failure rate in Polish MV networks" Eksploatacja i Niezawodność 20 (2018).
- [15] G. Jose, R. Chacko, "A review on wind turbine transformers", 2014 Annual International Conference on Emerging Research Areas: Magnetism, Machines and Drives (AICERA/iCMMD), Kottayam, India, (2014): 1-7, doi: 10.1109/AICERA.2014.6908172.
- [16] L. Yang, "Influence of vegetable oil on the thermal aging of transformer paper and its mechanism", IEEE Transactions on Dielectrics and Electrical Insulation 18.3, (2011): 692-700.
- [17] J. Singh, Y. Raj Sood, P. Verma, "The influence of service aging on transformer insulating oil parameters", IEEE Transactions on Dielectrics and Electrical insulation 19.2, (2012): 421-426.
- [18] I. Fofana, "Aging of transformer insulating materials under selective conditions", European transactions on electrical power 17.5 (2007): 450-470.
- [19] R. Singh, A. Singh, "Aging of distribution transformers due to harmonics", Proceedings of 14th International Conference on Harmonics and Quality of Power-ICHQP 2010. IEEE, (2010).
- [20] G. N. Wu, "Experimental study on further thermal aging of transformer oil-paper insulation by organic acid catalysis", High Voltage Eng. 41.3 (2015): 832-839.

- [21] M. D. Judd, "Intelligent condition monitoring and asset management. Partial discharge monitoring for power transformers", *Power Engineering Journal* 16.6 (2002): 297-304.
- [22] A. Cavallini, "Diagnosis of EHV and HV transformers through an innovative partial-discharge-based technique" *IEEE Transactions on Power Delivery* 25.2 (2009): 814-824.
- [23] M. Mondal, G. B. Kumbhar, "Detection, measurement, and classification of partial discharge in a power transformer: Methods, trends, and future research" *IETE Technical Review* 35.5 (2018): 483-493.
- [24] M. D. Judd, L. Yang, I. Hunter, "Partial discharge monitoring of power transformers using UHF sensors. Part I: sensors and signal interpretation", *IEEE Electrical Insulation Magazine* 21.2 (2005): 5-14.
- [25] H. H. Sinaga, B. T. Phung, T. R. Blackburn, "Partial discharge localization in transformers using UHF detection method", *IEEE Transactions on Dielectrics and Electrical Insulation* 19.6 (2012): 1891-1900.
- [26] M.D. Judd, G. P. Cleary, C. J. J. Bennoch, "Applying UHF partial discharge detection to power transformers", *IEEE Power Engineering Review* 22.8 (2002): 57-59.
- [27] M. Wang, "Partial discharge pattern recognition of current transformers using an ENN", *IEEE Transactions on Power Delivery* 20.3 (2005): 1984-1990.
- [28] J. Ramírez-Niño, A. Pascacio, "Acoustic measuring of partial discharge in power transformers", *Measurement Science and Technology* 20.11 (2009): 115-108.
- [29] E. T. N. Howells, E. T. Norton, "Location of partial discharge sites in on-line transformers", *IEEE transactions on power Apparatus and systems* 1 (1981): 158-162.
- [30] B. Castro, "Partial discharge monitoring in power transformers using low-cost piezoelectric sensors", *Sensors* 16.8 (2016): 12-66.
- [31] Y. Wang, "Acoustic localization of partial discharge sources in power transformers using a particle-swarm-optimization-route-searching algorithm", *IEEE Transactions on Dielectrics and Electrical Insulation* 24.6 (2017): 3647-3656.
- [32] S. Qian, "High sensitivity detection of partial discharge acoustic emission within power transformer by sagnac fiber optic sensor", *IEEE Transactions on Dielectrics and Electrical Insulation* 25.6 (2018): 2313-2320.
- [33] S. Yoshida, "Light emission spectrum depending on propagation of partial discharge in SF₆", *Conference Record of the 2008 IEEE International Symposium on Electrical Insulation. IEEE*, (2008).
- [34] S. Sarma, G. N. S. Kalyani, "ANN approach for condition monitoring of power transformers using DGA", *2004 IEEE Region 10 Conference TENCN 2004. Vol. 100. IEEE*, (2004).
- [35] O. E. Gouda, S. H. El-Hoshy, H. H. El-Tamaly, "Proposed heptagon graph for DGA interpretation of oil transformers", *IET Generation, Transmission & Distribution* 12.2 (2018): 490-498.
- [36] L. L. Li, N. Zhou, G. Sheng, X. Jiang, "A Novel Partial Discharge Localization Method in Substation Based on a Wireless UHF Sensor Array", *MDPI, Basel, Switzerland*, 10.3390/s17081909, Aug, (2017).
- [37] D. Benzerouk, "Pulse Sequence Analysis and Pulse Shape Analysis: Methods to Analyse Partial Discharge Processes", *Universität Siegen, Dr.-Ing. Dissertation, Germany*, (2008).
- [38] P. H. F. Morshuis, "Partial discharge mechanisms, mechanisms leading to break-down, analysed by fast electrical and optical measurements", *PhD Thesis, Delft U-niversity, Netherlands*, (1993).
- [39] D. Antony, P. Mishra, A. Todi, "Partial discharge localisation in transformers using UHF technique: non-iterative method", *Int. j. inf. tecnol.* 13, 291–297 (2021).
- [40] B. M. Ibrahim, S. Taha, R. Dessouky, S.S.M. Ghaly Ghoneim, "Enhanced partial discharge location determination for transformer insulating oils considering allocations and uncertainties of acoustic measurements", *Alexandria Engineering Journal, Volume 59, Issue 6*, (2020): 4759-4769, ISSN 1110-0168,

- [41] M. Duval, L. Lamarre, "The duval pentagon-a new complementary tool for the interpretation of dissolved gas analysis in transformers", *IEEE Elect. Insul. Mag.*, Vol. 30, Issue: 6, (2014): 9-12.
- [42] IEEE Guide for the Detection and Location of Acoustic Emissions from Partial Discharges in Oil-Immersed Power Transformers and Reactors, *IEEE Std C57.127™* (2007).
- [43] S. Hawking, "A Brief History of Time from the Big Bang to Black Holes", Bantam Dell Publishing Group, (1988).
- [44] S. L. Jones, "The detection of partial discharges in power transformers using computer aided acoustic emission techniques", Conference record of the 1990 IEEE international symposium on electrical insulation, Toronto, Canada, (1990).
- [45] E. Howells, E. Norton, "Location of Partial Discharge sites in on-line transformers", *IEEE Trans. Power App. Syst.*, Vol. PAS -100, No 1, (1981): 158-161.
- [46] R. Patsch, F. Berton, "Pulse Sequence Analysis - a diagnostic tool based on the physics behind partial discharges", *2001 J. Phys. D: Appl. Phys.* (2001): 25-35.
- [47] H. Illias, T. S. Yuan, A. H. A. Bakar, H. Mokhlis, G. Chen, P. L. Lewin, "Partial discharge patterns in high voltage insulation," *2012 IEEE International Conference on Power and Energy (PECon)*, (2012): 750-755, doi: 10.1109/PECon.2012.6450316.
- [48] M. Hoof, R. Patsch, "Analyzing partial discharge pulse sequences-a new approach to investigate degradation phenomena," *Proceedings of 1994 IEEE International Symposium on Electrical Insulation*, (1994): 327-331, doi: 10.1109/ELINSL.1994.401501.
- [49] L. E. Kinsler, A. R. Frey, A. B. Coppens, J. V. Sanders, "Fundamentals of Acoustics", New York: John Wiley & Sons, Inc. ISBN 0-471-84789-5, (2000).
- [50] A. S. Dukhin, P. J. Goetz, "Fundamentals of Acoustics in Homogeneous Liquids: Longitudinal Rheology", Elsevier, Volume 24, (2010): 91-125.
- [51] P. M. Morse, K. U. Ingard, "Theoretical Acoustics", Princeton University Press, ISBN: 0-691-08425-4, (1968).
- [52] F. G. Friedlander, "The diffraction of sound pulses. I. Diffraction by a semi-infinite plane" *Proceedings of the Royal Society A: Mathematical, Physical and Engineering Sciences*, 186, (1946): 322-344.
- [53] S. E. Rigby, A. Tyas, T. Bennett, S. D. Clarke, S. D. Fay, "The Negative Phase of the Blast Load", *International Journal of Protective Structures*, Vol. 5, NO. 1, (2014): 1-20.
- [54] P. He, "Simulation of ultrasound pulse propagation in lossy media obeying a frequency power law," *IEEE Trans. Ultra. Ferro. Freq. Contr.* Vol. 45, No. 1, (1998).
- [55] W. Lijing, S. Liping, Z. Yuerong, "Simulation of piezoelectric sensor-actuators based on multi-piezoelectric effect," *2010 2nd International Asia Conference on Informatics in Control, Automation and Robotics (CAR 2010)*, (2010): 402-404, doi: 10.1109/CAR.2010.5456580.
- [56] M. Beyer, H. Borsi, M. Hartje, "Some Aspects about Possibilities and Limitation of Acoustic Partial Discharges (PD) Measurements in Insulation Fluids" *5th International Symposium on High Voltage Engineering (ISH)*, (1987): 41.04.
- [57] S. A. M. Najafi, A. Peimankar, E. Gockenbach, H. Borsi, "Correlation Between Electrical Measured Partial Discharges And Acoustic Emission Signals From New And Thermal Aged Pressboards In Oil", *18th International Symposium on High Voltage Engineering (ISH)*, Seoul, South Korea, (2013).
- [58] L.M. Brekhovskikh, O.A. Godin, "Sound Reflection from a Medium with Arbitrarily Varying Parameters. In: *Acoustics of Layered Media I*", Springer Series on Wave Phenomena, vol 5. Springer, Berlin, Heidelberg. https://doi.org/10.1007/978-3-642-52369-4_10 (1990).
- [59] T. Bengtsson, M. Leijon, L. Ming, "Acoustic frequencies emitted by partial discharges in oil," *ISH-93*, (1993).

- [60] P. Janus, "Acoustic Emission Properties of Partial Discharges in the time-domain and their applications", Electromagnetic Engineering School of Electrical Engineering Kungliga Tekniska Högskolan, Masters' Degree Project, Stockholm, Sweden, (2012).
- [61] S. A. M. Najafi, E. Gockenbach, H. Borsi, "Correlation between electric and acoustic signals of discharge phenomenon at different electrical stress", 18th International Symposium on High Voltage Engineering (ISH), Seoul, South Korea, (2013).
- [62] R. Madarshahian, "Hsu-Nielsen source acoustic emission data on a concrete block." Data in brief vol. 23 103813. 6 Mar. 2019, doi:10.1016/j.dib.2019.103813
- [63] Tatro, C. A. , " Design Criteria For Acoustic Emission Experiment", In Acoustic Emission, ASTM STP 505, Philadelphia, PA: American Society for Testing and Materials; (1972).
- [64] K. Endoo, Y. Uwano; K. Hiraishi; T. Oonuma, R. Uemura, "Improvement of dielectric strength on transformer winding using new aramid paper", *Electr. Eng. Jpn.* (1995): 41–51
- [65] J. Gielniak, A. Graczkowski, H. Moranda, P. Przybyłek, K. Walczak, Z. Nadolny, H. Moscicka-Grzesiak, K. Feser, S. M. Gubanski, "Moisture in Cellulose Insulation of Power Transformers – Statistics", *IEEE Transactions on Dielectrics and Electrical Insulation* Vol. 20, No. 3; June (2013).
- [66] S. A. Boggs, "Partial Discharge: Overview and signal Generation", *IEEE Elect. Insul. Mag*, Vol. 6, No. 4, (1990).
- [67] Suwarno, "In Comparison Between Corona Discharge in Air and Streamer Discharge in Silicone Oil", 2008 International Conference on High Voltage Engineering and Application, (2008): 553-556, doi: 10.1109/ICHVE.2008.4773995.
- [68] L. Loïselle, UM. Rao, I Fofana, "Influence of Aging on Oil Degradation and Gassing Tendency for Mineral oil and Synthetic Ester under Low Energy Discharge Electrical Faults", *Energies*. 2020; 13(3):595.
- [69] G. Berg, L. Lundgaard, "Discharges in combined oil/paper insulation", *Proceeding of the 1999 IEEE 13th International Conference on Dielectric Liquids*, Nara, Japan, July (1999):144–147.
- [70] C. Dervos, P. D. Bourkas, E. A. Kayafas,, I. A. Stathopoulos, "Enhanced partial discharges due to temperature increase in the combined system of a solid-liquid dielectric", *IEEE Trans. Electr. Insul.* vol. 25, no. 3 June, (1990): 469-474.
- [71] H. C. Miller, "Surface flashover of insulators", in *IEEE Transactions on Electrical Insulation*, vol. 24, no. 5, Oct. (1989): 765-786, doi: 10.1109/14.42158.
- [72] R. Anderson, J. Brainard, "Mechanism of pulsed surface flashover involving electron stimulated desorption", *J. Appl. Phys.*, 51(1980): 1414-1421.
- [73] M. Liu, Y. Liu, Y. Li, P. Zheng, H. Rui, "Growth and partial discharge characteristics of electrical tree in XLPE under AC-DC composite voltage", in *IEEE Transactions on Dielectrics and Electrical Insulation*, vol. 24, no. 4, (2017): 2282-2290, doi: 10.1109/TDEI.2017.006537.
- [74] K. Hillermeier, "Prospects of Aramid as a Substitute for Asbestos", *Textile Research Journal*, (1984): 575-580.
- [75] O. M. Zodeh, R. J. Whearty, "Thermal Characteristics of a Meta-Aramid and Cellulose at Loads Beyond Nameplate", *IEEE Trans. Dielectr. Electr. Insul.*, Vol. 12, no. 1, January (1997): 234-248.
- [76] F. Barsoum, J. Suleman, A. Korcak, E.V. K. Hill, "Acoustic emission monitoring and fatigue life prediction in axially loaded notched steel specimens", *Journal Acoustic Emission*, (2009): 40-63.
- [77] M. Carlos, F. Vallen, "Acoustic Emission Signal Processing", in P. O. Moore (ed.), *Acoustic Emission Testing*, 3rd edn, Vol. 6 of *Nondestructive testing handbook*, American Society for Nondestructive Testing, Inc., Columbus, (2005): 153–154.
- [78] R. Unnpórsson, "Hit Detection and Determination in AE Bursts, Acoustic Emission", *Research and Applications*, Wojciech Sikorski, IntechOpen, DOI: 10.5772/54754, (2013).

- [79] Physical Acoustic corporation website; <https://www.physicalacoustics.com/>
- [80] Math work Image Processing Toolbox Available: <http://www.mathworks.com/products/image/>
- [81] K. E. Seralathan, A. Mahajan, N. Gupta, "Modelling of Electric Tree Progression due to Space Charge modified Field", *J. Phys. D: Appl. Phys*, Vol 41, (2008): 1-9.
- [82] S. A. M. Najafi, E. Gockenbach, H. Borsi, "Effect of Carbonized Patterns on Oil-Impregnated Pressboards Surface on Acoustic Emission Signals at Inhomogeneous Electric Field", *IEEE Trans. Dielectr. Electr. Insul.* vol. 25, no. 5, Oct. (2018): 1644-1650, doi: 10.1109/TDEI.2018.006939.
- [83] L. A. Dissado, J. C. Fothergill, "Electrical degradation and breakdown in polymers", Peter Peregrinus Ltd., London, (1992).
- [84] H. Reather, "Electron avalanches and breakdown in gases", Butterworths, London, (1964).
- [85] Y. Kitamura, S. Hirabayashi, "Partial discharge deterioration of epoxy resin for electronic parts", *Ann. Rep. Conf. Elect. Insul. & Diel. Phenom.*, (1985): 485-490.
- [86] T. Tanaka, "Internal partial discharge and material degradation" *IEEE Trans. On Electr. Insulation*, Vol. EI-21, (1986): 899-905.
- [87] J. C. Devins, "The Physics Of Partial Discharges In Solid Dielectrics" *IEEE Trans. On Electr. Insulation*, Vol. EI-19, (1984): 475- 494.
- [88] L Ziegler, E Gonzalez, T Rubert, U Smolka, J J. Melero, "Lifetime extension of onshore wind turbines: A review covering Germany, Spain, Denmark, and the UK" *Renewable and Sustainable Energy Reviews*, Volume 82, Part 1, (2018): 1261-1271.
- [89] A. J. M. Cardoso, L. M. R. Oliveira, "Condition monitoring and diagnostics of power transformers," *Int. J. COMADEM*, vol. 2, Jul. (1999): 5–11.
- [90] S. Li, J. Li, "Condition monitoring and diagnosis of power equipment: Review and prospective", *High Voltage*, vol. 2, no. 2, Jun. (2017): 82–91.
- [91] M. Bigdeli, M. Vakilian,, E. Rahimpour, "Transformer winding faults classification based on transfer function analysis by support vector machine", *IET Electr. Power Appl.*, vol. 6, no. 5, May (2012): 268–276.
- [92] N. Hashemnia, A. Abu-Siada,, S. Islam, "Detection of power transformer bushing faults and oil degradation using frequency response analysis", *IEEE Trans. Dielectrics Electr. Insul.*, vol. 23, no. 1, Feb. (2016): 222–229.
- [93] Q. Fu, J. Zhu, Z.-H. Mao, G. Zhang, T. Chen, "Online condition monitoring of onboard traction transformer core based on core-loss calculation model", *IEEE Trans. Ind. Electron.*, vol. 65, no. 4, Apr. (2018): 3499–3508.
- [94] C. Aj, M. A. Salam, Q. M. Rahman, F. Wen, S. P. Ang, W. Voon, "Causes of transformer failures and diagnostic methods—A review", *Renew. Sustain. Energy Rev.*, vol. 82, Feb. (2018): 1442–1456.
- [95] Y. Han, Y. H. Song, "Condition monitoring techniques for electrical equipment-a literature survey", *IEEE Trans. Power Del.*, vol. 18, no. 1, Jan. (2003): 4–13.
- [96] S. Tenbohlen et al., "Development and results of a worldwide transformer reliability survey", in *Proc. CIGRE SC A2 Colloq.*, Shanghai, China, Sep. (2015).
- [97] IEC Power transformers – Part 13: Self-protected liquid-filled transformers, IEC Standard 60076-13, (2006).
- [98] E. Kuffel, W. S. Zaengl, J. Kuffel, *High Voltage Engineering Fundamentals*. Newnes, Elsevier Butterworth-Heinemann, 2nd ed. (2000).
- [99] N. Izeki, A. Kurahashi, K. Matsuura, "Behavior of Oil Corona and Damage of Transformer Insulation", in *IEEE Transactions on Power Apparatus and Systems*, vol. PAS-90, no. 5, Sept. (1971): 2330-2338, doi: 10.1109/TPAS.1971.293081.
- [100] P. H. F. Morshuis, "Degradation of solid dielectrics due to internal partial discharge: some thoughts on progress made and where to go now", in *IEEE Transactions on Dielectrics*

- and Electrical Insulation, vol. 12, no. 5, Oct. (2005): 905-913, doi: 10.1109/TDEI.2005.1522185.
- [101] U. Kogelschatz, B. Eliasson, W. Egli, „Dielectric-Barrier Discharges. Principle and Applications”, Journal de Physique IV Colloque, pp.C4-47-C4-66, (1997).
- [102] IEC 60270: High-voltage test techniques-Partial discharge measurements, International Electrotechnical Commission - Edition, Geneva, Switzerland, (2000).
- [103] "IEEE Guide for the Interpretation of Gases Generated in Mineral Oil-Immersed Transformers," in IEEE Std C57.104-2019 (Revision of IEEE Std C57.104-2008), Nov. (2019): 1-98, doi: 10.1109/IEEESTD.2019.8890040.
- [104] S. J. Dala, "Future Development in Solid Dielectric Insulators for Compressed Gas Insulated Transmission Systems", Annual Report of CEIDP, (1981): 404-409.
- [105] H. Helmholtz, "Über einige Gesetze der Verteilung elektrischer Ströme in körperlichen Leitern mit Anwendung auf die thierisch-elektrischen Versuche", Ann. Phys. Chem. 165, (1853): 211–233.
- [106] P. M. Mitchinson, P. L. Lewin, B. D. Strawbridge and P. Jarman "Tracking and Surface Discharge at the Oil-Pressboard Interface", IEEE Electrical Insulation Magazine, March/April -Vol. 26, No. 2, (2010).
- [107] M. E. Banda, D. Malec, J. P. Cambronne, "Simulation of Space Charge Impact on Partial Discharge Inception Voltage in Power Busbars Dedicated to Future Hybrid Aircrafts. Circuits and Systems", 9, (2018): 196-212.
- [108] CIGRE TF 15/33.03.05, "PD Detection Systems for GIS: Sensitivity Verification for the UHF Method and the Acoustic Method", No. 183; CIGRE Electra: Paris, France, (1999).
- [109] CIGRE WG D 1.33, "Guidelines for Unconventional Partial Discharge Measurements", CIGRE Technical Brochure TB 444; CIGRE: Paris, France, (2010).
- [110] R. Patsch, M. Hoof, "The influence of space charge and gas pressure during electrical tree initiation and growth," Proceedings of 1994 4th International Conference on Properties and Applications of Dielectric Materials (ICPADM), (1994): 397-400 vol.1, doi: 10.1109/ICPADM.1994.414024.
- [111] W. Sima, P. Sun, M. Yang, Q. Yang, J. Wu, "Effect of space charge on the accumulative characteristics of oil paper insulation under repeated lightning impulses," in IEEE Transactions on Dielectrics and Electrical Insulation, vol. 22, no. 5, October (2015): 2483-2490, doi: 10.1109/TDEI.2015.004843.
- [112] F. H. Kreuger, "Discharge Detection in High Voltage Equipment", Temple Press Books Ltd, London, (1964).
- [113] B. Eliasson, U. Kogelschatz, "Modeling and Applications of Silent Discharge Plasma", IEEE Trans. On Plasma Science, Vol. 19, No. 2, (1991).
- [114] R. Brandenburg, "Dielectric barrier discharges: progress on plasma sources and on the understanding of regimes and single filaments", Plasma Sources Sci. Technol. (2017): 1-29.
- [115] S. A. M. Najafi, H. Saadati, P. Werle, E. Gockenbach, H. Borsi, "UHF characteristics of silent discharges", in Proceedings of the 20th International Symposium on High Voltage Engineering, (2017).
- [116] PDIX Complete Product Brochure: <https://www.pdix.com/downloads/brochure-and-brochure-pages.html>
- [117] E. Lemke, "A new partial discharge measuring procedure based on the evaluation of the cumulative charge", Conf. on PD in Electrical Insulation Bangalore/India, (1976): 1-22.
- [118] MIDEL oil moisture tolerance https://www.midel.com/app/uploads/2018/05/MIDEL_7131_Moisture_Tolerance.pdf
- [119] ABB, "Transformer Handbook", 3rd ed., ABB Ltd Transformers, (2010): 169-188.
- [120] L. Niemeyer, "A generalized approach to partial discharge modeling," IEEE Trans. Dielectr. Electr. Insul., Vol. 2, (1995): 510-528.

- [121] M. Ghaffarian Niasar, "Mechanisms of Electrical Ageing of Oil impregnated Paper due to Partial Discharges", Doctoral thesis, Stockholm, Sweden (2015).
- [122] A. R. Rezk, H. Ahmed, S. Ramesan, Y. L. Yeo, "High Frequency Sonoprocessing: A New Field of Cavitation-Free Acoustic Materials Synthesis, Processing, and Manipulation", *Adv. Sci.* (2021), 2001983. <https://doi.org/10.1002/adv.202001983>
- [123] R. T. Harrold, "Acoustic waveguides for sensing and locating electrical discharges in H.V. power transformers and other apparatus", *Trans. IEEE PAS98* (1979): 449–457.
- [124] T. Young, "The Bakerian Lecture: On the Theory of Light and Colours", *Philosophical Transactions of the Royal Society of London Vol. 92*, (1802): 12-48,
- [125] M Borovcnik, R Kapadia "A Historical and Philosophical Perspective on Probability", Springer Science+Business Media Dordrecht, DOI 10.1007/978-94-007-7155-0_2, (2014).
- [126] Omicron Measuring devices: <https://www.omicronenergy.com/en/product-overview/>
- [127] M. Roos, "Introduction to Cosmology", John Wiley & Sons, Ltd, ISBN 0 470 84909 6, (2003).
- [128] D. Marcus, K. S. Hickcox, N. Narendran, J. P. Freyssonier, J. Taylor, R. Leslie, "The Lightning Field Guide", Rensselear Polytechnic Institute, (2013).
- [129] N. C. Sahoo, M. M. A. Salama, R. Bartnikas, "Trends in Partial Discharge Pattern Classification: A Survey", *IEEE Trans. Dielectr. Electr. Insul.*, Vol. 12, No.2, (2005): 248-264.
- [130] S. Tenbohlen, D. Denissov, S. M. Hoek, "Partial Discharge Measurement in the Ultra High Frequency (UHF) Range", *IEEE Trans. Dielectr. Electr. Insul.*, Vol. 15, No.6, (2008): 1544-1552.
- [131] A. Akbari, P. Werle, H. Borsi, E. Gockenbach, "Transfer function-based partial discharge localization in power transformers: a feasibility study", in *IEEE Electrical Insulation Magazine*, vol. 18, no. 5, Sept.-Oct. (2002): 22-32, doi: 10.1109/MEI.2002.1044318.
- [132] L. Bao, J. Li, J. Zhang, X. Li, "Influences of moisture content on surface partial discharge behaviors of oil-impregnated paper insulation under pulsating DC voltage", *IEEE International Conference on High Voltage*, (2016).
- [133] M. Suwarno, H. Prakoso, "Effects of Water Content on Dielectric Properties of Mineral Transformer Oil", *World Academy of Science, Engineering and Technology International Journal of Electrical and Computer Engineering*, Vol:9, No:10, (2015).
- [134] 756/831 KF Coulometer Instructions for Use, Metrohm AG 2010, Switzerland <http://www.metrohm.com/>



Seyed Amir Mahmood Najafi

Erfahrung

10.2021–Heute

Lead Engineer Digitalization und Innovation • Siemens-Energy AG

- Projektleiter für die Digitalisierung und Sensformer®
- Entwicklung neuer Sensoren und Programmierung für Überwachung der Transformatoren und Schaltanlagen
- Preisoptimierung der Digitalisierungsmethode mithilfe der Marktbewertung

10.2020–09.2021

PLM und Projektleiter • Siemens-Energy AG

- Projektleiter für Spezialprojekte, Entwicklung der größten Offshore-Windanlage und komplexer Transformatoren
- Entwicklung von Methoden zur Optimierung des Stromnetzes über intelligente Ladestationen

10.2018–09.2020

Projektleiter und Vertriebsingenieur • Siemens AG

- Erstellung von Angeboten
- Projektabwicklung der Transformatoren weltweit (USA, Afrika und Asien)
- Betreuung von in- und ausländischen Kunden und Vertretungen am Standort
- Betreuung von Kunden bei Abnahmen im Herstellerwerk

02.2015–09.2018

Senior System Engineer (Electric Validation) • Servion GmbH

- Stetige Qualitätsverbesserung von Mittelspannungstransformatoren, Schaltanlagen, Generatoren, Kabeln und Stromschienen
- Optimierung von Standards für Typ- und Stückprüfungen
- Zusammenarbeit mit verschiedenen Universitäten und Instituten zur Entwicklung von neuen Validierungsmethoden



Mahmood.najafi@posteo.de



<https://www.linkedin.com/in/mahmood-najafi-61a1823a/>



Deutsch: Fließend
Englisch: Fließend
Farsi: Muttersprache



Doktor-Ingenieur in Elektrotechnik
(2023)
Masterstudium in Elektrotechnik
(2021)



Gute Teamfähigkeit, Kreative,
Tatkräftig, Selbstbewusst,
Zielstrebig



Ehrungen und Auszeichnungen

Gewinner des renommierten €300.000 Awards für eine bahnbrechende Idee in der Digitalisierung (2021)

Erfindung im Bereich Überwachung der Mittelspannungskomponenten
International Veröffentlichungsnummer WO2019215162A1 (2019)

Best Student Paper Award
20th International Symposium on High Voltage Engineering (ISH 2017)

Ausgezeichneter Student für 3 Semesters (2003 bis 2007)
Islamic Azad University of Gonabad, Gonabad, Iran

Publikationen

S. A. M. Najafi, A. Peymankar, H. Saadati, E. Gockenbach, H. Borsi; "The influence of corona near to the bushing of a power transformer on partial discharge measurement with an acoustic emission sensor", Electrical Insulation Conference (EIC 2013) Ottawa, Ontario, Canada

S. A. M. Najafi, A. Peymankar, E. Gockenbach, H. Borsi; "Correlation between electrical measured partial discharges and acoustic emission signals from new and thermal aged pressboards in oil", International Symposium on High Voltage Engineering (ISH 2013) Seoul, Republic of Korea

S. A. M. Najafi, E. Gockenbach, H. Borsi; "Correlation between electric and acoustic signals of discharge phenomenon at different electrode arrangements", International Symposium on High Voltage Engineering (ISH 2013) Seoul, Republic of Korea

S. A. M. Najafi, P. Werle; "Investigation on the possibility of silent partial discharges inside power transformers", Electrical Insulation Conference (EIC 2016) Montreal, Quebec, Canada

S. A. M. Najafi, H. Saadati, P. Werle; "Comparison of Acoustical Partial Discharge Signals under AC and DC Stress", Electrical Insulation Conference (EIC 2016) Montreal, Quebec, Canada

S. A. M. Najafi, H. Saadati, E. Gockenbach and H. Borsi; "UHF Characteristics of Silent Discharges", International Symposium on High Voltage Engineering (ISH 2017) Buenos Aires, Argentina

H. Saadati, S. A. M. Najafi, H. Movagharnejad, U. Schiefelbein and P. Werle; "Experimental Investigations on the Behavior of Partial Discharges in Dry Type Transformers as a Function of Temperature and Voltage Stress", International Symposium on High Voltage Engineering (ISH 2017) Buenos Aires, Argentina

S. A. M. Najafi, E. Gockenbach and H. Borsi; "Effect of Carbonized Patterns on Oil-Impregnated Pressboards Surface on Acoustic Emission Signals at Inhomogeneous Electric Field", IEEE Transactions on Dielectrics and Electrical Insulation

